Marta Guembe García
TESIS DOCTORAL
Año 2021

POLÍMEROS INTELIGENTES PARA EL CONTROL Y MONITORIZACIÓN DE HERIDAS CRÓNICAS

Directores:

Dr. Saúl Vallejos Calzada
Dra. Aránzazu Mendía Jalón

Universidad de Burgos

DEPARTAMENTO DE QUÍMICA
Área de Química Orgánica
Grupo de Polímeros

Dña. Aránzazu Mendía Jalón, Profesora del Área de Química Inorgánica, y **D. Saúl Vallejos Calzada**, investigador postdoctoral del Área de Química Orgánica del Departamento de Química de la Universidad de Burgos,

INFORMAN:

El trabajo original descrito en esta Memoria, titulada ***Polímeros sensores para el control y monitorización de heridas crónicas***, se ha realizado por **Dña. Marta Guembe García** en el Departamento de Química de la Universidad de Burgos, bajo su dirección, y autorizan su presentación para que sea calificada como **TESIS DOCTORAL**.

Burgos, 12 de mayo de 2021.

Fdo.:   Dra. Aránzazu Mendía Jalón   Fdo.:   Dr. Saúl Vallejos Calzada

Quisiera expresar mi más sincero agradecimiento a todas las personas que me han apoyado y ayudado, de manera que sin su contribución no hubiera sido posible culminar este trabajo con satisfacción:

A mis directores Saúl Vallejos y Aránzazu Mendía, por sus consejos, su paciencia y su dedicación, por acompañarme en el camino y por todo la aprendido.

A José Miguel García y Félix García, por darme la oportunidad de realizar esta Tesis y trabajar en el Grupo de Polímeros. Y a Satur por su ayuda en esta Tesis.

A las doctoras del Hospital Universitario de Burgos, Victoria Santaolalla y Natalia Moradillo, por dejarme colaborar con ellas.

A todos mis compañeros del grupo de polímeros, a los actuales, a los que se han ido y a los que acaban de llegar. En especial a Miriam, JA, Blanca, Patricia y Patricia Daniela. A todas las Robertas (Cintia, Carlos, Noelia, Marta, Fer…) y en especial a Claudia y a Kenia, a todos ellos gracias por todos los momentos que hemos vivido, los buenos y los no tan buenos, los viajes y las comidas convertidas en terapias, gracias por su amistad y su apoyo, por ser como mi familia cuando la mía estaba lejos.

A mis amig@s de toda la vida, en especial a Mari, por estar siempre.

A mis padres, a mi sister y a perrete, soy lo que soy gracias a ellos y sin ellos no hubiera llegado hasta aquí.

RESUMEN

A lo largo del desarrollo mi tesis he estado trabajando en el diseño, síntesis y caracterización de materiales poliméricos como sensores para el control y el seguimiento de las heridas crónicas en humanos. He realizado una búsqueda bibliográfica y un estudio con muestras reales para encontrar biomarcadores relacionados con el estado de este tipo de heridas, y he seleccionado los aminoácidos y el catión Zn(II) como posibles candidatos. He preparado dos sensores colorimétricos de aminoácidos, uno basado en sistemas de desplazamiento (IDAs, *Indicator–Displacement Assays*) y otro en dosímetros químicos, para evaluar de manera indirecta la actividad de las metaloproteasas, enzimas relacionadas con el estado de las heridas crónicas. Además, mi trabajo se ha completado con un tercer sensor fluorogénico de Zn(II), catión presente en este tipo de enzimas. Todos los sensores propuestos se han preparado en formato de *film* o membrana, concretamente para que su uso sea sencillo y orientado a su uso en una situación real. Estos sensores se han probado en muestras reales de heridas crónicas, demostrando su validez en el diagnóstico y su utilidad en el seguimiento de estas. Finalmente, se ha desarrollado una aplicación (*App*) para teléfonos inteligentes (*Colorimetric Titration*, *App* para Android y iOS) que facilita el uso de los polímeros inteligentes dando lugar a un sistema sensor integral, y que permite llevar a cabo un análisis cuantitativo de forma simple.

ABSTRACT

Throughout my thesis I have been working on the design, synthesis and characterization of polymeric materials as sensors for the control and monitoring of chronic wounds in humans. I have carried out a bibliographic search and a study with real samples to find biomarkers related to the state of these types of

wounds, and I have selected the amino acids and the Zn (II) cation as possible candidates. I have prepared two amino acid colorimetric sensors, one based on displacement systems (IDAs, Indicator–Displacement Assays) and the other on chemical dosimeters, to indirectly evaluate the activity of metalloproteases, enzymes related to the state of chronic wounds. In addition, my work has been completed with a third fluorogenic sensor for Zn (II), a cation present in this type of enzyme. All the proposed sensors have been prepared in film or membrane format, specifically so that their use is simple and oriented to their use in a real situation. These sensors have been tested in real samples of chronic wounds, demonstrating their validity in diagnosis and their usefulness in their follow-up. Finally, an application (App) for smartphones (Colorimetric Titration, App for Android and iOS) has been developed that facilitates the use of smart polymers, giving rise to an integral sensor system, and that allows a quantitative analysis to be carried out in a way simple.

CAPÍTULO 1

Introducción general

Los usos y aplicaciones de los polímeros han ido cambiando con el paso del tiempo. Su empleo se ha incrementado extraordinariamente dado que sus propiedades les permiten adaptarse a las necesidades de una sociedad tecnológica en continuo desarrollo. Hoy en día podemos encontrar a los polímeros en cualquier ámbito de la actividad humana, tanto en el día a día (como por ejemplo en los envases de productos de higiene, limpieza, cosmética y alimentación) como a nivel industrial como por ejemplo en automoción o en construcción y más recientemente, en medicina, donde desde hace décadas que se están empleando como biomateriales y como materiales inteligentes en el tratamiento, diagnóstico y prevención de enfermedades.

1.1. Antecedentes históricos de los polímeros.

Los polímeros son macromoléculas formadas por la unión covalente de moléculas más pequeñas (monómeros). Estos materiales se pueden clasificar en dos grandes grupos: polímeros naturales, como las proteínas o el ADN, y polímeros sintéticos, como el poliestireno o el nailon (*nylon*). Aunque los polímeros naturales son tan antiguos como la vida, e incluso ésta tiene su base en ellos, la historia de los polímeros sintéticos es muy reciente. El primer polímero completamente sintético fue la baquelita (polimerización de fenol y formaldehido) que se sintetizó en 1907 a partir de la experimentación sin una base científica sólida,[1] al igual que otros muchos polímeros que se desarrollaron en aquella época, puesto que no fue hasta 1920 cuando se contó con una teoría unificada sobre la estructura de los polímeros (y, sobre todo, sobre la relación estructura/propiedades).[2]

---

[1]   L. H. Baekeland, *Ind. Eng. Chem.*, **1909**, 1, 149–161.
[2]   H. Staudinger, *Berichte der Dtsch. Chem. Gesellschaft A B Ser.*, **1920**, 53, 1073–1085.

Con los años, los usos y las aplicaciones de los polímeros han ido cambiando para adaptarse a las necesidades del momento. Por ejemplo, inicialmente la baquelita supuso una gran revolución, y se utilizó en la fabricación de diferentes objetos, como las carcasas de radio y teléfono, los materiales de aislamiento eléctrico, las estructuras de los carburadores, e incluso en productos de la industria bélica. Sin embargo, hoy en día es un material con muchas menos aplicaciones y se ha sustituido por otro tipo de polímeros más avanzados y respetuosos con el medio ambiente, ya que el formaldehído, uno de los monómeros que interviene en su síntesis, está considerado como un producto químico perjudicial para la salud.

Los polímeros participan en prácticamente todos los aspectos de la actividad humana. Uno de los usos más conocidos de los polímeros es en el sector de los envases. En este caso, los polímeros no solo están presentes en la parte externa de productos de higiene, limpieza y cosmética, sino que además tienen un papel activo, mejorando algunas de sus propiedades y características.[3] Esto ocurre en la industria alimentaria, donde permiten un envasado ligero y favorecen la conservación de los alimentos que contienen. Otro de los ejemplos más conocidos es su empleo en revestimiento y aislamiento, en sectores que abarcan desde la automoción hasta la construcción. También son muy importantes sus aplicaciones en medicina, donde la biocompatibilidad general y la versatilidad en el diseño de estructuras poliméricas ha revolucionado la dosificación de medicamentos, la medicina dirigida y el reemplazo de tejidos y órganos.

1.2. Polímeros en medicina

De forma muy resumida, los requisitos más relevantes para que un material se pueda utilizar en el ámbito biomédico son:

---

[3]   S.H. Aswathy, U. Narendrakumar, I. Manjubala. *Heliyon*, **2020**, 6, e03719.

- *Debe ser un biomaterial*, es decir, debe ser biocompatible, implantable en el cuerpo humano (inerte o que su degradación dé lugar a especies que no causen efectos negativos).[4,5]

- *Pueden ser bioactivos e interactuar con el medio biológico en el que se encuentran* generando efectos positivos, como por ejemplo los apósitos de cicatrizado o las suturas.

- *Si tienen función estructural a medio y largo plazo, deben ser químicamente estables*, y tener adecuadas propiedades mecánicas, y poder adaptarse a las necesidades del tejido/entorno en el que se van a implantar, como por ejemplo una prótesis.

Teniendo en cuenta estas consideraciones previas, existen muchos polímeros que son considerados biomateriales, por lo que muchas ramas de la medicina como la odontología, la oftalmología o la cirugía los utilizan para el tratamiento o el diagnóstico de enfermedades y/o lesiones.

En odontología, los polímeros están presentes no solo en el instrumental y los equipos auxiliares, sino en las propias prótesis dentales,[6,7] en reconstrucciones (empastes), en cementos,[8] o en moldes que se utilizan para hacer piezas poliméricas removibles como las que se usan para tratar el bruxismo.[9]

En oftalmología, los materiales poliméricos se utilizan para hacer lentillas desechables,[3] para la reconstrucción ocular en forma de prótesis (total o parcial),

4   Williams DF. The Williams dictionary of biomaterials. Liverpool: Liverpool University Press; **1999**.

5   "Biomaterial." Merriam-Webster.com Dictionary, Merriam-Webster, https://www.merriam-webster.com/dictionary/biomaterial. Accessed 8 Mar. **2021**.

6   Z. Ma, X. Zhao, J. Zhao, Z. Zhao, Q. Wang and C. Zhang, *Front. Bioeng. Biotechnol.*, **2020**, 8, 620537.

7   M. Martín-del-Campo, D. Fernández-Villa, G. Cabrera-Rueda and L. Rojo, *Appl. Sci.*, **2020**, 10, 8371.

8   S. Soleymani Eil Bakhtiari, H. R. Bakhsheshi-Rad, S. Karbasi, M. Tavakoli, S. A. Hassanzadeh Tabrizi, A. F. Ismail, A. Seifalian, S. RamaKrishna and F. Berto, *Polym. Int*, **2020**, 12, 7, 1469.

9   C. Wesemann, B. C. Spies, D. Schaefer, U. Adali, F. Beuer and S. Pieralli, *J. Mech. Behav. Biomed. Mater.*, **2021**, 114, 104179.

como material de relleno en caso de atrofia, o para la reconstrucción de los canalículos y de las vías lagrimales.[10]

Los polímeros también tienen un papel relevante en la medicina vascular, ya que se utilizan para hacer catéteres o venas artificiales. A nivel óseo, los materiales poliméricos se utilizan en fabricación de prótesis, y en cirugía muchos de los materiales de sutura son también poliméricos (hilos, grapas, biopegamentos). También están presentes en la regeneración tisular, ya que son la base de todos los apósitos sanitarios. En este caso, los polímeros aportan una doble funcionalidad al producto para el tratamiento de heridas y úlceras.[11,] Por un lado protegen el tejido de agentes externos como bacterias, y por otro pueden liberar fármacos de forma controlada para una regeneración tisular más rápida y efectiva.

Estos son solo algunos ejemplos de las innumerables aplicaciones que tienen los polímeros en el campo de la biomedicina. Durante el desarrollo de mi tesis me he centrado en el uso de polímeros como biomateriales y de forma más precisa, en desarrollo de polímeros que interactúan con el medio que les rodea. Dicho de otra forma, en presencia de un estímulo específico son capaces de generar una respuesta, y se les conoce generalmente como polímeros inteligentes.[12,13]

1.3. Polímeros inteligentes

Los polímeros inteligentes son capaces de generar una respuesta ante un estímulo externo, tanto físico como químico. Los tipos de respuestas y de estímulos dependerán de la naturaleza y de las aplicaciones del sistema. En el ámbito biomédico, es habitual hoy en día encontrar estos polímeros inteligentes en algunas aplicaciones importantes como son la liberación controlada de

[10] A. Klapstova, J. Horakova, M. Tunak, A. Shynkarenko, J. Erben, J. Hlavata, P. Bulir and J. Chvojka, *Mater. Sci. Eng. C*, **2021**, 119, 111637.
[11] E. A. Kamoun, E. R. S. Kenawy and X. Chen, *J. Adv. Res.*, **2017**, 8, 217–233.
[12] Williams DF. The Williams dictionary of biomaterials. Liverpool: Liverpool University Press; **1999**.
[13] L. L. Hench, *J. Am. Ceram. Soc.*, **1991**, 74, 1487–1510.

fármacos,[14] la ingeniería de tejidos,[15,16] el reconocimiento e inmovilización de biomoléculas,[17] la medicina de precisión y la terapia celular.[18]

Los sistemas poliméricos empleados en la liberación controlada de fármacos están diseñados para producir la liberación del fármaco como respuesta ante un estímulo biológico o físico. La liberación del fármaco puede estar controlada por diferentes procesos de expansión/contracción, o solubilización/formación de gel, etc. Además, el estímulo que genera esa liberación puede ser de diferente naturaleza, como un cambio de pH, una señal electroquímica (provocada por una reacción redox), un cambio de temperatura, la presencia de una molécula biológica (glucosa, enzimas, proteínas, ácidos nucleicos…) o la exposición a radiación electromagnética. Esta versatilidad en lo referente a los estímulos hace que el término "liberación" se convierta en "liberación controlada", ya que se puede producir intencionadamente en un tejido/órgano concreto y a una velocidad determinada. Incluso, en algunos casos, la respuesta del sistema (liberación del fármaco) puede depender de la combinación de más de un estímulo.[14,19]

En el caso de la regeneración tisular, el objetivo es regenerar un tejido dañado o sustituirlo de manera funcional (prótesis). Para que esto sea posible los materiales que se utilizan deben permitir la adsorción de proteínas en su superficie que finalmente dará lugar a la adhesión celular. Las prótesis poliméricas representan una excelente opción en este tipo de medicina reconstructiva, ya que la interacción que se establecen entre el medio fisiológico y el material da lugar a superficies cargadas que favorecen la adsorción de proteínas previa a la adhesión celular.[15,16,20]

14 N. U. Khaliq, D. Chobisa, C. A. Richard, M. R. Swinney and Y. Yeo, *Ther. Deliv.*, **2021**, 12, 37–54
15 B. Naureen, A. S. M. A. Haseeb, W. J. Basirun and F. Muhamad, Mater. *Sci. Eng. C*, **2021**, 118, 111228.
16 G. C. J. Lindberg, K. S. Lim, B. G. Soliman, A. Nguyen, G. J. Hooper, R. J. Narayan and T. B. F. Woodfield, *Appl. Phys. Rev.*, **2021**, 8, 011301.
17 X. Chen and J. Li, *Mater. Chem. Front.*, **2020**, 4, 750–774.
18 H. J. Huang, Y. L. Tsai, S. H. Lin and S. H. Hsu, *J. Biomed. Sci.*, **2019**, 26, 1–11.
19 Namitha K. Preman, Rashmi R. Barki, Anjali Vijayan, Sandesh G. Sanjeeva, Renjith P. Johnson. Eur. J. Pharm. Biopharm., **2020**, 157, 121-153.
20 Doberenz, F., Zeng, K., Willems, C., Zhang, K., & Groth, T. J. Phys. Chem. B, **2020**, 8, 607-628.

Por su parte, la medicina de precisión y la terapia celular apuestan por la medicina personalizada, ya que las terapias en masa no siempre se adaptan a la heterogeneidad de los organismos y las circunstancias. Son terapias que se suelen aplicar en tratamiento de pacientes con cáncer, y los materiales que se utilizan deben cumplir tres requisitos: ser estables durante el tiempo que dura el tratamiento, pero fácilmente degradables una vez terminado el mismo; ser capaces de transportar genes y/o células madre del paciente; y ser capaces de liberar fármacos como respuesta a estímulos biólogos o físicos concretos del lugar para el que han sido diseñados.[18]

Los polímeros inteligentes también presentan aplicación en el reconocimiento e inmovilización de biomoléculas, es decir, como sensores. Un sensor es un dispositivo que transforma una señal química en una señal analítica cuantificable. Independientemente de la naturaleza del sistema de reconocimiento, los sensores se pueden clasificar en función del tipo de señal analítica que originen, los cuales se describen a continuación (**Figura 1.1.**):

- *Sensores poliméricos piezoeléctricos*: detectan cambios de presión en la superficie del material generando diferencias de potencial en la superficie del propio material.[21]

- *Sensores poliméricos quimio-mecánicos:* las interacciones entre el sensor y el analito generan un cambio en el tamaño, la forma y/o la estructura del material.[22]

- *Sensores poliméricos electroquímicos:* las interacciones entre el sensor y el analito generan un cambio en la conductividad eléctrica del sistema.[23]

---

[21] A. M. Sanjuán, J. A. Reglero Ruiz, F. C. García and J. M. García, *React. Funct. Polym.*, **2018**, 133, 103–125.

[22] A. Leronni and L. Bardella, *J. Mech. Phys. Solids*, **2021**, 148, 104292.

[23] B. S. Pascual, S. Vallejos, J. A. Reglero Ruiz, J. C. Bertolín, C. Represa, F. C. García and J. M. García, *J. Hazard. Mater.*, **2019**, 364, 238–243.

- *Sensores poliméricos colorimétricos:* las interacciones entre el sensor y el analito generan un cambio de color.[24,25]

- *Sensores poliméricos fluorescentes:* las interacciones entre el sensor y el analito generan un cambio de la fluorescencia del sistema. La presencia del analito puede aumentar o disminuir la fluorescencia del sistema.[26,27]
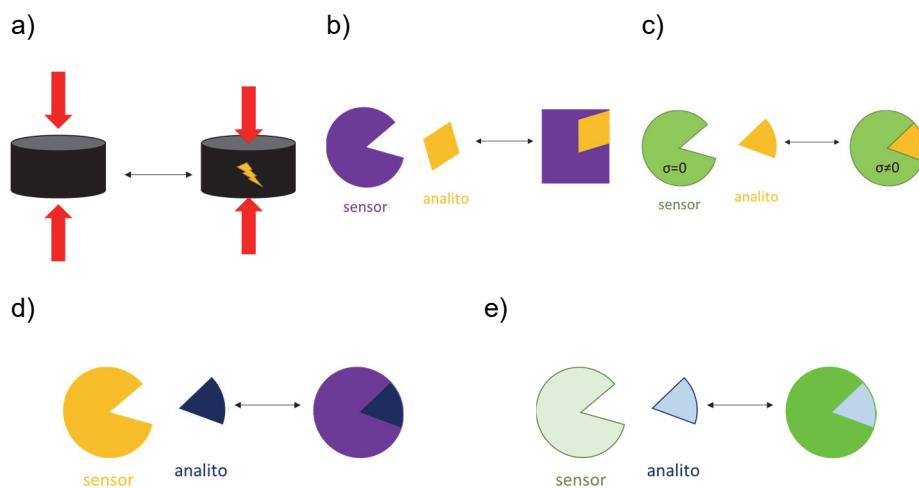
Figura 1.1. Clasificación de los sensores poliméricos en función de la señal analítica: a) sensores poliméricos piezoeléctricos; b) sensores poliméricos quimio-mecánicos; c) sensores poliméricos electroquímicos; d) sensores poliméricos colorimétricos; y e) sensores poliméricos fluorescentes.

Mi Tesis se centra en los **sensores colorimétricos y fluorimétricos**, cuyos cambios visuales del color y la fluorescencia se deben a procesos de reconocimiento/interacción molecular.

---

[24] S. Vallejos, A. Muñoz, S. Ibeas, F. Serna, F. C. García and J. M. García, *J. Mater. Chem. A*, **2013**, 1, 15435–15441.

[25] S. Vallejos, J. A. Reglero, F. C. García and J. M. García, *J. Mater. Chem. A*, **2017**, 5, 13710–13716.

[26] J. García-Calvo, S. Vallejos, F. C. García, J. Rojo, J. M. García and T. Torroba, *Chem. Commun.*, **2016**, 52, 11915–11918.

[27] S. Vallejos, A. Muñoz, S. Ibeas, F. Serna, F. C. García and J. M. García, *J. Hazard. Mater.*, **2014**, 276, 52–57.

Existen dos tipos de sensores en función del tipo de interacción que se produzca: reversibles (sensores químicos o quimiosensores) [28] o irreversibles (dosímetros químicos).[29] Dentro de las interacciones reversibles se pueden distinguir dos tipos: la formación de nuevas especies por reacción química o interacción física y los procesos de desplazamiento, tal y como se describe de manera esquemática en la **Figura 1.2**.
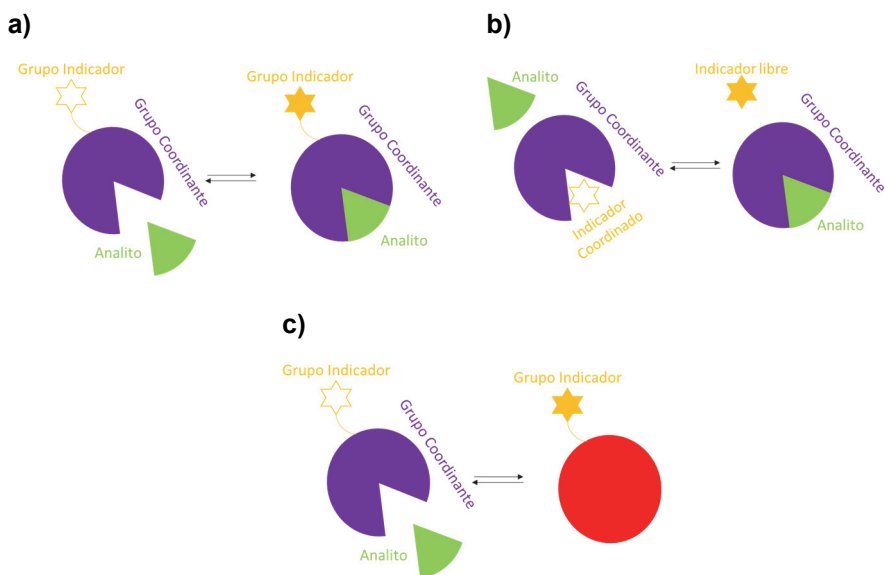
Figura 1.2. Comportamiento de los quimiosensores o sensores químicos reversibles. a) formación de complejos; b) procesos de desplazamiento y c) dosímetro químico o quimiodosímetro.

En el caso de las interacciones irreversibles lo que se produce es una reacción química especifica entre la unidad sensora y el analito, induciendo un cambio en alguna propiedad macroscópica medible en el sistema. Este tipo de sensores también se denominan dosímetros químicos o quimiodosímetros, y los cambios en las propiedades macroscópicas se deben a variaciones en la estructura electrónica de las moléculas.

---

[28] S. Vallejos, E. Hernando, M. Trigo, F. C. García, M. García-Valverde, D. Iturbe, M. J. Cabero, R. Quesada and J. M. García, *J. Mater. Chem. B*, **2018**, 6, 3735–3741.

[29] S. E. Bustamante, S. Vallejos, B. S. Pascual-Portal, A. Muñoz, A. Mendia, B. L. Rivas, F. C. García and J. M. García, J. Hazard. Mater., 2019, 365, 725–732.

Por una parte, el **color** depende de la diferencia de energía entre el HOMO (*Highest Occupied Molecular Orbital*) y el LUMO (*Lowest Unoccupied Molecular Orbital*). Por ejemplo, cuando esta es pequeña, la molécula absorbe en longitudes de onda entre 780-650 nm, es decir absorbe el color verde y refleja el complementario, el rojo. Si es grande, absorbe entre 435-480 nm (azul oscuro) y refleja el amarillo. Las longitudes de onda intermedias corresponden al resto de colores y diferentes magnitudes de diferencia de energía HOMO-LUMO (**Tabla 1**).

Tabla 1. Colores observados en función de la absorbancia de la muestra.

Luz absorbida			Color observado	
Lonqitud de onda (nm)	**Color**			
650-780	Rojo		Verde azulado	
595-650	Naranja		Azul verdoso	
560-595	Amarillo Verde		Morado	
500-560	Verde		Magenta	
490-500	Verde azulado		Rojo	
480-490	Azul verdoso		Naranja	
435-480	Azul		Amarillo	
380-435	Morado		Amarillo Verde	

Por su parte, **la fluorescencia** se debe a transiciones radiativas desde un estado electrónico excitado al estado fundamental. Es decir, siempre que se tenga una molécula electrónicamente excitada va a tender a volver a su estado electrónico fundamental, emitiendo una radiación. En función del tipo de transición que se produzca pueden darse dos fenómenos, fluorescencia o fosforescencia, que se pueden explicar con el diagrama de Jablonski[30] (**Figura**

---

[30] D. Frackowiak, *J. Photochem. Photobiol. B Biol.*, **1988**, 2, 399.

1.3). Si la emisión se produce desde un estado excitado (S_1) a uno inferior de igual multiplicidad (S_0) el proceso se denomina fluorescencia, si por el contrario la transición se produce entre estados de diferente multiplicidad (T_1-S_0), siempre de mayor a menor energía, el proceso se denomina fosforescencia. No todas las transiciones electrónicas están permitidas, de ahí que no todas las moléculas presenten fluorescencia o fosforescencia. En el caso de los sensores poliméricos fluorescentes, las interacciones de la especie sensora con el analito varían la configuración electrónica del sistema dando lugar a estados electrónicos entre los que se permiten transiciones (sensores *Off-On*),[27,31] o generando estados entre los que están prohibidas (sensores *On-Off*).[28]
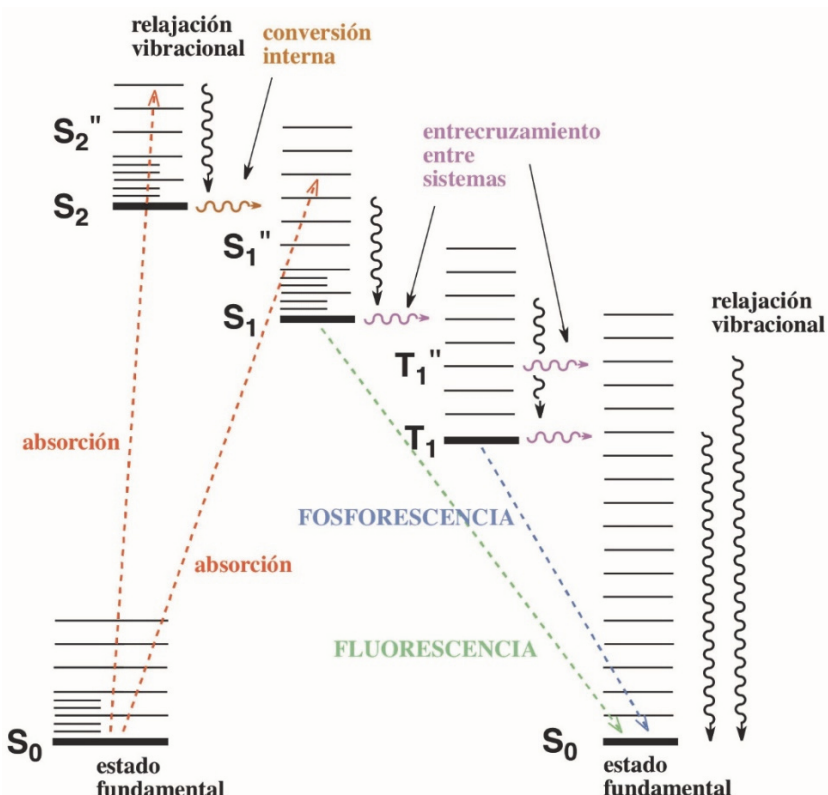
Figura 1.3. Diagrama de Jablonski (imagen tomado de la referencia 32).

[31] S. Vallejos, P. Estévez, S. Ibeas, F. C. García, F. Serna and J. M. García, Sensors, **2012**, 12, 2969–2982.

[32] http://www.ub.edu/talq/es/node/259 (Accessed 19 February 2021)

La hipótesis inicial de este trabajo fue que los sensores poliméricos (colorimétricos y fluorimétricos) pueden ser parte de la solución a un problema de salud de gran impacto social y económico, como son las heridas crónicas. Por eso, a lo largo de mi Tesis he desarrollado tres polímeros sensores para la detección de biomarcadores del estado de las heridas crónica, como son los aminoácidos y el catión Zn(II). Dos de esos polímeros sensores están basados en cambios de color para la detección de aminoácidos, uno basado en interacciones irreversibles (dosímetro químico) y el otro en procesos de desplazamiento (sensores IDAs). Además, también he desarrollado un sensor polimérico basado en un proceso *Off-On* de fluorescencia en presencia del catión Zn(II).

1.4. Planteamiento de la investigación

1.4.1. Problema detectado. Heridas crónicas

Las heridas crónicas son uno de los muchos problemas a los que se enfrenta la comunidad médica. Este tipo de lesiones son muy comunes, de hecho, se estima que afectan entre el 1 y el 2% de la población, y que solo en Europa se les dedica entre el 2-3% del presupuesto sanitario, lo que supone unos costes de entre 2,8 y 3,5 millones de euros por cada 100.000 habitantes al año.[33] Estas lesiones cutáneas necesitan un seguimiento diario, lo que se traduce en que cada profesional sanitario dedica anualmente de media 89 jornadas laborales (8h) al seguimiento y cura de las mismas. Además, se estima que los pacientes con estas lesiones ocupan entre 19.000 y 31.000 días de camas al año en los hospitales.[34] Todos estos factores agravan el impacto económico haciendo que los gastos derivados del tratamiento de las heridas crónicas puedan llegar a los 32.000 millones de dólares en Estados Unidos,[35] o que en España se dediquen 350 millones de euros al año a la causa.[33]

---

[33] P. Gómez Fernández, *RqR Enfermería Comunitaria*, **2015**, 3, 43–54.
[34] J. Posnett, F. Gottrup, H. Lundgren and G. Saal, *J. Wound Care*, **2009**, 18, 154–161.
[35] S. R. Nussbaum, M. J. Carter, C. E. Fife, J. DaVanzo, R. Haught, M. Nusgart and D. Cartwright, *Value Heal.*, **2018**, 21, 27–32.

Se puede decir que las heridas crónicas se han convertido en un problema de gran repercusión social y económica, debido a su difícil diagnóstico basado principalmente en un análisis visual del estado de la herida por parte del facultativo. El problema de esta valoración es la subjetividad, siendo muy probable que hasta pasados unos días no se tenga noción del estado real de la herida, es decir, si la herida evoluciona de manera correcta o si por el contrario se está convirtiendo en una herida crónica.

La causa principal de este tipo de lesiones es un desequilibrio entre los procesos de degradación/regeneración de las membranas celulares derivado de la actividad de un tipo concreto de enzimas, las metaloproteasas. En condiciones normales, estas enzimas degradan los tejidos dañados para que puedan ser remplazados por otros sanos y, cuando su actividad se descontrola, comienza a atacar indistintamente a los tejidos sanos y a los dañado, impidiendo así la cicatrización de las heridas. Por tanto, la determinación de la actividad enzimática de las metaloproteasas es el biomarcador más apropiado para la evaluación del estado de una herida. A su vez, la actividad metaloproteásica genera otros biomarcadores, como son los aminoácidos y el catión Zn(II), y es precisamente en lo que se centra mi tesis.

Actualmente no hay una manera rápida y sencilla de determinar la actividad metaloproteásica, y en la mayoría de los casos estas heridas solo pueden tratarse limpiando y cambiando los apósitos de manera frecuente. Las heridas están en constante evolución y la rapidez con la que se actúa sobre ellas es crucial. Por tanto, no tiene sentido el seguimiento de las heridas crónicas a través de análisis que pueden llevar días, e incluso puede llegar a ser contraproducente. Es por eso que sería de gran ayuda para el personal médico un apósito inteligente fácil de utilizar, y que dé una valoración objetiva del estado de la herida a través de un cambio de color. Esto ahorraría sufrimiento al paciente, tiempo y costes de material y personal. Este tipo de dispositivos podrían ser utilizados en una simple visita ambulatoria, o incluso por los propios pacientes en sus casas para un recuperación más rápida y efectiva.

1.4.2. Solución propuesta. Sensores poliméricos basados en cambios de color y fluorescencia.

A lo largo de los últimos años, una de las líneas de investigación del Grupo de Polímeros de la Universidad de Burgos ha sido la preparación de nuevos polímeros sensores de diferentes especies con especial interés. Inicialmente, la investigación del Grupo de polímeros se dirigía a la preparación de polímeros con receptores de moléculas discretas como aniones y cationes,[24,36] para avanzar posteriormente hacia aplicaciones orientadas a la vida cotidiana y relacionadas con la seguridad alimentaria, como la detección de mercurio en pescados,[26] polifenoles en vino,[37] o la determinación de la frescura del pescado a través de la medida de las aminas biógenas[38] o relacionadas con la seguridad civil como la detección de explosivos (TNT).[39] Más recientemente, y en lo que respecta a esta Tesis, el Grupo de Polímeros está dirigiendo su investigación hacia la detección de biomarcadores de enfermedades, como los cloruros en el caso de la fibrosis quística.[28]

Una de las ventajas que ofrecen los sensores poliméricos sobre otro tipo de sensores es la versatilidad de estos materiales que permite adaptar los sensores a distintos formatos como:

- *Aerosoles*, basados en disoluciones o dispersiones de polímeros lineales, especialmente útiles en el caso de detección de virus y bacterias en superficies o de cualquier otra cosa.[24]
- *Films o películas sensoras*, para la detección de sustancias en disolución.[24]

[36] S. Vallejos, P. Estévez, F. C. García, F. Serna, J. L. De La Peña and J. M. García, *Chem. Commun.*, **2010**, 46, 7951–7953.

[37] S. Vallejos, D. Moreno, S. Ibeas, A. Muñoz, F. C. García and J. M. García, *Food Control*, **2019**, 106, 106684..

[38] L. González-Ceballos, B. Melero, M. Trigo-López, S. Vallejos, A. Muñoz, F. C. García, M. A. Fernandez-Muiño, M. T. Sancho and J. M. García, *Sensors Actuators, B Chem.*, **2020**, 304, 127249.

[39] J. L. Pablos, M. Trigo-López, F. Serna, F. C. García and J. M. García, *Chem. Commun.*, **2014**, 50, 2484–2487.

- *Polvo fino*, lo que permite reducir el tiempo de respuesta del sensor en determinadas aplicaciones.
- *Espumas*, que combinan una buena manejabilidad con un tiempo de respuesta corto debido a su amplia superficie de contacto.[40]
- *Recubrimientos de fibras textiles*, fáciles de preparar a partir de un material soporte.[38]
- *Nanofibras electrohiladas*, con gran superficie de contacto y una metodología de producción orientada a la gran escala.

Desde el punto de vista de la composición, e independientemente del formato, todos los sensores poliméricos desarrollados en el Grupo de Polímeros de la Universidad de Burgos se basan en dos partes principales, la matriz inerte y el receptor. El nombre "matriz inerte" es simplemente una denominación para esta parte de los polímeros sensores que únicamente hace referencia a sus propiedades sensoras, ya que otras características como el formato del material, la hidrofilia o las propiedades mecánicas (entre otras) dependen directamente de la matriz inerte. Por su parte, el receptor es el encargado de interaccionar específicamente con las especies de interés, comúnmente conocidas como "especies diana", para producir el cambio de color o fluorescencia del material. Además, todos tienen en común una serie de características, como su fácil manejo por personal no especializado; su bajo coste debido a que los materiales de partida son reactivos (monómeros) donde la cantidad del receptor específico para las diferentes especies diana (monómero sensor) está en una proporción de un 1% como máximo, y el resto de los monómeros son comerciales y en general económicos; una estructura química biocompatible y comportamiento de gel; presentan respuesta colorimétrica o fluorimétrica, y por lo tanto se pueden detectar sustancias a simple vista (análisis semi-cuantitativo) o a través de un teléfono inteligente (análisis cuantitativo).[24]

---

[40] B. S. Pascual, S. Vallejos, C. Ramos, M. T. Sanz, J. A. R. Ruiz, F. C. García and J. M. García, Sensors (Switzerland), **2018**, 18, 4378.

Con respecto a las sondas colorimétricas o fluorimétricas convencionales, los polímeros sensores ofrecen una serie de ventajas (**Figura 1.4.**). Son fáciles de utilizar, no requieran de reactivos o disolvente, no necesitan de personal especializado que lleve a cabo las medidas, ni de equipos de protección individual, además permiten hacer una valoración cualitativa, e incluso cuantitativa a simple vista.

Figura 1.4. Ventajas de las polímeros sensores sobre las sondas sensoras convencionales.

Otra de las grandes ventajas que diferencian a los sensores poliméricos de las sondas colorimétricas o fluorimétricas convencionales es que en disolución las interacciones que deben darse entre el receptor y la especie diana suelen estar muy impedidas debido a interacciones de ambos con el disolvente, generalmente agua. Sin embargo, cuando los sensores son poliméricos, la matriz polimérica genera un entorno de protección que aísla en cierto modo a los receptores y las especies dianas del disolvente, produciéndose una interacción entre ambos mucho más favorecida, más selectiva, y más eficaz. Esta ventaja se ha estudiado y demostrado en esta tesis doctoral, ya que fue objeto de uno de los artículos científicos que se han publicado, y se encuentra descrita a fondo en el **Capítulo 2** de esta Memoria.

A la hora de diseñar nuevos polímeros sensores, la metodología de trabajo siempre comienza con la búsqueda de dianas relacionadas con necesidades/demandas concretas de la sociedad, y que pueden ser contaminantes, especies relacionadas con la seguridad alimentaria, o como en lo que a esta tesis respecta, especies biológicas de interés médico.

Una vez seleccionada esta especie diana, el segundo paso es la elección, tras una búsqueda bibliográfica, de receptores específicos que interaccionen con ella y si es posible, que además, la interacción produzca un cambio -óptico (cambio de color y/o fluorescencia). A continuación, se sintetizan monómeros que contengan estas estructuras receptoras a partir de rutas sintéticas conocidas. El resultado de esa síntesis es lo que denominamos monómero sensor, y que tendrá por lo tanto un grupo polimerizable (metacrilato, metacrilamida, vinilo, etc) y una subunidad receptora.

Finalmente, el monómero sensor se polimerizará junto con otros monómeros comerciales que forman la matriz inerte, y de la que dependen algunas propiedades finales del polímero sensor, como la manejabilidad o el grado de hinchamiento en agua, su grado de entrecruzamiento (sobre todo cuando se obtienen filmes o membranas con comportamiento de gel) o su solubilidad en agua (sobre todo cuando se obtienen polímeros lineales no entrecruzados).

Como alternativa, se pueden sintetizar o adquirir comercialmente compuestos intermedios de la ruta sintética, que cumplan el requisito indispensable de tener un grupo polimerizable, y sobre los cuales sea posible realizar reacciones en fase sólida. Este procedimiento abarata costes, es muy eficaz, y supone una opción muy recurrente a la hora de preparar polímeros sensores. Por ejemplo, en el **Capítulo 2** de esta memoria se describe un polímero sensor basado en grupos receptores derivados de la ninhidrina, que se preparó a través de esta metodología.

Desde el primer momento quise orientar mis sensores a un uso sencillo y orientado a personal no especializado. En este sentido, las nuevas tecnologías ofrecen muchas posibilidades, que he aprovechado para desarrollar una aplicación para dispositivos móviles que acompaña al usuario en el proceso de detección de aminoácidos o Zn(II), haciendo el seguimiento de las heridas crónicas muy intuitivo, muy sencillo, y solo con el uso de un teléfono.

En esta Memoria se presenta el trabajo realizado relacionado en el ámbito de sistemas sensores dirigidos a la mejora del seguimiento de heridas crónicas, que de cara a facilitar la comprensión de este se ha dividido en los siguientes bloques:

- El diseño, la síntesis, y la evaluación de polímeros sensores para la detección colorimétrica y fluorimétrica de aminoácidos y Zn(II), respectivamente. El objetivo de estos polímeros sensores fue determinar de manera indirecta la actividad de las metaloproteasas, ya que:

  1. Los aminoácidos son una consecuencia directa de la actividad descontrolada de las metaloproteasas presentes en la herida. Es por esto que se puede relacionar la concentración de aminoácidos con la actividad protésica, y de esta forma poder diagnosticar el estado de la misma para establecer el mejor tratamiento médico.

  2. Las metaloproteasas son enzimas dependientes de Zn(II). Presentan dos átomos de Zn(II) en su estructura, uno estructural que le confiere la estructura necesaria para ser activa, y otro catalítico, ubicado en el centro activo, que le permite llevar acabo la función catalítica de hidrolizar proteínas como el colágeno y la elastina en aminoácidos.

- El estudio de muestras de heridas crónicas realizado a través de un proyecto de colaboración con el Hospital Universitario de Burgos (HUBU) (MAT2017-84501-R), que ha permitido relacionar la cantidad de aminoácidos presentes en las heridas con el estado de estas.

- El desarrollo de una aplicación para teléfonos inteligentes que complementa el dispositivo sensor, y que permite que cualquier ciudadano (incluso sin conocimientos previos en ciencia) pueda cuantificar de forma muy sencilla e intuitiva la concentración de una especie de interés a través de una simple fotografía digital.

1.5. Objetivos.

El objetivo principal de la Tesis consiste en desarrollar diferentes polímeros inteligentes para la detección y el seguimiento de las heridas crónicas. Estas son un problema de gran impacto social y poca visibilidad, para el que la comunidad médica no tiene herramientas de diagnóstico y/o seguimiento.

Los objetivos parciales que se plantean para conseguir el objetivo principal son:

- Diseño de sensores poliméricos para la detección y cuantificación de aminoácidos.
- Establecer una relación entre la concentración aminoácidos, la actividad proteásica y el estado de las heridas.
- Diseño de un sensor polimérico para la detección y cuantificación de Zn(II).
- Establecer una relación entre la concentración de Zn(II) y estado de las heridas crónicas.
- Combinación de los sensores poliméricos desarrollados con la aplicación para teléfonos inteligentes (*Colorimetric Titration*).

1.6. Estructura de la Memoria

El trabajo realizado para la consecución de los objetivos planteados se presenta en esta Memoria dividida en 5 capítulos, que incluye en primer lugar esta introducción, en la que se explica de manera general el contexto y objetivos del trabajo llevado a cabo.

Los capítulos siguientes son una descripción de la metodología y los trabajos realizados para la consecución de dichos objetivos. En el **Capítulo 2** se describe la síntesis y caracterización de polímeros sensores para la detección y cuantificación de aminoácidos basados en sistemas IDAs y en derivados de la ninhidrina. Además, se estudió el efecto de la matriz sobre el comportamiento de

los sistemas sensores y se evaluó su funcionamiento sobre muestras reales (heridas).

El **Capítulo 3** se centra en la síntesis y caracterización de un sensor polimérico fluorescente de Zn(II), basado en quinolinas derivadas del Zinquin (CAS: 151606-29-0)[41] y su aplicación sobre muestras biológicas.

Finalmente, el **Capítulo 4** describe el desarrollo de la aplicación para dispositivos móviles (Android y iOS) *Colorimetric Tiration*, que permite el empleo del móvil como una herramienta complementaria a los materiales sensores elaborados. Así, esta aplicación posibilita la valoración y cuantificación automática de las especies de interés a partir de las fotografías tomadas por el propio teléfono inteligente a los materiales sensores.

Por último, se recogen las conclusiones extraídas en el desarrollo del trabajo, se analiza el cumplimiento de los objetivos fijados y se plantean perspectivas de futuro.

---

[41] https://www.sigmaaldrich.com/catalog/product/sial/z2376?lang=es&region=ES (Accessed 4 May 2021)

CAPÍTULO 2

Polímeros sensores para la detección de aminoácidos como nuevos marcadores de la evolución de heridas crónicas humanas

Los aminoácidos son un marcador indirecto de la actividad de las metaloproteasas en las heridas crónicas. De ahí que el diseño y desarrollo de sensores poliméricos para estas especies sea uno de los primeros pasos hacia el desarrollo de sistemas capaces de evaluar el estado de dichas heridas. Aunque en la bibliografía existe un gran número de técnicas/métodos para la determinación y/o cuantificación de aminoácidos, describimos a continuación dos sensores poliméricos para su detección. Estos se basan en otros sensores en disolución descritos previamente, como los sistemas IDAs y la ninhidrina. Además, se estudió el efecto de la matriz polimérica sobre el rendimiento y características del sistema sensor.

2.1. Introducción

En primer lugar, será planteada la base del problema que se afronta en esta tesis, y alrededor del cual gira todo el trabajo experimental, es decir, las heridas

crónicas. Según la organización mundial de la salud (OMS) las enfermedades con mayor índice de mortalidad son las cardiopatías isquémicas y los accidentes cerebrovasculares, seguidas por las enfermedades obstructivas pulmonares crónicas y el cáncer de pulmón, tráquea y bronquios.[42] Sin embargo, existen otras muchas afecciones de baja visibilidad y gran repercusión económica y social que también preocupan a la comunidad médica. Un ejemplo son las heridas crónicas, un tipo de heridas caracterizadas porque su proceso de cicatrización es muy lento, o incluso no llega a completarse.

El proceso de cicatrización en heridas normales tiene 4 fases: coagulación o homeostasis, inflamación o fase defensiva, proliferación y maduración (**Figura 2.1)**. La fase de coagulación empieza inmediatamente después de producirse la lesión y dura unas 24 h. Su objetivo es recuperar el efecto barrera, frenar la pérdida de sangre. La fase inflamatoria se inicia unas pocas horas después de producirse la lesión y en condiciones normales dura unos 3 días. Su objetivo es limpiar la herida de bacterias y de estructuras celulares dañadas. En esta fase es donde entran en juego las metaloproteasas o MMPs (por sus siglas en inglés *matrix metalloproteases*), cuya función es la degradación de las proteínas de matriz dañadas. La fase de proliferación se inicia al tercer día después de producirse la lesión y se puede prolongar hasta la tercera semana. Su objetivo es el desarrollo del tejido granulado (precursor del tejido nuevo que remplazará a los tejidos dañados) y la revascularización. Finalmente, está la fase de maduración, que puede durar entre 21 días y 2 años. Su objetivo es la maduración de los nuevos tejidos y su cicatrización final.[43]

Las heridas crónicas se quedan estancadas en la fase inflamatoria, y no son capaces de continuar el proceso de cicatrización. El mayor problema de estas lesiones es su difícil diagnóstico temprano. A simple vista no se puede

---

[42] World Health Organitation:https://www.who.int/news-room/fact-sheets/detail/the-top-10-causes-of-death (Accesed 18 October 2020)

[43] K. Las Heras, M. Igartua, E. Santos-Vizcaino and R. M. Hernandez, *J. Control. Release*, **2020**, 328, 532–550

evaluar si el proceso de cicatrización está siendo el correcto o no, y generalmente los tratamientos están orientados a limpiar bien las heridas y esperar. Para cuando la herida muestras señales de no estar cicatrizando correctamente, ya se ha convertido en una herida crónica, complicando su tratamiento y/o recuperación y provocando el sufrimiento de los pacientes.
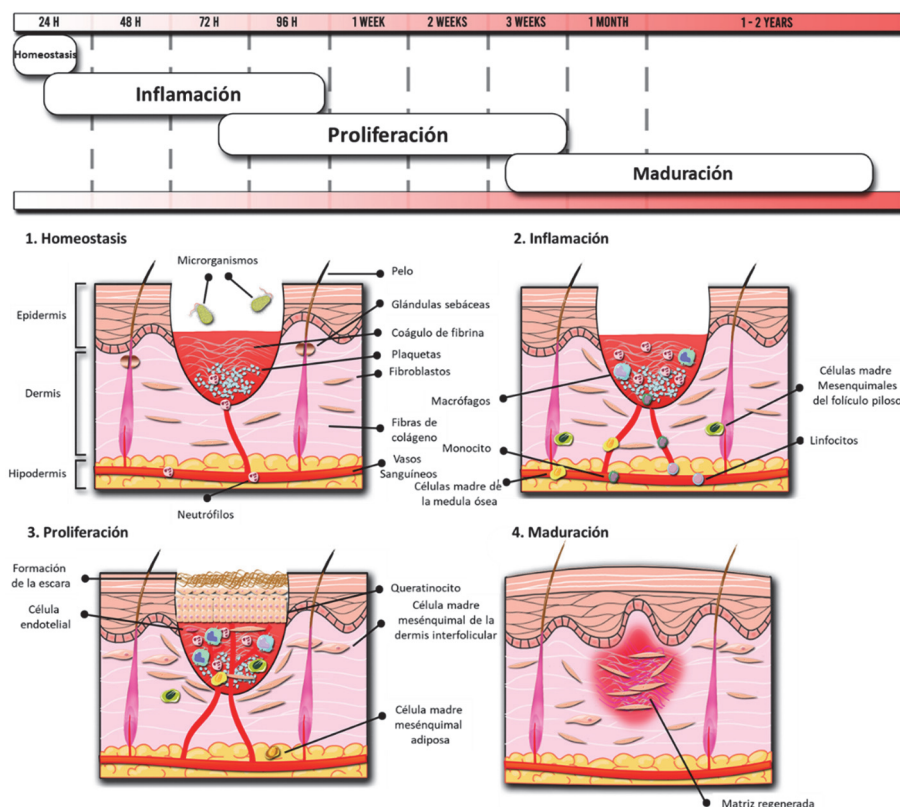

Figura 2.1. Fases del proceso de cicatrización (imagen tomado de la referencia 43).

A día de hoy no existe una solución clara para este problema ni para su diagnóstico, aunque sí existe un consenso médico acerca de ello. Según *the World Union of Wound Healing Societies* "el aumento de la actividad de las proteasas es actualmente el mejor marcador disponible para tratar estos trastornos cuando se han excluido otras causas, y el uso eficaz de un kit de

detección de proteasas tiene el potencial de cambiar el tratamiento de estas heridas".[44] El tipo de proteasas implicadas en los procesos de cicatrización se llaman metaloproteasas, y su papel es fundamental, ya que se encargan de la degradación de las proteínas dañadas de la matriz extracelular (fase inflamatoria). El problema está asociado a un desequilibrio en la formación/degradación de proteínas, generalmente alterado por una actividad descontrolada de las metaloproteasas, que destruyen dichas proteínas de forma muy rápida, y el proceso de cicatrización no avanza y empeora. Es por esto por lo que la determinación de la actividad de estas enzimas es fundamental para el diagnóstico temprano y tratamiento de las heridas crónicas.

Una vez contextualizado el problema de las heridas crónicas, se hablará brevemente de las diferentes formas de determinar la actividad enzimática. Las técnicas más utilizadas para la determinación de la actividad enzimática son la zymografia en gel y los ensayos ELISA (de las siglas en inglés *Enzyme-Linked Immunosorbent Assay*). Son técnicas en las que se emplean anticuerpos para la detección de las dianas (enzimas) y, en general, se basan en procedimientos tediosos y costosos. [45-47] Sin embargo, los aminoácidos y pequeños péptidos son producto directos de la actividad proteásica y, por tanto, los consideramos como marcadores en el diseño inicial del trabajo conducente a mi Tesis doctoral, de tal forma que se planteó la hipótesis de la determinación de forma indirecta de la actividad metaloproteásica a través de la cuantificación de aminoácidos.

---

[44] K. Becker, J. Boykin, M. Crossland, P. Davis, D. Doughty, V. Driver, C. von Eiff, K. Harding, C. Lindholm, M. Lubbers, M. Millar, Z. Moore, S. Morbach, D. Queen, M. Romanelli, N. Santamaria, G. Schultz, G. Sibbald, M. Stacey, P. Vowden and H. Wallace, *Diagnostics and wound. A consensus document. World Union of Wound Healing Societies (WUWHS). Principles of best practice: A World Union of Wound Healing Societies' Initiative.*, 2008.

[45] D. E. Kleiner and W. G. Stetlerstevenson, *Anal. Biochem.*, **1994**, 218, 325–329.

[46] Z. S. Calis, G. K. Sukhova and P. Libby, *FASEB J.*, **1995**, 9, 974–980.

[47] M. F. Clark and A. N. Adams, *J. Gen. Virol.*, **1977**, 34, 475–483.

En la bibliografía podemos encontrar muchas técnicas para la detección de aminoácidos, como la cromatografía de gases,[48-50] la resonancia magnética nuclear,[51] la espectroscopia de UV-Vis,[52,53] la electroforesis,[54,55] la espectroscopia de fluorescencia[54,55] o cromatografía líquida de alta eficacia (HPLC).[56,57] Sin embargo, y al igual que en el caso de la determinación de la actividad enzimática, todas ellas se tienen que llevar a cabo por personal cualificado y, en la mayoría de los casos, requieren del empleo de mucho tiempo y de equipamiento avanzado. Por eso, propusimos el diseño de un polímero sensor en forma de film para la detección y cuantificación de manera sencilla y directa de aminoácidos. Se escogió como punto de partida un sistema perteneciente a la familia de sensores colorimétricos por desplazamiento, sistema sencillo, intuitivo y fácil de adaptar para su uso por personal no especializado.

2.2. Preparación de los polímeros sensores

2.2.1. Estudio de la matriz inerte. Aproximación a un polímero sensor de aminoácidos.

Tal y como se ha descrito en el **Capítulo 1**, la matriz inerte es una parte clave del diseño de polímeros sensores, y de ella dependen propiedades tan importantes en ciencia de polímeros como el hinchamiento en agua del material en forma de film, o la manejabilidad del mismo, entre otras. Por ello, en esta etapa de mi tesis realicé un estudio profundo de esta matriz. El Grupo lleva trabajando una década con films que tienen comportamiento de gel (fase solida),

---

[48] A. Szeinberg, B. Szeinberg and B. E. Cohen, *Clin. Chim. Acta*, **1969**, 23, 93–95.

[49] A. Saifer, *Adv. Clin. Chem.*, **1971**, 14, 145–218.

[50] K. Adriaenssens, R. Vanheule and M. van Belle, *Clin. Chim. Acta*, **1967**, 15, 362–364.

[51] S. Katsikis, I. Marin-Montesinos, C. Ludwig and U. L. Günther, *J. Magn. Reson.*, **2019**, 305, 175–179.

[52] P. M. Nielsen, D. Petersen and C. Dambmann, *J. Food Sci.*, **2001**, 66, 642–646.

[53] A. H. Aubaid, A. Z. Risan and A. K. Naem, *Mycoses*, **1999**, 42, 249–253.

[54] M. T. Veledo, M. de Frutos and J. C. Diez-Masa, *Electrophoresis*, **2006**, 27, 3101–3107.

[55] A. E. Pasieka and M. E. Thomas, *Clin. Biochem.*, **1968**, 2, 423–429.

[56] P. Lindroth and K. Mopper, *Anal. Chem.*, **1979**, 51, 1667–1674.

[57] K. Petritis, C. Elfakir and M. Dreux, *LC GC Eur.*, **2001**, 14, 389–395.

y ya se había observado que esta matriz podía ejercer un entorno protector hacia los receptores,[29] generando un ambiente en el que la especie diana y el receptor podían interaccionar de forma más efectiva. De forma adicional, en la bibliografía también se pueden encontrar otros ejemplos de sistemas que se comportan de manera diferente en disolución que en fase sólida. Por ejemplo, la síntesis en fase sólida de Merrifield permite sintetizar péptidos de hasta 50 aminoácidos de forma muy efectiva y con altos rendimientos, mientras que la síntesis en disolución solo permite obtener pequeños péptidos (8 aminoácidos), con rendimientos muy bajos, y procesos de purificación tediosos.[58]

Por lo tanto, estudiamos a fondo el efecto de la matriz inerte en el reconocimiento molecular entre especie diana y receptor, a través de un estudio solvatocrómico. Para llevar a cabo este tipo de estudio fue necesaria la elección de un sistema sensor con el que poder estudiar la matriz, para lo que escogimos como modelo un receptor previamente estudiado en la bibliografía para la detección de aminoácidos.[52] El receptor está basado en un compuesto de coordinación cobre (II), y un derivado de etilendiamina.[59] Así que, se diseñó una ruta sintética para introducir un grupo polimerizable en el mismo. En la **Figura 2.2.** se muestra la estructura química del receptor descrito en la bibliografía, la estructura química del receptor modificado con grupos polimerizables, y la ruta sintética llevada a cabo para su obtención.

Al abordar el reto principal de esta línea de trabajo, es decir, el estudio de la matriz inerte, el sistema sensor se analizó en varios disolventes y de tres formas diferentes:

❖ Estudiando la absorbancia del receptor en disolución.

❖ Estudiando la absorbancia del receptor disperso en la matriz inerte.

❖ Estudiando la absorbancia del receptor (anclado covalentemente) como uno de los comonómeros que conforman la matriz inerte.

---

[58] R. B. Merrifield, *J. Am. Chem. Soc.*, **1963**, 85, 2149–2154.

[59] J. Frantz Folmer-Andersen, M. Kitamura and E. V. Anslyn, *J. Am. Chem. Soc.*, **2006**, 128, 5652–5653
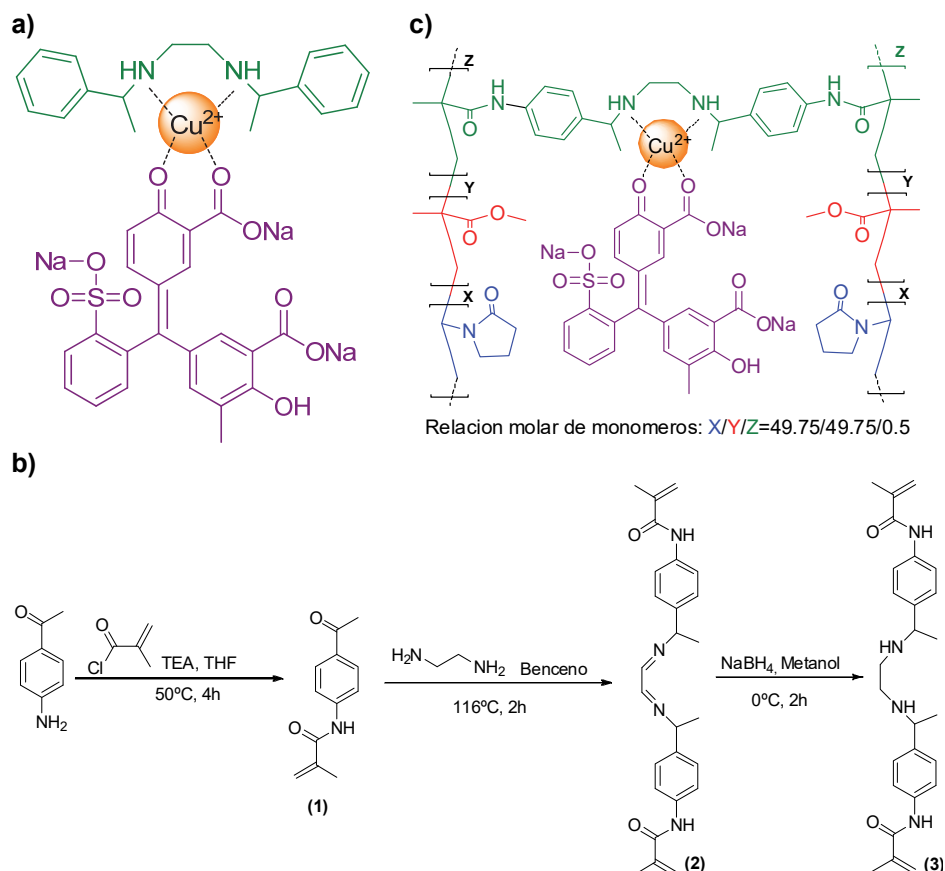
Figura 2.2. Sistema sensor basado en IDAs: a) sistema sensor descrito en la bibliografía[59]; b) ruta sintética llevada a cabo para la obtención del derivado polimerizable de etilendiamina y c) sistema sensor polimérico modificado.

Los resultados se interpretaron con el modelo de Taft-Kamlet,[60-63] y se observó que las interacciones dipolo-dipolo entre el receptor y el disolvente son mucho mayores en disolución que dentro de la matriz inerte. Dicho de otra forma, se demostró que la matriz polimérica proporciona un entorno protector que disminuye la interacciones receptor-disolvente, y por lo tanto, haciendo que las

[60] M. J. Kamlet and R. W. Taft, *J. Am. Chem. Soc.*, **1976**, 98, 377–383.
[61] R. W. Taft and M. J. Kamlet, *J. Am. Chem. Soc.*, **1976**, 98, 2886–2894.
[62] M. J. Kamlet, J. L. Abboud and R. W. Taft, *J. Am. Chem. Soc.*, **1977**, 99, 6027–6038.
[63] M. J. Kamlet, J. L. M. Abboud, M. H. Abraham and R. W. Taft, *J. Org. Chem.*, **1983**, 48, 2877–2887.

interacciones entre diana y receptor estén más favorecidas. De esta manera, el reconocimiento molecular es mucho más eficiente.

El estudio completo de nuestro trabajo se publicó en la revista *Polymers*,[64] trabajo que incluyó una prueba de concepto utilizando el polímero sensor desarrollado. Para esta prueba, se hidrolizó una muestra de carne simulando una acción desmedida de metaloproteasas en heridas crónicas. Los aminoácidos generados durante el proceso se cuantificaron tanto con el polímero sensor como con un método de referencia para la determinación de estas especies, y se obtuvieron resultados prometedores.

Esta primera aproximación con un polímero sensor está basada en un sensor por desplazamiento, y teniendo en cuenta la futura aplicación del material en herida, el siguiente paso fue el diseñó de un nuevo polímero cuyo mecanismo sensor se debe a una reacción química irreversible entre el receptor y la especie diana y cuyo desarrollo se describe a continuación.

2.2.2. Optimización del receptor. Estudio con muestras reales de heridas crónicas.

En la siguiente etapa de mi tesis doctoral propusimos la optimización del receptor para la detección y cuantificación de aminoácidos presentes en heridas. Todo el planteamiento de la investigación se basaba en la hipótesis de que los aminoácidos eran un marcador del estado de las heridas. Así que en esta etapa también se estudió la relación entre el estado de las heridas, y la concentración de aminoácidos en las mismas.

Los pacientes de heridas crónicas fueron examinados por el personal médico del hospital que colaboró con el Grupo de Polímeros en este proyecto. En este diagnóstico de las heridas, se evaluaron de forma subjetiva (a través del personal sanitario profesional) diferentes variables, como el aspecto visual de la

---

[64] M. Guembe-García, P. D. Peredo-Guzmán, V. Santaolalla-García, N. Moradillo-Renuncio, S. Ibeas, A. Mendía, F. C. García, J. M. García and S. Vallejos, *Polymers (Basel)*., 2020, **12**, 1249.

herida o la presencia de necrosis, entre otros. Después, las muestras provenientes de esas heridas se analizaron, y se determinó la concentración de aminoácidos utilizando un método validado de referencia.[52] Gracias a este estudio demostramos que, efectivamente, la concentración de aminoácidos está directamente relacionada con el estado y evolución de las heridas crónicas, lo que nos dio pie a optimizar nuestro polímero sensor con un nuevo receptor mucho más orientado a la futura aplicación de estos materiales.

Uno de los métodos colorimétricos primigenios para detectar aminoácidos fue el método de la ninhidrina.[65-68] Este compuesto orgánico reacciona con los grupos amino primarios de los aminoácidos, y forma un producto de color morado (morado de Ruhemann) (**Figura 2.3.**). Durante años fue muy utilizado en ciencia forense,[69-71] ya que es un método muy fácil de utilizar. Sin embargo, cuando es necesario no solo detectar, sino cuantificar, las técnicas más utilizadas son la electroforesis,[55,72] la cromatografía líquida de alta eficacia o HPLC (de sus siglas en inglés: *high performance liquid chromatography*),[57,73] RMN (resonancia magnética nuclear)[51] o la cromatografía de gases.[48,49,74] Por otro lado, aunque son técnicas muy potentes y muy precisas, requieren de personal cualificado y equipos de medida avanzados.
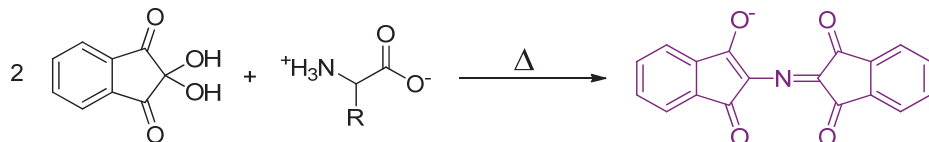
Figura 2.3. Reacción de la ninhidrina con aminoácidos para formar el morado de Ruhemann.[65-68,75]

[65] S. Ruhemann, *J. Chem. Soc. Trans.*, **1910**, 97, 1438–1449.
[66] S. Ruhemann, *J. Chem. Soc. Trans.*, **1911**, 99, 792–800.
[67] S. Ruhemann, *J. Chem. Soc. Trans.*, **1911**, 99, 1306–1310.
[68] S. Ruhemann, *J. Chem. Soc. Trans.*, **1911**, 99, 1486–1492.
[69] D. Kumar, M. Abdul Rub, M. Akram and Kabir-Ud-Din, *Tenside, Surfactants, Deterg.*, **2014**, 51, 157–163.
[70] M. Friedman, *J. Agric. Food Chem.*, **2004**, 52, 385–406.
[71] D. J. McCaldin, *Chem. Rev.*, **1960**, 60, 39–51.
[72] M. T. Veledo, M. De Frutos and J. C. Diez-Masa, *J. Chromatogr. A*, **2005**, 1079, 335–343.
[73] K. Mopper and P. Lindroth, *Limnol. Oceanogr.*, **1982**, 27, 336–347.
[74] K. Adriaenssens, R. Vanheule, D. Karcher and Y. Hardens, *Clin. Chim. Acta*, **1967**, 18, 351–354.
[75] C. B. Bottom, S. S. Hanna and D. J. Siehr, *Biochimie*, **1973**, 55, XIV.

En este trabajo se diseñó un polímero sensor que reuniera las ventajas del método de la ninhidrina, y que tuviera la precisión de los equipos más avanzados sin necesidad de utilizarlos. De esta forma se consiguió preparar un polímero sensor **(Figura 2.4.)** para la detección y cuantificación de aminoácidos mediante una técnica colorimétrica fácil de seguir a través del análisis de los parámetros de color digital RBG (*Red, Blue, Green*) de una fotografía digital tomada con un smartphone. El estudio completo se publicó en la revista *Sensors*
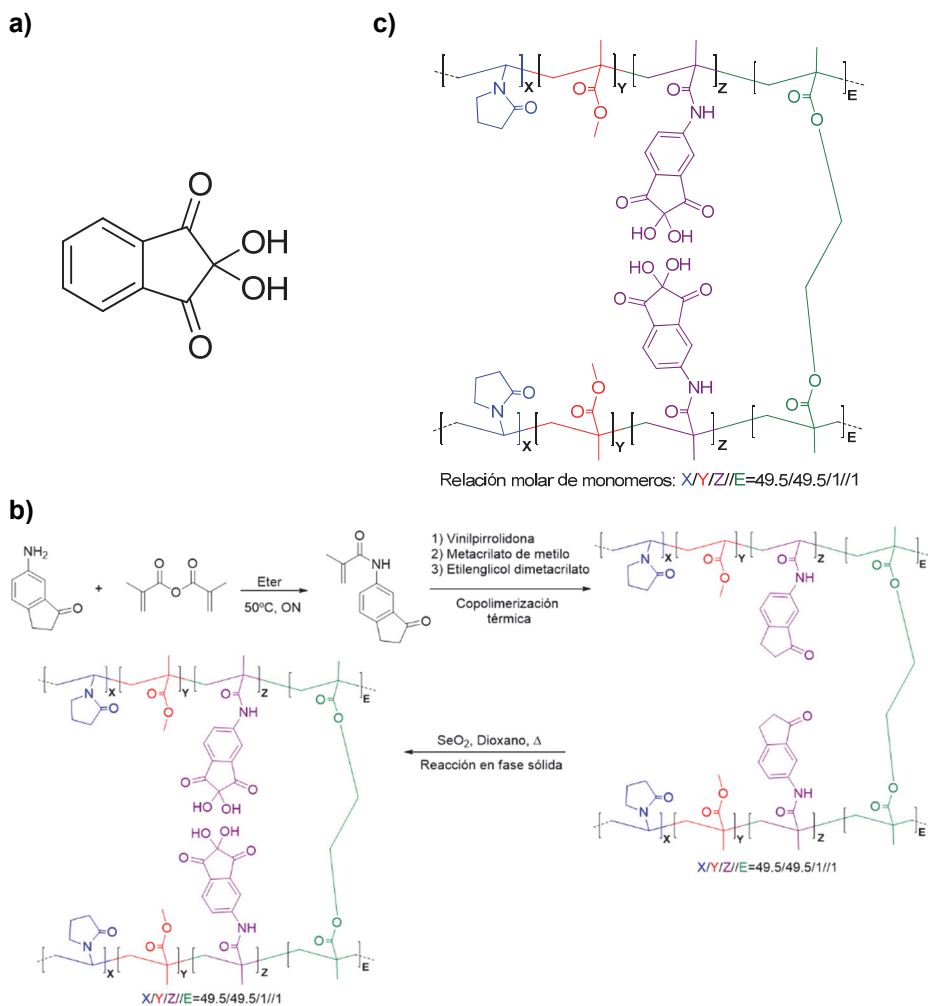
Figura 2.4. Sistema sensor basado en ninhidrina: a) Estructura ninhidrina; b) Ruta sintética llevada a cabo para la obtención del polímero sensor y c) Sistema sensor polimérico con ninhidrina modificada.

and Actuators B: Chemical,[76] y el material se encuentra patentado (**Figura 2.5.**, Número de solicitud: P202030077).[77]

Figura 2.5. Justificante de presentación electrónica de solicitud de patente. Número de solicitud: P202030077.

[76] M. Guembe-García, V. Santaolalla-García, N. Moradillo-Renuncio, S. Ibeas, J. A. Reglero, F. C. García, J. Pacheco, S. Casado, J. M. García and S. Vallejos, *Sensors Actuators, B Chem.*, **2021**, 335, 129688.
[77] Guembe García, M., Vallejos Calzada, S., García Pérez, J. M., García García, F., Ibeas Cortés, S., & Yagüe Fernández, P. (2020). Copolímeros de estructura derivada de la ninhidrina, películas o membranas obtenidas a partir de los mismos y su utilización. No P202030077. Priority country: Spain. Ownership: University of Burgos

2.3. Resultados

A continuación, se describen los resultados obtenidos a través de la transcripción íntegra de los dos trabajos publicados:

- *Why the sensory response of organic probes is different in solution and in the solid-state within a polymer film? Evidence and application to the detection of amino acids in human chronic wounds.*

- *Monitoring of the evolution of human chronic wounds the easy way. Analyses using a ninhydrin based sensory polymer and a smartphone.*

Why the sensory response of organic probes is different in solution and in the solid-state within a polymer film? Evidence and application to the detection of amino acids in human chronic wounds

Why the sensory response of organic probes is different in solution and in the solid-state within a polymer film? Evidence and application to the detection of amino acids in human chronic wounds

Marta Guembe-García,[1] Patricia D. Peredo-Guzmán,[1] Victoria Santaolalla-García,[2] Natalia Moradillo-Renuncio,[2] Saturnino Ibeas,[1] Aranzazu Mendía,[1] Félix C. García,[1] José Miguel García,[1,*] Saúl Vallejos[1,*]

[1]Departamento de Química, Facultad de Ciencias, Universidad de Burgos, Plaza de Misael Bañuelos s/n, 09001 Burgos, Spain. Email: svallejos@ubu.es (SV); jmiguel@ubu.es (JMG)

[2]Complejo Asistencial Universitario de Burgos, Burgos, Spain

* Correspondence: svallejos@ubu.es, jmiguel@ubu.es; Tel.: (+34 947258085)

Abstract

We anchored a colourimetric probe, comprising a complex containing copper (Cu(II)) and a dye, to a polymer matrix obtaining film-shaped chemosensors with *induced* selectivity toward glycine. This sensory material is exploited in the selectivity detection of glycine in complex mixtures of amino acids mimicking elastin, collagen and epidermis, and also in following the protease activity in a beefsteak and chronic human wounds. We use the term *inducing* because the probe in solution is not selective toward any amino acid and we get selectivity toward glycine using the solid-state. Overall, we found that the chemical behaviour of a chemical probe can be entirely changed by changing its chemical environment. Regarding its behaviour in solution, this change has been achieved by isolating the probe by anchoring the motifs in a polymer matrix, in an amorphous state, avoiding the interaction of one sensory motif with another. Moreover, this selectivity change can be further tuned because of the effectiveness of the transport of targets both by the physical nature of the interface of the polymer matrix/solution, where the target chemicals are dissolved, for instance, and inside the matrix where the recognition takes place. The interest

in chronic human wounds is related to the fact that our methods are rapid and inexpensive, and also considering that the protease activity can correlate with the evolution of chronic wounds.

Keywords: Solid-state chemosensors; sensory polymers; amino acids; chronic wounds.

1. Introduction

From a chemical viewpoint, it is well known that chemicals in the solid-state exhibit completely different properties than in solution. This is because of the usual dense packaging and inter-molecule interactions in the former and the solvated state in the later, where the interaction of solvent molecules-chemical play a crucial role. This fact is well known and has been intensely exploited for different purposes, e.g., luminescence, for the preparation of cleaners, liquid crystals, catalysts, plasticisers, coatings, buffers, etc [1]. More recently, the properties of chemicals dispersed in a polymer matrix, or chemically anchored to a polymer backbone, in the solid-state, have been exploited [2–6].The substances, isolated one from another by the polymer chains or sections in the solid-sate, in an amorphous-state and interacting with the macromolecules, within as highly-motion-restricted environment, behave completely different than in solution or in conventional crystalline solid-state [2].

In this paper, we analyse the behaviour within a solid polymer matrix of a well know dye that has been previously exploited as a probe for detection of amino acids, Chromoxame Cyanine R (D), and take advantage of its different behaviour in this state than in solution to explore the ability of the new solid sensory materials, or polymer chemosensors, to detect and recognise amino acids in complex environments, such as chronic human wounds. The advantage of the solid polymer chemosensors in the tuning of the properties of the chemical probes but also in the manageability of the polymer chemosensors prepared as

films, that can be safely managed and stored at ambient conditions even by untrained personnel [7–9].

Human chronic wounds constitute a significant health societal problem. Approximately 1-2% of people worldwide suffer from a health problem that hampers the regular activity of the cutaneous wound healing process, which ultimately results in chronic wounds. Compared with cancer or with HIV, chronic wounds may not be as well known, but this condition is no less common a problem. In Spain alone, €350 million per year is devoted to the care of this health problem. In Europe, the total cost of chronic wounds (including nursing, medical and surgical time, hospital bed days and cost of materials) amounts to €144.000 per 100 patients. This constitutes 2–3% of the total health care budget in Europe. The USA has also performed an economic evaluation of the impact, cost, and Medicare policy implications of chronic non-healing wounds, and has concluded that the cost is nearly 32.000 million dollars [10–13]. Currently, there is no solution to this problem, although there is a medical consensus (WUWHS) [14] "that the increased activity of proteases is currently the best available marker for healing disorders when other causes have been excluded, and that the effective use of a protease analysis kit has the potential to change the treatment of wounds Worldwide" [15,16]. The major players in the healing process are the proteases, these enzymes are responsible for degrading damaged proteins of the extracellular matrices (EM) in peptides and amino acids, leading to the formation of new tissues, that is, to orderly healing. The problem lies in the degradation/protein formation equilibrium, which is delicate and when it is altered by high activity of the proteases, it can lead to destroying the EM that has just been formed and other proteins such as the growth factor and its receptors giving rise to difficulties in healing. Then, knowing the level of activity of the proteases in a wound allows for the evaluation of the risk of (ulceration and the) bad prognosis and the probability of healing, and with this to establish palliative measures to reduce the activity of the proteases. Currently, it is complicated to evaluate the level of proteases in wounds. Regarding the analytical tests, some research studies have assessed the activity levels of the proteases in exudates

used several different techniques at the laboratory level, p. ex. Zymography in gelatine and ELISA that uses antibodies to measure protease levels. In practice, the analytical evaluation of protease activity is not feasible for most health professionals. Concerning clinical evaluation, excessive activity of proteases may be suspected in wounds that do not heal, although clinical signs of inflammation are difficult to differentiate from those of infection.

The use of sensory materials in physiological media with medical applications has been a topical issue during last years [17–26]. Thus, we propose herein an indirect quantification of protease activity from the quantitative detection of amino acids using sensory films. These sensory films are acrylic polymers with bidentate *N*-donor motifs (based on ethylenediamine) in the short-chain that crosslink the polymer structure, whose colourimetric sensory behaviour is based on the indicator-displacement assay (IDA) [27,28]. The ethylenediamine motifs form a complex with copper (Cu(II)) and a dye (D) giving rise to the solid sensory film. Upon immersion of the film in a water solution containing amino acids, the dye is displaced by the amino acid giving rise to a dual colourimetric signal, i.e., the colour change of the film and the colour development of the initially colourless water solution. This process is easily followed by ultraviolet/visible spectroscopy (UV/Vis) and, importantly, visually and by analysing pictures taken with conventional smartphones.

2. Materials and Methods

All materials and solvents were commercially available and used as received unless otherwise indicated. They included 4'-aminoacetophenone (99%, Alfa Aesar), triethylamine (99%, VWR-Prolabo), methacryloyl chloride (97%, Alfa Aesar), tetrahydrofuran (THF, 100%, VWR-Prolabo), diethyl ether (99.7%, VWR-Prolabo), deuterated dimethyl sulfoxide (DMSO-d_6, 99.8%D, VWR-Prolabo), ethane-1,2-diamine (99%, Alfa Aesar), benzene (99%, Fluka), methanol (MeOH, 100%, VWR-Prolabo), $NaBH_4$ (98%, Alfa Aesar), ethyl acetate (99.9%, VWR-Prolabo), 2,2′-azobis(2-methylpropionitrile) (AIBN) (Aldrich, 98%), 1-vinyl-2-pyrrolidone (VP) (99%, Acros Organics), methylmethacrylate (MMA) (Merck, 99%),

phenolphthalein (98%, Alfa Aesar), thymol blue (98%, Alfa Aesar), bromophenol blue (100%, Alfa Aesar), Eosin Y (99%, Sigma-Aldrich), fluorescein (100%, Fluka), chromoxame cyanine R (100%, Acros Organics), catechol violet (100%, Acros Organics), chorophenol red (100%, Alfa Aesar), chrome Azurol S (100%, MP), trans-4-hydroxi-L-proline (≥99%, Sigma-Aldrich), L-aspartic acid (98%, Alfa Aesar), L-threonine (98%, Alfa Aesar), serine (≥99%, Fluka), L-arginine (98%, Alfa Aesar), L-glutamic acid (+99%, Alfa Aesar), L-lysine (97%, Sigma-Aldrich), L-proline (99%, Alfa Aesar), L-histidine (+98%, Alfa Aesar), Glycine (99%, Alfa Aesar), L-alanine (99%, Alfa Aesar), L-cysteine (+98%, Alfa Aesar), L-valine (≥98%, Sigma-Aldrich), L-methionine (+98%, Alfa Aesar), L-isoleucine (98%, Sigma-Aldrich), L-tyrosine (+99%, Acros Organic), L-phenylalanine (98%, Alfa Aesar), N,N-dimethylacetamide (DMA, ≥ 99%, Sigma-Aldrich), 1-butanol (99,8%, Sigma-Aldrich), ethanol absolute (EtOH, 100%, VWR-Prolabo), 1,4-dioxane (100%, VWR-Prolabo), chloroform (99.2%, VWR-Prolabo), acetone (99%, VWR-Prolabo), acetonitrile (99.95%, VWR-Prolabo), nitromethane (95%, Sigma-Aldrich), ethylene glycol (99.9%, VWR-Prolabo), $NaNO_3$ (≥ 99%, LabKem), NaH_2PO_4 ≥ 98%, Sigma-Aldrich), NaOH (99%, VWR-Prolabo), HCl(37%, VWR-Prolabo), sodium dodecyl sulfate (≥97%, Fluka), di-sodium tetraborate (99%, Sigma-Aldrich), phthaldialdehyde (97%, Merk), 2-mercaptoethanol (98+%, Alfa Aesar), $CsNO_3$ (≥99%, Fluka), $Mn(NO_3)_2$ (98+%, Alfa Aesar), $HAuCl_4$ $3H_2O$ (99.9+%, Sigma-Aldrich), $K_2Cr_2O_7$ (≥99.5%, Sigma-Aldrich), $BaCl_2$ (pure, Labkem), $Zn(NO_3)_2 \cdot 6H_2O$ (98%, Aldrich), $Co(NO_3)_2 \cdot 6H_2O$ (≥99%, Labkem), NH_4NO_3 (≥98%, Sigma-Aldrich), $Ca(NO_3)_2 \cdot 4H_2O$ (≥99%, Sigma-Aldrich), $Cr(NO_3)_3 \cdot 9H_2O$ (98.5%, Alfa Aesar), $Hg(NO_3)_2$ (98%, Alfa Aesar), $RbNO_3$ (99.95%, Sigma-Aldrich), $Dy(NO_3)_3$ (99.9%, Alfa Aesar), LiCl (≥ 99%, Sigma-Aldrich), $Cd(NO_3)_2$ (98.5%, Alfa Aesar), $Fe(NO_3)_3 \cdot 9H_2O$ (VWR-Prolabo), $CeCl_3 \cdot 4H_2O$ (≥99.99%, Sigma-Aldrich), $ZrCl_4$ (98%, Alfa Aesar), $La(NO_3)_3 \cdot 6H_2O$ (99.9%, Alfa Aesar), KNO_3 (99+%, Sigma-Aldrich), $Sm(NO_3)_3$ (99.9%, Alfa Aesar), $Mg(NO_3)_2 \cdot 6H_2O$ (≥ 99%, Labkem), $Al(NO_3)_2 \cdot 9H_2O$ (≥ 98.9%, Sigma-Aldrich), $AgNO_3$ (≥99.9, Sigma-Aldrich), $Nd(NO_3)_3$ (99.9%, Alfa Aesar), $Pb(NO_3)_2$ (≥ 99%, Fluka), $Sr(NO_3)_2$ (99+%, Sigma-Aldrich), $Cu(NO_3)_2 \cdot 3H_2O$ (98%, Sigma-Aldrich), $Ni(NO_3)_2 \cdot 6H_2O$ (98.5%, Sigma-Aldrich),

sodium cyanide (>97%, Sigma-Aldrich), sodium acetate (>99%, Aldrich), lithium hydroxide (>98%, Sigma-Aldrich), sodium fluoride (≥99.9%, Sigma-Aldrich), potassium perchlorate (>99%, Sigma-Aldrich), sodium dodecyl sulphate (≥98.5%, Sigma-Aldrich), sodium nitrite (>97%, Aldrich), sodium ethoxide (95%, Sigma-Aldrich), potassium hydrogen phthalate (99.95%, Sigma-Aldrich), sodium pyrophosphate tetrabasic (>95%, Sigma-Aldrich), potassium persulfate (>99%, Sigma-Aldrich), sodium methanesulfonate (98%, Sigma-Aldrich), sodium pyrophosphate dibasic (>99%, Sigma-Aldrich), lithium trifluoromethanesulfonate (96%, Sigma-Aldrich), sodium p-toluenesulfonate (95%, Sigma-Aldrich), potassium bromide (>99%, Sigma-Aldrich,), potassium thiocyanate (>99%, Sigma-Aldrich), potassium oxalate monohydrate (>98.5%, Sigma-Aldrich), sodium carbonate (>99%, Sigma-Aldrich), sodium benzoate (>99.5%, Sigma-Aldrich), lithium phosphate monobasic (99%, Sigma-Aldrich,), sodium sulfate (99%, Sigma-Aldrich), sodium chloroacetate (98%, Sigma-Aldrich), sodium trifluoroacetate (>99%, Sigma-Aldrich), sodium periodate (99.78%, Sigma-Aldrich, 99.8%).

3. Experimental

3.1. Measurement techniques

^{1}H and ^{13}C{^{1}H} NMR spectra were recorded with a Varian Inova 400 spectrometer operating at 399.94 MHz for ^{1}H, and 100.6 MHz for ^{13}C, using deuterated dimethyl sulfoxide (DMSO-d_6) or deuterated chloroform (CDCl$_3$) as solvents at 25°C. Infrared spectra (FTIR) were recorded with an FT/IR-4200 FT-IR Jasco Spectrometer with an ATR-PRO410-S single reflection accessory.

The material was thermally and mechanically characterised using thermogravimetric analysis (TGA, 10–15 mg of the sample under synthetic air and nitrogen atmosphere with a TA Instruments Q50 TGA analyser at 10°C·min^{-1}), differential scanning calorimetry (DSC, 10–15 mg of the sample under a nitrogen atmosphere with a TA Instruments Q200 DSC analyser at 20°C·min^{-1}), and tensile properties analysis (5 × 9.44 × 0.122mm samples using a Shimadzu EZ Test Compact Table-Top Universal Tester at 1mm·min^{-1}).

High-resolution electron-impact mass spectrometry (EI-HRMS) was carried out on a Micromass AutoSpect Waters mass spectrometer (ionisation energy: 70 eV; mass resolving power: >10,000). Inductively coupled plasma mass spectrometry (ICP-MS) measurements were recorded on an Agilent 7500 ICP-MS spectrometer.

UV/Vis spectra were recorded using a Hitachi U-3900 UV/Vis spectrophotometer. The standard experimental procedure for all measurements consisted of placing the sensory material in the bottom of a standard cuvette (1 cm side), in MeOH: pH=7 Buffer. Next, a certain amount of amino acids is added, and the diffusion process of the dye from the sensory material to the solution was observed. The solution was always homogenised before each measurement, using a pasteur pipette.

RGB method was carried out by taking digital pictures of the sensory discs (8 mm diameter) with an iPhone 6S smartphone after immersion in aqueous media with different concentrations of amino acid. To obtain a good reproducibility of the results, as well as to avoid possible external influences in the photographs, these were taken in a dark room. The digital pictures were analysed with a generic image software to obtain the RGB parameters of the entire surface of the sensory disc. Photographs were taken three-fold for the error's calculations, and the average of each RGB parameter was calculated. This easy and cheap method allows the quantification of amino acid in aqueous media, by only taking a photo, and we have widely used it in previous works [3,7].

Principal component analysis (PCA) was carried out using the Statgraphics Centurion XVI software installed on a personal computer in a Windows 7 environment. The variable (principal component) values were standardised and accounted for >99% of the variance in all experiments

Biological samples were weighed, and for each 1g of samples, 20 mL of pH = 7 buffer was added. Then the samples were boiled at 100° C for 10 min to stop the hydrolysis. Finally, they were filtered hot.

3.2. Preparation of the sensory monomer

Synthesis of N-(4-acetylphenyl)methacrylamide (1). A mixture of 4'-aminoacetophenone (10g, 74mmol), triethylamine (1.6 equiv., 96.18mmol, 9.73g, 13.41mL), methacryloyl chloride (1.2 equiv., 88.78mmol, 9.28g, 8.68mL) and 100 mL of THF was stirred in a pressure flask at 50°C. After four hours, the reaction mixture was filtered and the solvent was removed under reduced pressure. The solid was washed with water and then with diethyl ether. ^{1}H NMR (300 MHz, CDCl$_3$) δ =7.93 (d, J = 8.7Hz, 2H), 7.87 (s, 1H), 7.68 (d, J = 8.7Hz, 2H), 5.82 (s, 1H), 5.51 (s, 1H), 2.57 (s, 1H), 2.06(s, 1H).^{13}C NMR (75 MHz, CDCl$_3$) δ =196.97 (C), 166.72 (C), 142.23 (C), 140.63 (C), 132.92 (CH), 129,68 (CH), 120.49 (CH), 119.16 (CH$_2$), 26.41 (CH$_3$), 18.67 (CH$_3$). HRMS (EI) m/z [M+H]$^+$ calc for [C$_{12}$H$_{13}$NO$_2$] 204.1019; found: 204.1022 and HRMS (EI) m/z [M+Na]$^+$ calc for [C$_{12}$H$_{13}$NO$_2$] 226.0838; found: 226.0840. FT-IR (Wavenumbers, cm^{-1}): ν$_{>N-H+}$, 3350.

Synthesis of N,N'-(((ethane-1,2-diylidenebis(azanylylidene))bis(ethane-1,1-diyl))bis(4,1-phenylene))bis(2-methacrylamide) (2). A mixture of ethane-1,2-diamine (0.6g, 9.9mmol, 0.667mL), **(1)** (1.04 equiv., 20.6mmol, 4.2g) and 50mL of benzene was stirred in a round bottom flask with Dean-Stark at 116°C. After two hours, the reaction mixture was filtered. The filtered solid was washed with diethyl ether. ^{1}H NMR (300 MHz, DMSO) δ =9.89 (s, 2H), 7.89-7.65 (m, 8H), 5.83 (s, 2H), 5.54 (s, 1H), 5.51 (s, 2H), 3.79 (s, 4H), 3.34 (s, 2H), 2.23 (s, 6H) 1.96(s, 6H).^{13}C NMR (75 MHz, DMSO) δ =167.26 (C), 164.39 (CH), 140.75 (CH), 135.97 (Ch), 127.28 (CH), 120,56 (CH), 120.49 (CH), 119.77 (CH$_2$), 53.25 (CH), 19.16 (CH$_3$), 15.43 (CH$_3$). HRMS (EI) m/z [M+H]$^+$ calc for [C$_{26}$H$_{30}$N$_4$O$_2$] 431.2442; found: 431.2445 and HRMS (EI) m/z [M+Na]$^+$ calc for [C$_{26}$H$_{30}$N$_4$O$_2$] 453.2261; found: 453.2261.. FT-IR (Wavenumbers, cm^{-1}): ν$_{>N-H+}$, 3300, ν$_{C-N=+}$, 1660.

Synthesis of N,N'-(((ethane-1,2-diylbis(azanediyl))bis(ethane-1,1-diyl))bis(4,1-phenylene))bis(2-methacrylamide) (3). **(2)** was dissolved in 25mL of MeOH at 0°C. Next NaBH$_4$ (6 equiv., 30mmol, 1.14g) was added little by little.

After half an hour, the reaction mixture was stirred during 2 hours at room temperature. Then the reaction mixture was filtered, and the organic solvent was evaporated under vacuum yielding the impure solid. Finally, the impure solid was washed with ethyl acetate. ^{1}H NMR (300 MHz, DMSO) δ = 9.71 (s, 2H), 7.59 (d, J = 8.5 Hz, 4H), 7.22 (dd, J = 8.5, 1.7 Hz, 4H), 5.79 (s, 2H), 5.50 (s, 2H), 3.58 (dd, j= 8.5, 6.6 Hz, 2H), 3.33 (s, 2H), 2.35 (d, J =2, 4H), 1.95 (s, 6H), 1.20 (d, J =6.5Hz, 6H). ^{13}C NMR (75 MHz, DMSO) δ =167.04 (C), 141.99 (C), 140.91 (C), 137.77 (C),126.91 (CH),120.56 (CH), 120.12 (CH_2), 57.57 (CH), 47.57 (CH_2), 24.94 (CH_3), 19.21 (CH_3). HRMS (EI) m/z $[M+H]^+$ calc for $[C_{26}H_{30}N_4O_2]$ 435.2755; found: 435.2756 and HRMS (EI) m/z $[M+Na]^+$ calc for $[C_{26}H_{30}N_4O_2]$ 457.2574; found: 457.2575. FT-IR (Wavenumbers, cm^{-1}): $\nu_{>N-H+}$, 3336.

Scheme 1 summarised the synthetic steps followed to prepare the sensory monomer (3). The NMR and FTIR spectra of intermediates ((1) and (2)) and monomer (3) are depicted in **SI**, section **S1**, **Figures S1- S3**.
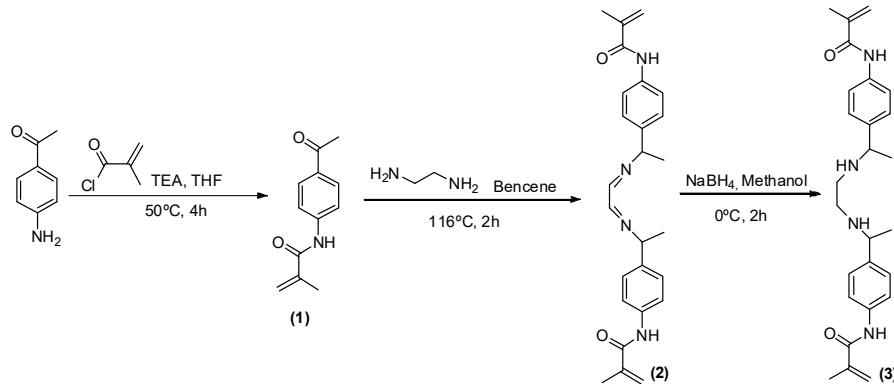
Scheme 1. Synthetic route of sensory monomer (3).

3.3. Preparation of the sensory film

The starting material **F(3)** was obtained by radical copolymerization of the different monomers: vinylpyrrolidone (VP) as the hydrophilic monomer, methylmethacrylate (MMA) as the hydrophobic monomer, and (3) (*N,N'*-(((ethane-1,2-diylbis(azanediyl))bis(ethane-1,1-diyl))bis(4,1-phenylene))bis(2-methacrylamide)) as the anchorage monomer. The bulk radical polymerisation

was carried out in a silanised glass mould (100 μm thick) in an oxygen-free atmosphere at 60°C overnight. Regarding the molar ratio of the monomers, this can be adjusted for different purposes. In our case, the colorimetric response of the material toward amino acid was modulated by adjusting this molar ratio, i.e., 49.75/49.75/0.5 (VP/MMA/(3)). After the bulk radical polymerisation, the material was immersed in an aqueous solution of CuSO$_4$ 0.1 M overnight. Next, the material was washed with water 5 times and the membrane **F$_{(3)-Cu}$** was obtained. Then, the material was immersed in 100mL of water with 1 mL of Chromoxame Cyanine R at 5x10^{-3} M in MeOH. Finally, the material was washed with water (3 times), acetone (twice), water:acetone (80:20) (once) and water (once) for obtaining the final sensory material **F$_{(3)-Cu-D}$**. The chemical structure of the films used to prepare the sensory materials is depicted in Scheme 1.

X/Y/Z=49.75/49.75/0.5
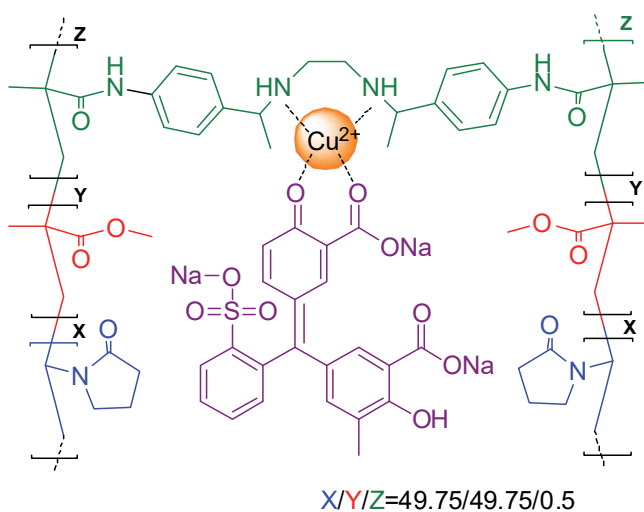
Scheme 2. Chemical structure of sensory material F$_{(3)-Cu-D}$.

3.4. Ethical statement

We have performed all experiments with human subjects based on the use and ethics of the *Hospital Universitario de Burgos* policy for trials with humans. The ethics committee of clinical experimentation of the region of Burgos, Spain, approved this study (minute 13/2017, internal code: 2017.200) on November 16, 2017. Informed consent was obtained from all participants of the study according

to Spanish Organic Law 15/199, December 13, related to Spanish Personal Data Protection Regulation and Royal Decree-Law 1720/2007, December 21.

4. Results and discussion

The colourimetric the discrimination of enantiomeric amino acids in solution using probes of Cu(II) complexes of bidentate *N*-donor ligands was described by Anslyn *et al.* [27]. With this work on mind, we envisaged solid polymeric materials having bidentate *N*-donor moieties in the polymer structure to prepare complexes with Cu(II) to detect amino acids in chronic human wounds to try to correlate the response with the protease activity measured by an accepted method. Thus, our idea was to have an easy-to-manage material for the detection of amino acids, cost-effective, rapid in response.

Firstly, we prepared a crosslinked polymer with bidentate *N*-donor motifs crosslinking main polymer chains. For this purpose, a difunctional monomer (3) was synthesised following conventional procedures (Scheme 1). Then, the crosslinked film was prepared by bulk thermally induced radical polymerisation of a small quantity of the crosslinked (3) (mol 0.5%) and two commercial monomers, VP and MMA, in mol 49.75% each, to obtain a material with a proper balance of mechanical properties and gel behaviour. In this sense, VP provides hydrophilicity and MMA hydrophobicity to the prepared polymer, and the crosslinker tunes further the water swelling percentage of the materials, by physical means, giving rise to a manageable film (**F(3)**), even after swelling. The weight percentage of water taken up by the films upon soaking in pure water at 20°C until reaching equilibrium (water-swelling percentage, WSP) was obtained from the weight of a dry sample film (ω_d) and its water-swelled weight (ω_s) using the following expression: $WSP = 100 \times [(\omega_s - \omega_d)/\omega_d]$. The water swelling percentage was 58.40% for **F(3)**, and envisaged good value for the diffusion of chemicals, such as amino acids, into the water swelled sensory film [2,7,9].

After preparing the film, the complex of diethyamine motifs-Cu(II) within the material was easily prepared by immersing the film in a water solution of $CuSO_4$

overnight (film **F$_{(3)}$-Cu**). Then, the sensory film (**F$_{(3)}$-Cu-D**) was prepared by immersion of the **F$_{(3)}$-Cu** in a water solution of the dye.

The dye was chosen after screening experiments with ten different commercial dyes (**Figure 1**). The chosen one presented the most drastic change of colour in the presence of amino acids.
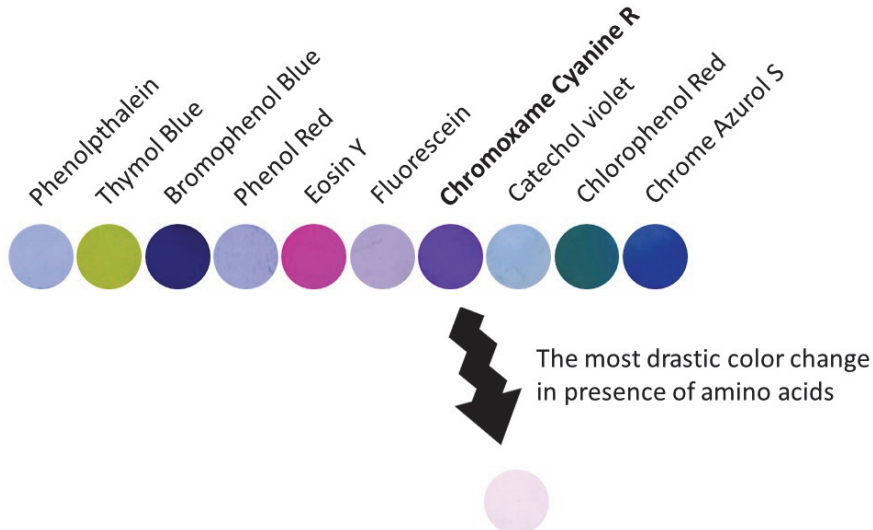
Figure 1. 10 discs (8 mm of diameter) of **F$_{(3)}$-Cu** after immersion in solutions of different dyes.

4.1. Mechanical and thermal properties of the films

The manageability of the films is visually observed upon handling and can also be analysed by measuring the mechanical properties of the materials. Thus, Young's moduli values for **F$_{(3)}$**, **F$_{(3)}$-Cu** and **F$_{(3)}$-Cu-D** were obtained from strips of the water swelled films (**Table 1**). The Young's modulus of the water swelled materials are right, ranging from 98 to 116 MPa, showing slight worsening upon diminishing the interchain interactions by the formation of the complexes between the diethylamine motifs of the polymer with Cu(II) and with Cu(II)-dye. Also, good manageability, in the broad sense, implies a reasonably good thermal behaviour, with thermal resistance well above the higher temperatures expected in the environment. Thus, the data of the thermogravimetric analysis (TGA) for the 5%

(T_5) and 10% (T_{10}) weight loss under nitrogen atmosphere are higher than 300°C (**Table 1**). The thermal analysis was completed with the evaluation of the glass transition temperatures (Tg) of the materials, that were calculated by DSC analysis at 20 °C min^{-1}, obtaining values around 140 °C, higher for hybrid polymers due to the restricted motion derived from the formation of the polymer-Cu(II) and polymer-Cu(II)-dye complexes. The TGA and DSC patterns are graphically depicted in the **SI-S2**, **Figure S4**.

Table 1. Mechanical (Young modulus, MPa) and thermal behaviour (degradation temperatures: 5% (T_5) and 10% (T_{10}) weight loss; thermal transition: glass transition (Tg)) of films.

Polymers	Mechanical properties of water swelled films, Young modulus (MPa)	Thermal properties, in N$_2$		
		Thermal resistance		Thermal transition
		T_5 (°C)	T_{10} (°C)	Tg (°C)
F$_{(3)}$	116	355	372	137
F$_{(3)\text{-Cu}}$	108	355	374	144
F$_{(3)\text{-Cu-D}}$	98	347	366	140

4.2. The behaviour of the sensory film at different pH

The use of sensory materials usually needs specific conditions in terms of pH. For this reason, discs of **F$_{(3)\text{-Cu-D}}$** were dipped in water solutions with pHs ranging all the conventional scale (from 1 top 14). The behaviour is depicted in **SI-S3**. According to the results, the sensory material can be used in a broad pH range (5 to 10). Thus, a biological pH was used for this study, pH = 7.

4.3. Interference study

The discs of sensory film **F$_{(3)\text{-Cu-D}}$** were immersed for 24 hours in a buffered solution of water/MeOH with a broad set of cations and anions (see **SI-S4**). The blue colour of the film changed its colour only in the presence of three cations, Au(III), Fe(III) and Nd(III). Among these cations, only Fe(III) can be considered an interferent because it is present in biological samples. For this reason, a

thorough study was carried out with this cation, at a concentration of 2.7×10^{-5} M (1.5 ppm), the maximum content of iron in the blood. Moreover, as biological samples are diluted 20 times their weight in the proper mixture of solvents, previous measurement, the maximum concentration of iron in the derived solution is 1.4×10^{-6} M (75 ppb). This concentration caused no interference at any measuring time, and accordingly, the sensory material can be used safely without the interference of any cation or anion.

4.4. Why films are not only a support but deeply influence the performance of the sensory probe?

It is usually found in the bibliography that solid polymers having sensory motifs chemically anchored to the polymer backbone behave in a different way than the sensory chemicals in solution beyond the lack of migration of the sensory motifs to the solution. It is stated that these systems mimic enzymes in water solutions that have a broad hydrophilic body that maintains the protein hydrated (tertiary structure) and small hydrophobic active sites where selective reactions take place without the competition of water [2,3,5,29].

Herewith we demonstrate the influence of the polymer matrix in outperforming the performance of conventional probes by two means: analysing the interaction of the probe or sensory motifs in solution and chemically anchored to a polymer in the solid-state and analysing the influence of the diffusion of species in solution into the swelled film.

4.5. Analysis of the interaction of the dye with solvents both in solution and in the amorphous and solid-state (within the solvent swelled film)

As has been previously mentioned, chemicals in the solid-state exhibit different properties than in solution, and this fact can be exploited for other purposes. Thus, chemicals dispersed in a polymer matrix, or chemically anchored to a polymer backbone, in the amorphous state, and isolated one from another by polymers chains, or sections, with high restriction in movement, exhibit different

properties because their chemical environment is different. For instance, highly thermally labile chemical groups, that cannot be isolated in conventional organic chemistry, such as diazonium salts, can be used without care at room temperature, for weeks, and exploited as sensors in sensing harmful chemicals in water media, when anchored to polymer backbones [2]. It is as if the polymer chains generate a protective environment for the labile group, and generalising, the polymer chains deeply influence the interactions that the chemicals within the polymer matrix can establish with others.

For getting the insight of the environment of a chemical in solution and the isolated amorphous state within a polymer matrix, we have analysed the interaction of solvents with the dye D by UV/Vis spectroscopy.

The influence of the solvent on the absorption spectra in the visible/ultraviolet range is due to the differences in solvation between the fundamental and excited state of the chemical (solute) [1]. These appear when there is an appreciable difference in the distribution of the population between the two states, often accompanied by a significant change in the dipole moments. The effect of the solvent is called solvatochromism and is described in terms of the displacement of the position of the peak of lower energy, with a greater wavelength, in the absorption spectrum. This can be to shorter wavelengths, hypsochromic (blue shift, negative solvatochromism), or to longer wavelengths, bathochromic (redshift, positive solvatochromism). The first effect takes place when the fundamental state is more dipolar than the excited state, while the opposite occurs when the excited state is more dipolar. These changes refer to the variation of energy between the states [30].

Non-polar solutes in the presence of polar or non-polar solvents, mainly experience dispersive forces, the effect thereof being very small and bathochromic, which increases with the polarity of the solvent. For polar solutes in non-polar solvents, the two types of displacements increase with solvent polarizability, depending on the dipole moment of the fundamental or excited state. When both are polar, the situation is more complex, since there is a

rearrangement of the solvent around the solute in both the fundamental and the excited state, so that both the polarizability and polarity of the solvent and the induced polarisation of the solute influence the displacements.

The absorption spectra are generally due to transitions n→π*, π→π* and electronic charge transfer. The most popular solvatochromic model currently in use is the Taft-Kamlet method [31–34]. In this model, multiple parameters are implemented to characterise different solvent-solute interactions, in the form of Eq. (1):

$$v = v_o + s(\pi^* + d\delta) + a\alpha + b\beta \qquad (1)$$

Where v is the energy of the transition, the inverse of the wavelength, v_o is the energy of the transition in the absence of solvent, π^*, α y β describe the polarity of the solvent, acidity or ability to donate a proton to a hydrogen bond (HBD) and the basicity or ability to accept a proton from a hydrogen bond (HBA) respectively (**SI-S5**, **Table S9**) [33,35]. δ is a correction term introduced due to the different polarizability of aromatic and polychlorinated solvents concerning aliphatic and non-polychlorinated solvents, 0 being for aliphatic solvents not substituted with chlorine, 0.5 for polychlorinated aliphatic and 1 for aromatic. If the solvent causes positive solvatochromism, this correction term is not necessary, and the coefficient d is zero. The coefficients *s, d, a* and *b* quantify the contributions of these properties. When working with non-chlorinated or non-aromatic solvents and if *a* and *b* are very small, the equation can be simplified to Eq. (2), and s can be easily obtained from the slope of the linear fitting of π^* and v data (**SI-S5**, **Figure S10**).

$$v = v_o + s\pi^* \qquad (2)$$

Following the results obtained, it follows that the predominant effect is the polarity of the solvent on the dye, stabilising the fundamental state more than the excited one, producing displacements at shorter wavelengths as the polarity of the solvent increases. Meaningful dipole-dipole interaction is observed in the case of dyes in solution, with a value of s = 3.22. However, when the dye is in the

film, having Cu(II) or not, the value of *s* is very small, around 0.6. This data indicates that the environmental surroundings of dye motifs prevent or hinders the dipole-dipole interactions between the dye motifs and the solvent swelling the film. Somehow it can be said that the structure of the film protects the dye.

4.6. Diffusion of species in solution into the swelled film

In the literature, we find numerous works dealing with adsorption of substances, generally pollutants, in different substrates with variable particle size [36–40]. In this work, we may consider the sensor as an adsorbent and the target amino acids as adsorbant. In our case, the adsorbent is not a particle of a certain size, but a 100 μm thick membrane.

In the adsorption processes in solution, several stages of transport take place in series: a) external transport of the adsorbate moving within the solution to nearby of the nearness of the sensory film. This is a quick process; b) diffusion of the adsorbate towards the surface of the sensory film, or external mass transfer; c) intraparticle diffusion; d) adsorption itself on the sensory motifs.

There are two approaches in mathematical modelling for the kinetic study of adsorption: surface reaction model (SRM), where the mass transfer is assumed to be rapid and the adsorption reaction (step d) is the stage that limits speed; and model of mass transfer reaction (MTM), where the mass transfer is the slow stage while the adsorption reaction is rapid. In this late-model there are two possibilities, single resistance model (intraparticle or external diffusion) or dual resistance model, i.e., both intraparticle and external diffusion playing an important role where steps b) and c) control the adsorption speed.

All these models were analysed in-depth, and the results are shown in the **SI,** Section **S6**. The model that gave us better results was the dual resistance model that considers both intraparticle and external diffusion in the analysis of the data, where relevant data were obtained following the methodology described by Crank [41] from Eqs. 3-5, where q_t is the milligrams of adsorbate per gram of adsorbent at a time t, q_e are equilibrium sorbate concentration in sorbent (mg/g),

B_i is Biot number, i.e., ratio of external film diffusivity to intraparticle diffusivity, D_s diffusion coefficient of sorbate within the sorbent (cm^2/min) and k_f are external or film mass transfer coefficient, (cm/min).

$$\frac{q_t}{q_e} = 1 - \sum_{n=1}^{\infty} \frac{2B_i^2 exp(-\beta_n^2 D_s t/l^2)}{\beta_n^2 (\beta_n^2 + B_i^2 + B_i)} \quad (3)$$

$$\beta_n tan\beta_n = B_i \quad (4)$$

$$B_i = \frac{k_f l}{D_s} \quad (5)$$

With Eqs. 3-5 the parameters *Ds* and *kf* were optimised by a non-linear fitting by least squares. This model, for spherical particles, has been used by other researchers [42]. In this way, following by UV-Vis technique the liberation of D in the presence of amino acid is possible to calculate the adsorbed mg of amino acid, i.e., the adsorption curve. **Figure 2** shows the results obtained for one of the amino acids, glycine.
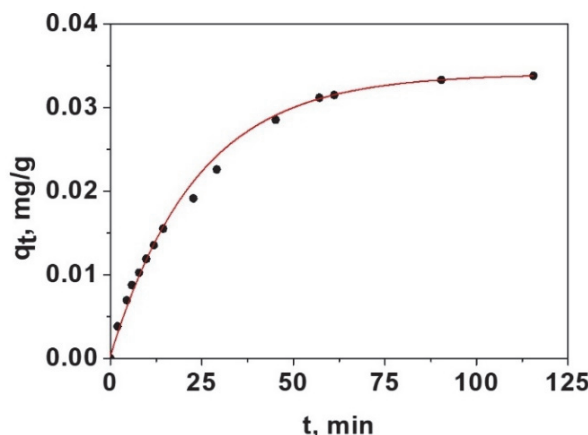
Figure 2. Non-linear fitting of the data of adsorption of glycine in the sensory film using the Crank model of dual resistance (Eqs. 3-5).

Once estimated the external and internal diffusion coefficients for a given adsorption system, the speed limitation step can be determined in terms of the number of Biot, Bi, which relates the external mass transfer resistance to the

resistance of internal mass transfer, Eq. 5. When the Bi >> 1, the adsorption process mainly controls by intraparticle diffusion, and if Bi << 1, it is the external diffusion that primarily controls the speed [43–45]. Once the values of Bi have been checked, **Table 2**, the stage that mainly controls this adsorption process is diffusion over the boundary layer or the transport of external mass.

Table 2. Parameters obtained by non-linear least-squares adjustment of Eq. 3.

Amino acid	k_f 10^4, cm/min	D_s 10^4, cm^2/min	B_i	R
Arginine	0.31 ±0.07	0.009±0.001	0.17±0.06	0.9975
Aspartic Acid	0.47 ±0.02	0.021±0.006	0.11±0.04	0.9977
Phenylalanine	0.57±0.09	0.024±0.004	0.12±0.04	0.9989
Glutamic Acid	0.89±0.02	0.038±0.007	0.12±0.02	0.9989
Hidroxiproline	1.18±0.04	0.041±0.003	0.14±0.02	0.9977
Proline	1.41±0.05	0.049±0.003	0.14±0.01	0.9968
Alanine	1.75±0.05	0.067±0.003	0.13±0.01	0.9981
Valine	2.00±0.1	0.082±0.004	0.12±0.01	0.9975
Glycine	2.20±0.1	0.092±0.003	0.12±0.01	0.9973

In our sensory system, this fact means that the solid sensory film exerts, because of the diffusion over the boundary layer, restrictions in the transport of chemicals favouring the diffusion of one chemical species against others, thus introducing a physical selectivity that does not apply for probes in solution. In our case, this selectivity favours glycine (**Table 2**). Furthermore, one the glycine is inside the solid sensory films, its interaction with the sensory motifs is facilitated by the limited interaction of these sites with the solvent, in our case water.

4.7. Analysis of the complex formation between the polymer, Cu(II) and dye

For getting an insight of the complex formation of the polymer with Cu(II) and the dye, we have analysed by UV/Vis the complex formation in a solution of the monomer (3) with Cu(II) and the dye D. Thus, to a DMA solution of D increasing concentration of a solution of (3) and Cu(II) in a molar ratio of 1:1. The UV/Vis spectra (**SI-S7**, **Figure S17**) showed one isosbestic point at about 350 nm

(confirming the interaction between D and {(3)-Cu(II)} at 1:1 stoichiometry), allowing for the analysis of three processes corresponding to the formation complexes {(3)-Cu(II)}$_n$D$_m$ with stoichiometries n:m of 1:1, 2:1, and 3:1. The later was also estimated with a Job's plot (**SI-S7**, **Figure S18**). However, at high ratios of dye to (3)-Cu(II), as it is in the preparation of the sensory film, the expected stoichiometry is 1:1. The study of the behaviour of the dye D and the complex {(3)-Cu(II)}$_n$D$_m$ (n:1, m:1) at different pH by UV/Vis allowed for the determination of the pK$_a$s of the acid protons. **Figure 3** depicts the pK$_a$s, both reported in previously [46] (aqueous media) and calculated by us (methanol: pH=7 buffer solution, 1:1). pK$_1$ values given in the literature are outside of the pH scale; thus, we have determined only pK$_2$, pK$_3$ and pK$_4$.
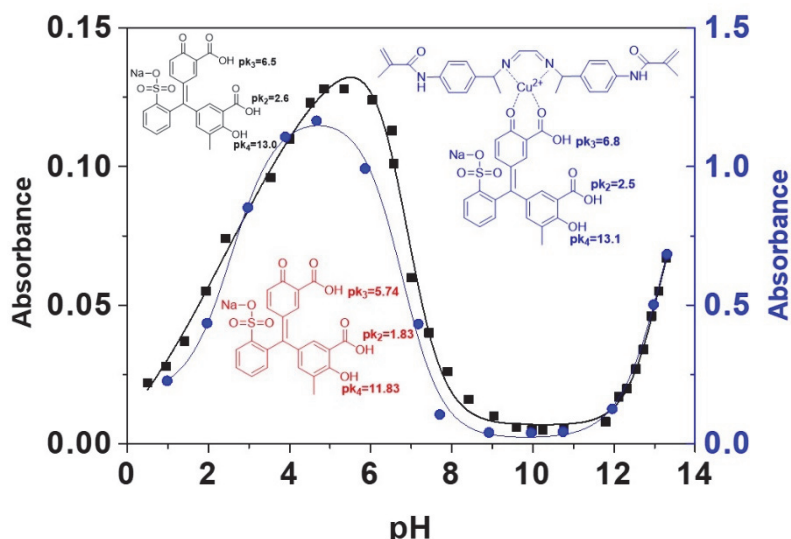
Figure 3. **Red**: pKa values for D according to the literature in aqueous media. **Black**: pH study and obtained pKa values for D in methanol:pH 7 buffer solution (1:1) media. **Blue**: pH study and obtained pKa values for the complex {(3)-Cu(II)}nDm (n:1, m:1) in methanol:pH 7 buffer solution (1:1) media.

4.8. Colourimetric sensing of amino acids

The immersion of discs of **F$_{(3)\text{-Cu-D}}$** in an aqueous/methanol solution buffered at physiological pH gave rise to the discolouration of the initially blue films and the

colouration initially colourless solution. The interaction of the amino acids with the $F_{(3)-Cu-D}$ lead to the initial material $F_{(3)}$, with the concomitant displacement of the dye and the formed new colourless complex Cu-(amino acid) [47–58], initially to the swelled film and finally to the solution.

Both the discolouration of the films (image analysis of pictures taken to the film) and the colour evolution of the solution (UV/Vis technique) can be used to sense the presence of amino acids in solution, and to measure their concentration upon previously construction of titration curves using a known concentration of amino acids.

Starting with the UV/Vis analysis based on the colour evolution of the solution, and to test the viability of the sensory system in complex environments, solutions of 7, 4 and 18 amino acids mimicking collagen, elastin and epidermis were initially prepared (see **SI-S8**, **Tables S19-S21**).[59–61] Then, discs of $F_{(3)-Cu-D}$ were immersed in water/methanol buffered at pH=7 in different vials and they were spiked with these solutions to give different apparent concentrations (sum of the concentration of amino acids in each solution). The absorbance along time for all the vials allowed for the calculation of the kinetic rate constants inside the sensory film [62], which are shown for collagen, elastin and epidermis in the **SI-S9**, **Tables S22-S24**. Since the absorbance value is proportional to the concentration of adsorbed glycine, the ratio between A and time is a point measure of rate. In the first measures of the reaction, the graphical representation of A/t against t is a straight line, and its origin is the value of the initial rate. The time for kinetic measurements ranged 1-5 min.

Thinking in the idea that the sensory film may be selective to one amino acid, as commented before, specifically glycine, the data of rate these rate constants were plotted against the concentration of glycine, giving a straight line, as shown in **Figure 4**. Moreover, the data for the three complex systems is fully

comparable with that of one with only glycine. This relevant information means that we have selective sensory material toward glycine, even though the sensory motif in solution responds equally to all amino acids. The good fitting of the

different systems (collagen, elastin and epidermis) to a pseudo-first-order model (as glycine), is due to the high molar proportion of glycine in this system (37.15 %, 46.71 % and 44.71 % respectively). The limits of detection and quantification of glycine are 1.9×10^{-5} and 5.7×10^{-5} M, respectively.
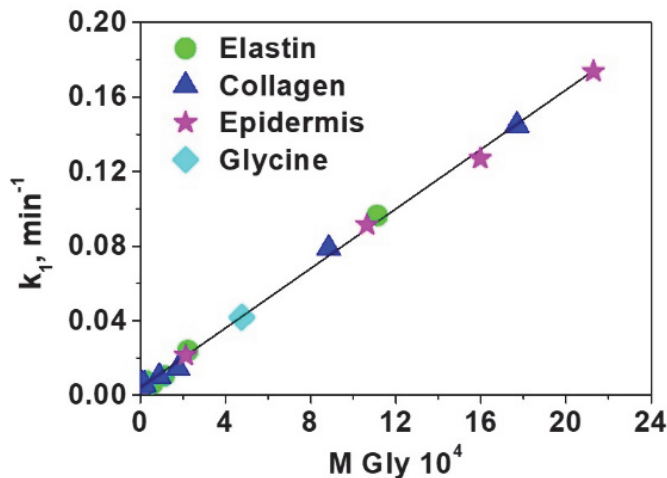
Figure 4. Kinetic rate constants of the kinetic of displacement of the dye by amino acids in the solid sensory $F_{(3)-Cu-D}$. The rate constants were calculated using the UV/Vis absorption data obtained from the solution where the sensory discs were immersed.

To achieve lower detection times, initial rates at 2 and 5 min were also calculated and correlated with amino acid concentration. Methodology and results are shown in the **SI**, section **S10**.

Once analysed the selective detection of glycine in complex mixtures of amino acids by studying by UV/Vis the colouring of the solution in which a sensory film was immersed, the colour decreases of the sensory films upon contacting with glycine was studied. This time, the colour variation was analysed by studying the digital colour definition of a picture taken to the discs. The digital colour was defined by three variables according to the RGB model (Red, Green and Blue), having these variables values between 0 and 255. To have the meaning of the two relevant variables (R and G) in only one, they were reduced to a single variable call PC (principal component) by the principal component analysis (PCA) [8]. The titration curve is depicted in **Figure 5** for solutions containing different

concentration of glycine in which the sensory discs were immersed for 60 min (the RGB data are shown in **SI-S11, Figure S28**, along with relevant PCA data).
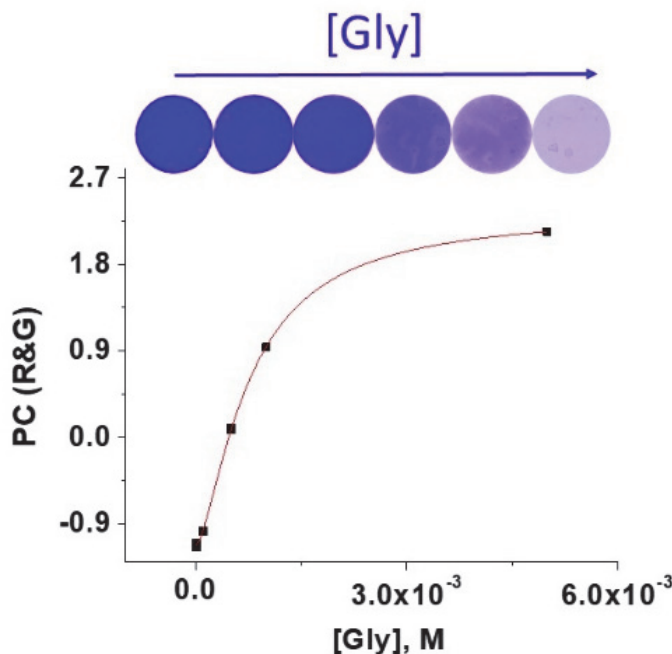
Figure 5. Titration of with Gly with **F$_{(3)-Cu-D}$** by RGB method. The top of the figure shows the photographs of **F$_{(3)-Cu-D}$** discs after immersion for 60 min in 0.63 ml of MeOH : pH 7 buffer solution (1:1) for concentrations of glycine ranging from 1×10^{-6} M to 5×10^{-3} M.

The limit of detection and quantification of glycine was 1.6×10^{-4} and 4.7×10^{-4} M, respectively. Though these values are one order of magnitude higher than those obtained with the previous method that uses UV/Vis spectroscopy, the lack of need of laboratory equipment using only a digital camera as analysing technique makes this method especially valuable. The analysis was also carried out with epidermis, at immersion times of 1 and 5 min, showing that quick measures can be carried out (**SI-S11, Figures S29 and S30**).

The comparison of published detection methods for amino acids is shown in **Table 3**. These methods have advantages and disadvantages, showing our proposal advantages related to the inexpensive methodology, visual detection and low response time.

Table 3. Comparative table of different amino acid analytical methods.

Method	Detection method	Low cost	Response time	Naked eye detection	Limit of detection	Reference
Reference method	UV-vis	no	15min	no	-	[63]
Screening method	Chromatography	yes	5min	yes	qualitative method	[64]
hyperpolarised ^{13}C-^{1}H-2D-NMR	NMR	no	4h	no	-	[65]
Trichophyton mentagrophytes var. erinacei	UV-vis	no	2 weeks	no	-	[66]
CE-LIF	Electrophoresis and Fluorimetry	no	4h	no	25-50 nM	[67]
HPLC	HPLC	no	3h	no	50-60 fmol	[68]
HPLC-CLND	HPLC (CLND)	no	3h	no	0.0025-.0075mM	[69]
High Voltage Electrophoresis	Electrophoresis	no	22h	no	-	[70]
Chromatography	Chromatography	no	3h	no	0.5-10µg	[71]
Screening method	Chromatography	no	24h	no	1.5-7.5w%	[72]
RGB	Digital pictures (RGB parameters defining the digital colours)	Yes	5-60 min	yes	1.58×10^{-4} M	This work
Kinetics	UV-vis	Yes	5-300 min	yes	1.89×10^{-6} M	This work
Initial rate	UV-vis	yes	1-5 min	yes	1.2×10^{-4} M	This work

4.9. Proof of concept. Sensing amino acids from a beefsteak and a human chronic wound

The first proof of concept carried out was the detection of amino acids coming from the action of the proteinase papain (papaya proteinase I) on a beefsteak bought in the local market (**SI-S12, Figure S31**). The degree of hydrolysis (DH%) caused by papain is usually followed by UV/Vis using the procedure described by Nielsen *et al*. [63](**Figure 6a**). We have also analysed the digital colour of our sensory discs dipped in partially hydrolysed beef steak samples and correlated with the previously calculated DH%, showing a good correlation and confirming the viability of our analytical procedure for providing information about the content of amino acids of a solution (**Figure 6b**, black line). Similarly, both the kinetic rate

constants of the kinetic of displacement of the dye by amino acids of the partially hydrolysed beef steak in the solid sensory $F_{(3)-Cu-D}$ (**Figure 6b,** blue line) and the initial rates at 1 and 5 min calculations (**SI-S12, Figure S32**) achieved using the UV/Vis absorption data obtained from the solution where the sensory discs were immersed, showed a good correlation with the DH% obtained with the method of Nielsen *et al.* [63].
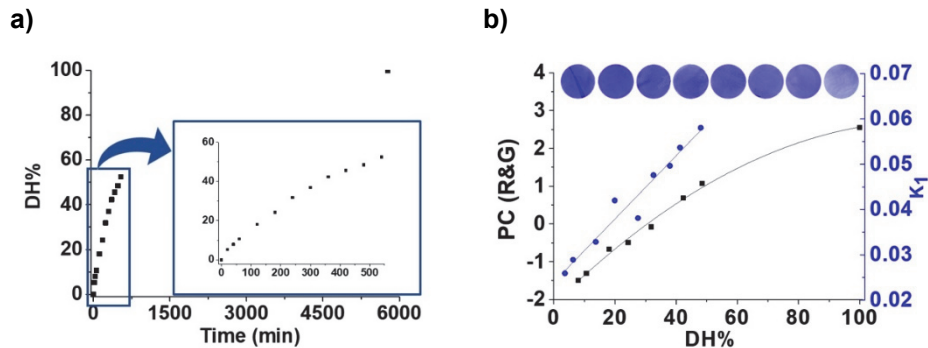
Figure 6. a) Degree of hydrolysis of a beefsteak obtained by UV/Vis using the Nielsen *et al.* procedure (DH% = [(A_{sample}-A_{blank})/($A_{100\%}$-A_{blank})]x100; A=absorbance) *vs* time [63]. *Experimental conditions*: 12.5 g of beefsteak and 62.5 mg of papain were made up to 250 ml with pH 7 buffer solution. The mixture was stirred at 50°C and aliquots of 5 mL were taken at different times. Additional information in **SI-S12**. **b)** *Blackline:* Correlation of the RGB method with DH%. PC (R&G) parameter was obtained by multivariable analysis of parameter R & G from digital images of the discs of $F_{(3)-Cu-D}$, after immersion for 60 min in the filtered aliquots from the hydrolysis reaction. *Blueline*: Correlation of the kinetic rate constants of the kinetic of displacement of the dye by amino acids in the solid sensory $F_{(3)-Cu-D}$. The rate constants were calculated using the UV/Vis absorption data obtained from the solution where the sensory discs were immersed.

The second proof of concept was carried with different types of samples (swab, wound bed, edge, capsular tissue and bone) of a chronic wound of the same patient. After, treating samples according to the procedure described in the **SI-S13**, the supernatant has the amino acids of the samples derived from the action of the different proteases over the proteins. The amino acid content of samples was characterised by the reference method, as previously explained. Then sensory discs were immersed at different times in the biological samples, and the colour of the films was analysed by the previously described procedure from the pictures taken to them. No results were obtained, probably because of the low concentration of the amino acids in these solutions. Also, after the immersion of each disc in the biological samples, they were evaluated by UV/Vis along time, and the kinetic rate constants evaluated. This time the method was

sensitive enough to detect the amino acids, and this is so because the limits of detection and quantification of this method are one order of magnitude lower than those obtained analysing the pictures taken to the film. Accordingly, the rate constants were proportional to the absorbance at 330 nm. This means that the sensory material can probably be used to follow the evolution of the chronic wounds and may be of help to assist doctors treating chronic wounds, especially because the analysis in rapid (less than 60 min after taken the samples) and costless (each disc can be fabricated at a lab-scale for less than 0.1 euros).

4.10. Reusability of the sensory material

The sensory discs can be used to detect amino acids, washed and used again for at least 6, as shown in the **SI-S14**, **Figure S34**, without an apparent loss of performance.

5. Conclusions

The research presented deals with the differences in the chemical behaviour of chemical probes in solution and the solid-state and the way of exploiting these differences in the field of polymeric chemical sensors. Thus, we previously looked for a sensory complex, previously exploited in solution for the colourimetric detection of amino acids, and then we anchored this sensory motif to a polymer backbone in the solid-state that gives rise to a film-shaped sensory material for discussing the selectivity and sensitivity of the solid materials compared with that of the probe in solution. Therefore, we report herein on the influence of the chemical environment of the amorphous and isolated sensory motifs within the solid polymer matrix, and also on the influence of this matrix in developing selectivity due to restrictions in the transport of target species into the material where the sensory motifs can interact with the target. More precisely, we have found that the sensory material, as a whole, is selective to glycine among several amino acids, whereas the probe in solution it is not, and we have applied it to the detection of amino acids in human chronic wounds, as a first step in the correlation of chronic wound evolution with the protease activity within the wound.

Furthermore, the solid-state is promising for exploiting organic or inorganic motifs with different and tuned properties related with the lack of interaction between these motifs that are in the amorphous state, the interaction with the polymer chains that can be tuned in terms of hydrophilic or hydrophobic behaviour, and the interface between the polymer matrix and the liquid or gaseous media.

Supplementary Materials: The following are available online at www.mdpi.com/2073-4360/12/6/1249/s1, FTIR, UV/Vis and CIE diagrams, SEM images, 1H-NMR and 13C-NMR spectra of model molecules, synthesised organometallic polymers and films obtained.

References

1. Nathan, A.J.; Scobell, A. *How China sees America*; Wiley, 2012; Vol. 91; ISBN 0 471 98369 1.

2. Bustamante, S.E.; Vallejos, S.; Pascual-Portal, B.S.; Muñoz, A.; Mendia, A.; Rivas, B.L.; García, F.C.; García, J.M. Polymer films containing chemically anchored diazonium salts with long-term stability as colorimetric sensors. *J. Hazard. Mater.* **2019**, *365*, 725–732, doi:10.1016/j.jhazmat.2018.11.066.

3. Vallejos, S.; Reglero, J.A.; García, F.C.; García, J.M. Direct visual detection and quantification of mercury in fresh fish meat using facilely prepared polymeric sensory labels. *J. Mater. Chem. A* **2017**, *5*, 13710–13716, doi:10.1039/c7ta03902f.

4. Bustamante Fonseca, S.E.; Rivas, B.L.; García Pérez, J.M.; Vallejos Calzada, S.; García, F. Synthesis of a polymeric sensor containing an occluded pyrylium salt and its application in the colorimetric detection of trimethylamine vapors. *J. Appl. Polym. Sci.* **2018**, *135*, 46185, doi:10.1002/app.46185.

5. Vallejos, S.; Hernando, E.; Trigo, M.; García, F.C.; García-Valverde, M.; Iturbe, D.; Cabero, M.J.; Quesada, R.; García, J.M. Polymeric chemosensor for the detection and quantification of chloride in human sweat. Application to the diagnosis of cystic fibrosis. *J. Mater. Chem. B* **2018**, *6*, 3735–3741, doi:10.1039/c8tb00682b.

6. González-Ceballos, L.; Melero, B.; Trigo-López, M.; Vallejos, S.; Muñoz, A.; García, F.C.; Fernandez-Muiño, M.A.; Sancho, M.T.; García, J.M. Functional aromatic polyamides for the preparation of coated fibres as smart labels for the visual detection of biogenic amine vapours and fish spoilage. *Sensors Actuators, B Chem.* **2020**, *304*, 127249, doi:10.1016/j.snb.2019.127249.

7. Vallejos, S.; Muñoz, A.; Ibeas, S.; Serna, F.; García, F.C.; García, J.M. Solid sensory polymer substrates for the quantification of iron in blood, wine and water by a scalable RGB technique. *J. Mater. Chem. A* **2013**, *1*, 15435–15441, doi:10.1039/c3ta12703f.

8. Vallejos, S.; Estévez, P.; Ibeas, S.; García, F.C.; Serna, F.; García, J.M. An organic/inorganic hybrid membrane as a solid "Turn-On" fluorescent chemosensor for coenzyme a (CoA), cysteine (Cys), and glutathione (GSH) in aqueous media. *Sensors* **2012**, *12*, 2969–2982, doi:10.3390/s120302969.

9. Vallejos, S.; Moreno, D.; Ibeas, S.; Muñoz, A.; García, F.C.; García, J.M. Polymeric chemosensor for the colorimetric determination of the total polyphenol index (TPI) in wines. *Food Control* **2019**, *106*, 106684, doi:10.1016/j.foodcont.2019.06.010.

10. Nussbaum, S.R.; Carter, M.J.; Fife, C.E.; DaVanzo, J.; Haught, R.; Nusgart, M.; Cartwright, D. An Economic Evaluation of the Impact, Cost, and Medicare Policy Implications of Chronic Nonhealing Wounds. *Value Heal.* **2018**, *21*, 27–32, doi:10.1016/j.jval.2017.07.007.

11. Nherera, L.; Digby, L.; Di Vincenzo, P.; Clark, J.; Gilpin, C. *Quantifying the economic value of diagnostics in wound care in the UK Background : The burden of chronic wounds*; 2013;

12. Posnett, J.; Gottrup, F.; Lundgren, H.; Saal, G. The resource impact of wounds on health-care providers in Europe. *J. Wound Care* 2009, *18*, 154–161.

13. Gómez Fernández, P. Revisión del tratamiento de las úlceras venosas: terapia compresiva. *RqR Enfermería Comunitaria* **2015**, *3*, 43–54.

14. Becker, K.; Boykin, J.; Crossland, M.; Davis, P.; Doughty, D.; Driver, V.; von Eiff, C.; Harding, K.; Lindholm, C.; Lubbers, M.; et al. *Diagnostics and wound. A consensus document. World Union of Wound Healing Societies (WUWHS). Principles of best practice: A World Union of Wound Healing Societies' Initiative.*; 2008;

15. International Consensus The role of proteases in wound diagnostics. An expert working group review. *London Wounds Int.* **2011**.

16. Westby, M.J.; Norman, G.; Dumville, J.C.; Stubbs, N.; Cullum, N. Protease-modulating matrix treatments for healing venous leg ulcers. *Cochrane Database Syst. Rev.* 2016, *2016*, 12.

17. Shang, K.; Song, S.; Cheng, Y.; Guo, L.; Pei, Y.; Lv, X.; Aastrup, T.; Pei, Z. Fabrication of carbohydrate chips based on polydopamine for real-time determination of carbohydrate-lectin interactions by QCM biosensor. *Polymers (Basel).* **2018**, *10*, 1275, doi:10.3390/polym10111275.

18. Tavakoli, J.; Tang, Y. Hydrogel based sensors for biomedical applications: An updated review. *Polymers (Basel).* **2017**, *9*, 364, doi:10.3390/polym9080364.

19. Jiang, Z.; Shangguan, Y.; Zheng, Q. Ferrocene-modified polyelectrolyte film-coated electrode and its application in glucose detection. *Polymers (Basel).* **2019**, *11*, 551, doi:10.3390/polym11030551.

20. Bagal-Kestwal, D.R.; Chiang, B.H. Exploration of chitinous scaffold-based interfaces for glucose sensing assemblies. *Polymers (Basel).* **2019**, *11*, 1958, doi:10.3390/polym11121958.

21. Zhang, X.; Khan, I.M.; Ji, H.; Wang, Z.; Tian, H.; Cao, W.; Mi, W. A Label-Free Fluorescent Aptasensor for Detection of Staphylococcal Enterotoxin A Based on Aptamer-Functionalized Silver Nanoclusters. *Polymers (Basel).* **2020**, *12*, 152, doi:10.3390/polym12010152.

22. Davies, M.L.; Murphy, S.M.; Hamilton, C.J.; Tighe, B.J. Polymer membranes in clinical sensor applications. III. Hydrogels as reactive matrix membranes in fibre optic sensors. *Biomaterials* **1992**, *13*, 991–999, doi:10.1016/0142-9612(92)90149-I.

23. Retama, JR; Lopez-Ruiz, B.; Lopez-Cabarcos, E. Microstructural modifications induced by the entrapped glucose oxidase in cross-linked polyacrylamide microgels used as glucose sensors. *Biomaterials* **2003**, *24*, 2965–2973, doi:10.1016/S0142-9612(03)00095-4.

24. Klueh, U.; Dorsky, D.I.; Kreutzer, D.L. Enhancement of implantable glucose sensor function in vivo using gene transfer-induced neovascularisation. *Biomaterials* **2005**, *26*, 1155–1163, doi:10.1016/j.biomaterials.2004.04.017.

25. Gerritsen, M.; Kros, A.; Sprakel, V.; Lutterman, J.A.; Nolte, R.J.M.; Jansen, J.A. Biocompatibility evaluation of sol-gel coatings for subcutaneously implantable glucose sensors. *Biomaterials* **2000**, *21*, 71–78, doi:10.1016/S0142-9612(99)00136-2.

26. Tian, Y.; Su, F.; Weber, W.; Nandakumar, V.; Shumway, B.R.; Jin, Y.; Zhou, X.; Holl, M.R.; Johnson, R.H.; Meldrum, D.R. A series of naphthalimide derivatives as intra and extracellular pH sensors. *Biomaterials* **2010**, *31*, 7411–7422, doi:10.1016/j.biomaterials.2010.06.023.

27. Frantz Folmer-Andersen, J.; Kitamura, M.; Anslyn, E. V. Pattern-based discrimination of enantiomeric and structurally similar amino acids: An optical mimic of the mammalian taste response. *J. Am. Chem. Soc.* **2006**, *128*, 5652–5653, doi:10.1021/ja061313i.

28. Nguyen, B.T.; Anslyn, E. V. Indicator-displacement assays. *Coord. Chem. Rev.* **2006**, *250*, 3118–3127, doi:10.1016/j.ccr.2006.04.009.

29. Gupta, V.K.; Goyal, R.N.; Sharma, R.A. Anion recognition using newly synthesised hydrogen bonding disubstituted phenylhydrazone-based receptors: Poly(vinyl chloride)-based sensor for acetate. *Talanta* **2008**, *76*, 859–864, doi:10.1016/j.talanta.2008.04.046.

30. Marcus, Y. *The properties of solvents*; 4th ed.; Wiley: England, 1998; ISBN 0-471-98369-1.

31. Kamlet, M.J.; Taft, R.W. The Solvatochromic Comparison Method. I. The β-Scale Of Solvent Hydrogen-Bond Acceptor (HBA) Basicities. *J. Am. Chem. Soc.* **1976**, *98*, 377–383, doi:10.1021/ja00418a009.

32. Taft, R.W.; Kamlet, M.J. The Solvatochromic Comparison Method. 2. The α-Scale of Solvent Hydrogen-Bond Donor (HBD) Acidities. *J. Am. Chem. Soc.* **1976**, *98*, 2886–2894, doi:10.1021/ja00426a036.

33. Kamlet, M.J.; Abboud, J.L.; Taft, R.W. The Solvatochromic Comparison Method. 6. The π* Scale of Solvent Polarities1. *J. Am. Chem. Soc.* **1977**, *99*, 6027–6038, doi:10.1021/ja00460a031.

34. Kamlet, M.J.; Abboud, J.L.M.; Abraham, M.H.; Taft, R.W. Linear Solvation Energy Relationships. 23. A Comprehensive Collection of the Solvatochromic Parameters, π, α, and β, and Some Methods for Simplifying the Generalised Solvatochromic Equation. *J. Org. Chem.* **1983**, *48*, 2877–2887, doi:10.1021/jo00165a018.

35. Kamlet, M.J.; Taft, R.W. The Solvatochromic Comparison Method. I. The β-Scale Of Solvent Hydrogen-Bond Acceptor (HBA) Basicities. *J. Am. Chem. Soc.* **1976**, *98*, 377–383, doi:10.1021/ja00418a009.

36. Mir, AA; Amooey, A.A.; Ghasemi, S. Adsorption of direct yellow 12 from aqueous solutions by an iron oxide-gelatin nanoadsorbent; kinetic, isotherm and mechanism analysis. *J. Clean. Prod.* **2018**, *170*, 570–580, doi:10.1016/j.jclepro.2017.09.101.

37. Zhang, L.; Song, X.; Liu, X.; Yang, L.; Pan, F.; Lv, J. Studies on the removal of tetracycline by multi-walled carbon nanotubes. *Chem. Eng. J.* **2011**, *178*, 26–33, doi:10.1016/j.cej.2011.09.127.

38. Hameed, B.H.; Tan, I.A.W.; Ahmad, A.L. Adsorption isotherm, kinetic modeling and mechanism of 2,4,6-trichlorophenol on coconut husk-based activated carbon. *Chem. Eng. J.* **2008**, *144*, 235–244, doi:10.1016/j.cej.2008.01.028.

39. Doğan, M.; Abak, H.; Alkan, M. Adsorption of methylene blue onto hazelnut shell: Kinetics, mechanism and activation parameters. *J. Hazard. Mater.* **2009**, *164*, 172–181, doi:10.1016/j.jhazmat.2008.07.155.
40. Kumar, K.V.; Ramamurthi, V.; Sivanesan, S. Modeling the mechanism involved during the sorption of methylene blue onto fly ash. *J. Colloid Interface Sci.* **2005**, *284*, 14–21, doi:10.1016/j.jcis.2004.09.063.
41. Crank, J. *Diffusion in a plane sheet*; Oxford University Press, 1975;
42. Chatterjee, A.; Schiewer, S. Multi-resistance kinetic models for biosorption of Cd by raw and immobilised citrus peels in batch and packed-bed columns. *Chem. Eng. J.* **2014**, *244*, 105–116, doi:10.1016/j.cej.2013.12.017.
43. Illanes, C.O.; Ochoa, N.A.; Marchese, J. Kinetic sorption of Cr(VI) into solvent impregnated porous microspheres. *Chem. Eng. J.* **2008**, *136*, 92–98, doi:10.1016/j.cej.2007.03.008.
44. Dávila-Guzman, N.E.; Cerino-Córdova, F.J.; Diaz-Flores, P.E.; Rangel-Mendez, J.R.; Sánchez-González, M.N.; Soto-Regalado, E. Equilibrium and kinetic studies of ferulic acid adsorption by Amberlite XAD-16. *Chem. Eng. J.* **2012**, *183*, 112–116, doi:10.1016/j.cej.2011.12.037.
45. Sun, X.; Chen, J.H.; Su, Z.; Huang, Y.; Dong, X. Highly effective removal of Cu(II) by a novel 3-aminopropyltriethoxysilane functionalised polyethyleneimine/sodium alginate porous membrane adsorbent. *Chem. Eng. J.* **2016**, *290*, 1–11, doi:10.1016/j.cej.2015.12.106.
46. Kiernan, J.A. Chromoxane cyanine R. II. Staining of animal tissues by the dye and its iron complexes. *J. Microsc.* **1984**, *134*, 25–39, doi:10.1111/j.1365-2818.1984.tb00501.x.
47. Levina, A.; Muzart, J. Enantioselective allylic oxidation in the presence of the Cu(I) Cu(II)-proline catalytic system. *Tetrahedron: Asymmetry* **1995**, *6*, 147–156, doi:10.1016/0957-4166(94)00370-Q.
48. Conato, C.; Contino, A.; Maccarrone, G.; Magrì, A.; Remelli, M.; Tabbì, G. Copper(II) complexes with L-lysine and L-ornithine: Is the side-chain involved in the coordination? A thermodynamic and spectroscopic study. *Thermochim. Acta* **2000**, *362*, 13–23, doi:10.1016/S0040-6031(00)00633-X.
49. Ilavarasi, R.; Rao, M.N.S.; Udupa, M.R. Synthesis and characterisation of copper(II) complexes of adenine and aminoacids. *Proc. Indian Acad. Sci. Chem. Sci.* **1997**, *109*, 79–87, doi:10.1007/BF02871153.
50. Valora, G.; Bonomo, R.P.; Tabbì, G. An EPR and voltammetric study of simple and mixed copper(II) complexes with L- or D-glutamate and L-arginate in aqueous solution. *Inorganica Chim. Acta* **2016**, *453*, 62–68, doi:10.1016/j.ica.2016.07.031.
51. Scarpa, M.; Vianello, F.; Signor, L.; Zennaro, L.; Rigo, A. Ascorbate Oxidation Catalysed by Bis(histidine)copper(II). *Inorg. Chem.* **1996**, *35*, 5201–5206, doi:10.1021/ic9600644.
52. Solans, X.; Ruíz-Ramírez, L.; Martínez, A.; Gasque, L.; Moreno-Esparza, R. Mixed chelate complexes. III. Structures of (L-alaninato)(aqua)(2,2'-bipyridine)copper(II) nitrate monohydrate and aqua(2,2'-bipyridine)(L-tyrosinato)copper(II) chloride trihydrate. *Acta Crystallogr. Sect. C Cryst. Struct. Commun.* **1992**, *48*, 1785–1788, doi:10.1107/s0108270192000568.
53. Su, C.C.; Tai, T.Y.; Wu, S.P.; Wang, S.L.; Liao, F.L. Spectroscopic and electronic properties of mixed ligand aminoacidatocopper(II) complexes: Molecular structure of [Cu(4,7-dimethyl-1,10-phenanthroline)(L-phenylalaninato)](ClO4). *Polyhedron* **1999**, *18*, 2361–2368, doi:10.1016/S0277-5387(99)00130-8.
54. Gala, L.; Lawson, M.; Jomova, K.; Zelenicky, L.; Congradyova, A.; Mazur, M.; Valko, M. EPR spectroscopy of a clinically active (1:2) copper(ii)-histidine complex used in the treatment of menkes disease: A fourier transform analysis of a fluid cw-epr spectrum. *Molecules* **2014**, *19*, 980–991, doi:10.3390/molecules19010980.
55. Fernandes, MCMM; Paniago, E.B.; Carvalho, S. Copper(II) mixed ligands complexes of hydroxamic acids with glycine, histamine and histidine. *J. Braz. Chem. Soc.* **1997**, *8*, 537–548, doi:10.1590/S0103-50531997000500017.
56. Marti, E.M.; Quash, A.; Methivier, C.; Dubot, P.; Pradier, CM Interaction of S-histidine, an amino acid, with copper and gold surfaces, a comparison based on RAIRS analyses. *Colloids Surfaces A Physicochem. Eng. Asp.* **2004**, *249*, 85–89, doi:10.1016/j.colsurfa.2004.08.055.
57. Mukherjee, G.; Ghosh, T. Metal ion interaction with penicillins: Part VIII. Equilibrium study of mixed ligand complex formation of Co (II), Ni (II), Cu (II) and Zn (II) with ampicillin and some

amino acids. *Proc. Indian Acad. Sci. Chem. Sci.* **1996**, *108*, 371–378, doi:10.1007/BF02871247.

58.   Estrader, M.; Diaz, C.; Ribas, J.; Solans, X.; Font-Bardía, M. Synthesis, characterisation and magnetic properties of six new copper(II) complexes with aminoacids as bridging ligand, exhibiting ferromagnetic coupling. *Inorganica Chim. Acta* **2008**, *361*, 3963–3969, doi:10.1016/j.ica.2008.03.028.

59.   Eastoe, J.E. The amino acid composition of proteins from the oral tissues-I. A comparison of human oral epithelium, epidermis and nail proteins. *Arch. Oral Biol.* **1963**, *8*, 449–458, doi:10.1016/0003-9969(63)90035-9.

60.   Keeley, F.W.; Partridge, S.M. Amino acid composition and calcification of human aortic elastin. *Atherosclerosis* **1974**, *19*, 287–296, doi:10.1016/0021-9150(74)90063-X.

61.   Eastoe, J.E.; Martens, P.; Thomas, N.R. The amino-acid composition of human hard tissue collagens in osteogenesis imperfecta and dentinogenesis imperfecta. *Calcif. Tissue Res.* **1973**, *12*, 91–100, doi:10.1007/BF02013724.

62.   Azizian, S. Kinetic models of sorption: A theoretical analysis. *J. Colloid Interface Sci.* **2004**, *276*, 47–52, doi:10.1016/j.jcis.2004.03.048.

63.   Nielsen, P.M.; Petersen, D.; Dambmann, C. Improved method for determining food protein degree of hydrolysis. *J. Food Sci.* **2001**, *66*, 642–646, doi:10.1111/j.1365-2621.2001.tb04614.x.

64.   Szeinberg, A.; Szeinberg, B.; Cohen, B.E. Screening method for detection of specific aminoacidemias. *Clin. Chim. Acta* **1969**, *23*, 93–95, doi:10.1016/0009-8981(69)90015-1.

65.   Katsikis, S.; Marin-Montesinos, I.; Ludwig, C.; Günther, UL Detecting acetylated aminoacids in blood serum using hyperpolarised 13C-1H-2D-NMR. *J. Magn. Reson.* **2019**, *305*, 175–179, doi:10.1016/j.jmr.2019.07.003.

66.   Aubaid, A.H.; Risan, A.Z.; Naem, A.K. Detection of sugars and aminoacids in antigens of Trichophyton mentagrophytes var. erinacei. *Mycoses* **1999**, *42*, 249–253, doi:10.1046/j.1439-0507.1999.00459.x.

67.   Veledo, M.T.; de Frutos, M.; Diez-Masa, J.C. On-capillary derivatisation and analysis of amino acids in human plasma by capillary electrophoresis with laser-induced fluorescence detection: Application to diagnosis of aminoacidopathies. *Electrophoresis* **2006**, *27*, 3101–3107, doi:10.1002/elps.200500781.

68.   Lindroth, P.; Mopper, K. High Performance Liquid Chromatographic Determination of Subpicomole Amounts of Amino Acids by Precolumn Fluorescence Derivatization with o-Phthaldialdehyde. *Anal. Chem.* **1979**, *51*, 1667–1674, doi:10.1021/ac50047a019.

69.   Petritis, K.; Elfakir, C.; Dreux, M. HPLC-CLND for the Analysis of Underivatized Amino Acids. *LC GC Eur.* **2001**, *14*, 389–395.

70.   Pasieka, A.E.; Thomas, M.E. The detection of β-alanine in biological fluids. *Clin. Biochem.* **1968**, *2*, 423–429, doi:10.1016/s0009-9120(68)80101-8.

71.   Saifer, A. Rapid screening methods for the detection of inherited and acquired aminoacidopathies. *Adv. Clin. Chem.* **1971**, *14*, 145–218, doi:10.1016/S0065-2423(08)60146-8.

72.   Adriaenssens, K.; Vanheule, R.; van Belle, M. A new simple screening method for detecting pathological amino-acidemias with collection of blood on paper. *Clin. Chim. Acta* **1967**, *15*, 362–364, doi:10.1016/0009-8981(67)90080-0.

Monitoring of the evolution of human chronic wounds the easy way.

Analyses using a ninhydrin based sensory polymer and a smartphone.

Monitoring of the evolution of human chronic wounds the easy way. Analyses using a ninhydrin based sensory polymer and a smartphone.

Marta Guembe-García,[1] Victoria Santaolalla-García,[2] Natalia Moradillo-Renuncio,[2] Saturnino Ibeas,[1] Jose A. Reglero,[1] Félix C. García,[1] Joaquín Pacheco,[3] Silvia Casado,[3] José M. García,[1,*] Saul Vallejos[1,*]

[1]Departamento de Química, Facultad de Ciencias, Universidad de Burgos, Plaza de Misael Bañuelos s/n, 09001 Burgos, Spain. Tel: (+) 34 947 258 085. E-mail: jmiguel@ubu.es (JMG), svallejos@ubu.es (SV)

[2]Complejo Asistencial Universitario de Burgos, Avenida de las Islas Baleares, 3, 09006 Burgos, Spain.

[3]Departamento de Economía Aplicada, Facultad de C. Económicas y Empresariales, Universidad de Burgos, Calle Parralillos, s/n, 09001 Burgos, Spain.Received: 11 May 2020; Accepted: 27 May 2020; Published: 29 May 2020

Abstract

The healing processes in cutaneous wounds, i.e., chronic wounds, represent a health problem affecting 1-2% of the population. The evaluation of these wounds is mainly based on subjective parameters, although there is a medical consensus on protease activity as the best marker for healing disorders. Here we show the correlation of the amino acid concentration on chronic wounds and with their evolution, and the development of a test kit to straightforward determining this evolution. Our test kit is a colorimetric sensory polymer film that change its colour upon contacting amino acids. The kit allows for quantification of the overall amino acid concentration by simply analysing the colour definition parameters of the sensory film obtained from of a photograph taken with a smartphone. We analysed with the kit the amino acid concentration of human chronic wounds of 34 patients and we mathematically demonstrate that there is a correlation with

the amino acid concentration, related with the protease activity, and the evolution of the wound's diagnoses. This kit can help diagnosis of human chronic wounds, usually evaluated and treated along time by different physicians, or even by different medical teams, providing an analytical tool not subjected to subjective evaluation.

1. Introduction

Nowadays, the medical researches related to the cure for cancer, or the development of new vaccines against viruses, such as HIV or coronavirus, are very current issues. But there are other health problems that a priori may seem milder but have a significant impact on society, both due to the large number of people who are affected by them and the economic costs they cause. In this work, we will focus on one of these well-known health problems [1,2], with high impact [3–7], and little visibility: the healing processes in cutaneous wounds, that is, chronic wounds. These types of low visibility injuries (affecting 1-2% of the population) represent 2-3% of the total European health budget [8]. According to estimates, in Europe, these wounds signify costs of 2.8-3.5 million euros per 100,000 habitants. Nurses dedicate the equivalent of 89 days to cures, and it is estimated that patients with these conditions occupy 19,000 to 31,000 bed days per year [9]. In the USA, the economic impact of chronic injuries has been estimated at 32,000 million dollars per year [10], and only in Spain 350 million € per year [8].

This type of wounds requires weekly monitoring (even daily, in case of hospitalised patients). This follow-up is carried out by a physicians through a form where the state of the wound is assessed, regarding factors such as the appearance of infection (Y/N), revascularisation (Y/N), date of revascularisation, evolution, necrosis (Y/N), ischemia (Y/N) or cell cultures performed (Pseudomonas aeruginosa, Proteus mirabilis, Staphylococcus aureus, Prevotella

bivia, Enterococcus faecalis, Escherichia coli). The problem with these evaluations is that many of the parameters are subjective. Additionally, due to the shifts and schedules of the health workers, throughout the same week, a patient can be attended by 2 or 3 different physicians, with varying opinions about the state of the wound, which generates a high variability on the results. At this point, the need for a methodology based on a simple kit becomes evident, which physicians can use to objectively determine the state/evolution of the wounds.

Although nowadays there are currently not clear solutions to this problem, there is a medical consensus among the World Union of Wound Healing Societies [11], "that increased protease activity is currently the best available marker for healing disorders when other causes have been excluded, and that the effective use of a protease test kit has the potential to change wound management globally" [12,13]. Proteases are the enzymes responsible for the degradation into peptides and amino acids of proteins. They are believed to play a crucial role in healing processes as they degrade damaged extracellular matrix (EM) proteins, thereby allowing new tissue formation in an orderly healing process. Healing problems appear when the degradation/regeneration balance is altered, due to the uncontrolled activity of the protease that not only breaks the damaged EM proteins but also degrades the newly formed EM and other essential EM proteins, like growth factors and their receptors. This uncontrolled degradation prolongs the inflammatory phase preventing the wound to progress to the proliferative phase.

Thus, determining the enzymatic activity of a wound seems to be the key to diagnosing this type of lesions at an early stage, since at first sight, they are not easy to detect in their early stages because clinical signs of inflammation are usually challenging to discriminate from the signs of infection. This is an important issue since there is currently no fast and reliable method for evaluating enzyme activity. Techniques such as gelatine zymography [14,15], and the Enzyme-Linked Immunosorbent Assay (ELISA) [16], determines protease levels using antibodies but, in most cases, they are beyond the reach of physicians.

Since proteases hydrolyse ME proteins, we hypothesise that the higher the enzyme activity, the higher the amino acid concentration. This hypothesis would allow us to address the problem indirectly by measuring the concentration of amino acids derived from enzyme activity and not the activity directly. Within the literature, the detection of amino acids is an intensely studied subject and for which there are several techniques such as electrophoresis [17,18], HPLC [19,20], NMR [21], or chromatography [22–24]. However, all of these methods require expensive equipment and advanced knowledge for amino acid detection.

One of the oldest and most studied methods [25,26] is that of ninhydrin [27–30], a colorimetric method widely used in forensic science [25,31,32]. However, this method implies both the manipulation of chemicals and the use of relatively costly equipment, which undoubtedly complicates their daily use in hospitals and/or health centres. Gel behaviour polymers have been widely used for sensory applications oriented to different areas [33–36], and for this reason, we propose a sensory film, with gel behaviour, simple, cheap and easy to use by non-specialized personnel, based on ninhydrin receptors but without the need to manipulate any chemical reagent, which determines enzymatic activity in the wounds indirectly, by measuring the amino acid concentration of exudates from a skin wound through a digital photo taken with a smartphone.

This work is focused in two correlated objectives. First, the development of a new sensory material for the detection of amino acids in and easy and rapid way, by only using a smartphone. Second, the demonstration that the level of amino acids is directly related to the state of a chronic wound, and subsequently with the protease activity. For the analysis of all this data, the statistical classification methods have boosted the proposed diagnostic tool based on a simple sensory film.

2. Experimental

2.1. Materials

We have used the following materials and solvents, as received, unless otherwise stated: 2,2′-azobis(2-methylpropionitrile) (AIBN) (98%, Aldrich), 1-vinyl-2-pyrrolidone (VP) (99%, Aldrich), methyl methacrylate (MMA) (99%, Aldrich), pH 4.66 Buffer (VWR), dioxane (100%, VWR), acetone (99%, VWR), trans-4-hydroxi-L-proline (≥99%, Sigma-Aldrich), L-aspartic acid (98%, Alfa Aesar), L-threonine (98%, Alfa Aesar), Serine (≥99%, Fluka), L-arginine (98%, Alfa Aesar), L-glutamic acid (+99%, Alfa Aesar), L-lysine (97%, Sigma-Aldrich), L-proline (99%, Alfa Aesar), L-histidine (+98%, Alfa Aesar), Glycine (99%, Alfa Aesar), L-alanine (99%, Alfa Aesar), L-cysteine (+98%, Alfa Aesar), L-valine (≥98%, Sigma-Aldrich), L-methionine (+98%, Alfa Aesar), L-isoleucine (98%, Sigma-Aldrich), L-tyrosine (+99%, Acros Organic), L-phenylalanine (98%, Alfa Aesar) zinc (II) nitrate hexahydrate (98%, Sigma Aldrich), Iron(III) nitrate nonahydrate (99%, Sigma Aldrich), cesium nitrate (≥99%, Fluka), manganese (II) nitrate hexahydrate (98+%, Alfa Aesar), tetrachloroauric(III) acid trihydrate (99.9+%, Sigma-Aldrich), potassium dichromate (≥99.5%, Sigma-Aldrich), barium chloride dehydrate (99%, Labkem), cobalt(II) nitrate hexahydrate (≥99%, Labkem), ammonium nitrate (≥98%, Sigma-Aldrich), calcium nitrate tetrahydrate (≥99%, Sigma-Aldrich), chromium(III) nitrate nonahydrate (98.5%, Alfa Aesar), mercury(II) nitrate (98%, Alfa Aesar), rubidium nitrate (99.95%, Sigma-Aldrich), dysprosium(III) nitrate (99.9%, Alfa Aesar), lithium chloride (≥ 99%, Sigma-Aldrich cadmium nitrate tetrahydrate (98.5%, Alfa Aesar), $Fe(NO_3)_3 \cdot 9H_2O$ (≥ 98%, VWR), cerium (III) chloride tetrahydrate (≥99.99%, Sigma-Aldrich), zirconium(IV) chloride (98%, Alfa Aesar), lanthanum(III) nitrate hexahydrate (99.9%, Alfa Aesar), potassium nitrate (99+%, Sigma-Aldrich), samarium(III) nitrate (99.9%, Alfa Aesar), magnesium nitrate hexahydrate (≥ 99%, Labkem), aluminum nitrate nonahydrate (≥ 98.9%, Sigma-Aldrich), silver nitrate (≥99.9, Sigma-Aldrich), neodymium(III) nitrate (99.9%, Alfa Aesar), lead(II) nitrate (≥ 99%, Fluka), strontium nitrate (99+%,

Sigma-Aldrich), copper(II) nitrate trihydrate (98%, Sigma-Aldrich), nickel(II) nitrate hexahydrate (98.5%, Sigma-Aldrich), sodium nitrate (99%, LabKem), tin (II) chloride (98%Aldrich), Sodium cyanide (>97%, Sigma-Aldrich), Sodium acetate (>99%, Aldrich), Lithium hydroxide (>98%, Sigma-Aldrich), Sodium fluoride (≥99.9%, Sigma-Aldrich), Potassium perchlorate (>99%, Sigma-Aldrich), Sodium dodecyl sulphate (≥98.5%, Sigma-Aldrich), Sodium nitrite (>97%, Aldrich), Sodium Ethoxide (95%, Sigma-Aldrich), Potassium hydrogen phthalate (99.95%, Sigma-Aldrich), Sodium pyrophosphate tetrabasic (>95%, Sigma-Aldrich), Potassium persulfate (>99%, Sigma-Aldrich), Sodium methanesulfonate (98%, Sigma-Aldrich), Sodium pyrophosphate dibasic (>99%, Sigma-Aldrich), Lithium trifluoromethanesulfonate (96%, Sigma-Aldrich), Sodium p-toluenesulfonate (95%, Sigma-Aldrich), Potassium bromide (>99%, Sigma-Aldrich), Potassium thiocyanate (>99%, Sigma-Aldrich), Potassium oxalate monohydrate (>98.5%, Sigma-Aldrich), Sodium carbonate (>99%, Sigma-Aldrich), Sodium benzoate (>99.5%, Sigma-Aldrich), Lithium phosphate monobasic (99%, Sigma-Aldrich,), Sodium sulfate (99%, Sigma-Aldrich), Sodium chloroacetate (98%, Sigma-Aldrich), Sodium trifluoroacetate (>99%, Sigma-Aldrich), Sodium periodate (99.78%, Sigma-Aldrich, 99.8%), bovine serum albumin (BSA) (>97%, Biowest), L-Glutathione reduced (GLUT) (VWR, >98%), SeO2 (99.4%, Alfa Aesar), HCl(37%, VWR-Prolabo), sodium dodecyl sulfate (≥97%, Fluka), di-sodium tetraborate (99%, Sigma-Aldrich), phthaldialdehyde (97%, Merk), 2-mercaptoethanol (98+%, Alfa Aesar), Selenium dioxide (98%, Fluka, Caution, toxic!).

We have prepared three solutions mimicking collagen (COL), elastin (ELA) and epidermis (EPI), following the procedure described in a previous work [37], by mixing different concentrations of the amino acids which these proteins are constituted of, as reported by Eastoe [38], Keeley and Partrige [39], and Eastoe et al. [40].

The concentration of COL, ELA and EPI are expressed as the summation of the molarities of each amino acid (μM).

Food matrix, beef, loin cut, was used to test the polymer described in this work as amino acid sensor. For it, the results of the proposed method in this work were compared with the results of the Nielsen method (reference method for the amino acids detection) [41]. The food matrix was purchased from a local supermarket (see ESI section S6, Figure S10).

The real biological samples (exudates) from patients with chronic wounds have been obtained following the established procedures at HUBU (university hospital of Burgos), directly from the damaged tissue. Thus, tissue sample collection was carried out with validated aseptic technique after mechanical dragging with physiological saline of any drug residue or detritus. In cases where there is dry crust or abundant accumulation of devitalized tissue, they are actively removed with a scalpel until a representative bed of the ulcer is obtained. The samples are two-ways collected: 1) by means of a bottom swab smear of the lesion; 2) by physical debridement with a scalpel in the different areas of loss of substance depending on the anatomical location of the lesion and its extension in surface and depth (edges, bottom, bone, tendon, etc.), obtaining a piece of vital tissue of the size to proceed according to the condition of the wound. The sample is deposited in a suitable means of transport that allows the correct later analysis. The study was carried out with five types of samples of a chronic wounds of each patient, and picked up from 35 patients: swab (A), wound bed (B), edge (C), capsular tissue (D) and/or bone (E). Samples were collected by physicians who previously performed a visual analysis of the wounds, evaluating also other factors such as age, type of sample (A, B, C, D, E), re-vascularised date, site injury, infectious appearance (Y/N), bad evolution (Y/N), necrosis (Y/N), ischemia (Y/N) and cell cultures (Pseudomonas aeruginosa, Proteus mirabilis, Staphylococcus aureus, Prevotella bivia, Enterococcus faecalis, Escherichia coli) and note about evolution. We understand by bad evolution of a wound if there are criteria of infection or lack of healing in a given period. Signs of infection are pain, heat, perilesional erythema, bad smell, gas, lymphangitis, crepitus in the area of the injury, and signs of lack of healing are progressive necrosis or reduced

granulation tissue at the bottom of the lesion in 4-6 weeks from the appearance of the lesion. All samples were boiled in pH 4.66 buffer solution for 10 min (20 ml of pH 4.66 buffer solution per gram of sample). Finally, samples were filtered at room temperature, and the resulting solutions were labelled as CWS (chronic wound samples).

2.2. Measurements and instrumentation

The method for measuring amino acid concentrations with pictures taken to sensory films (from now on RGB_method) was carried out by taking digital photography of the sensory discs (8 mm diameter) with an iPhone 6S smartphone after immersion in a mixture of 1:1 buffer pH=4,66: aqueous solutions with different concentrations of amino acids at 100oC for 1 hour. The pictures were made in a homemade retro-illumination box, manufactured with 3D printing, to obtain a good reproducibility of the results, as well as to avoid possible external influences in the photographs (for practical purposes, the influence of ambient light and digital camera could be disregarded using a colour reference, [42,43]). The digital pictures were analysed with a generic image software to obtain the R (red), G (green) and B (blue) parameters (RGB) of the entire surface of the sensory disc. Photos were made six-fold for the calculations of the errors, and the average of each RGB parameter was calculated. This easy and cheap method allows the quantification of amino acid in aqueous media, by only taking a photo, and we have widely used it in previous works [44,45].

Principal component analysis (PCA) was carried out using the Statgraphics Centurion XVI software installed on a personal computer in a Windows 7 environment. The principal component (PC) values were obtained from RGB parameters, carrying out a multivariate analysis of principal component. This mathematical method allows the simplification of 3 variables to a single one [46], transforming a colour in a number. Values were standardised and accounted for >99% of the variance in all experiments.

Infrared spectra (FTIR) were recorded with an FT/IR-4200 FT-IR Jasco Spectrometer with an ATR-PRO410-S single reflection accessory. 1H and 13C{1H} NMR spectra were recorded with a Bruker Avance III HD spectrometer operating at 300 MHz for 1H, and 75 MHz for 13C, using deuterated solvents like dimethyl sulfoxide (DMSO-d6) or deuterated chloroform (CDCl3) at 25°C. Solid-state 13C CPMAS NMR spectra were recorded on a Bruker AVANCE III, 9.4 T system equipped with a 4 mm MAS DVT Double Resonance HX MAS probe. Larmor frequencies were 400.17 MHz and 100.63 MHz for 1H and 13C nuclei, respectively. Chemical shifts were calibrated indirectly with glycine, carbonyl peak at 176 ppm. The sample rotation frequency was 10 kHz and the relaxation delay was 5 s. The number of scans were 10240. Polarization transfer was achieved with RAMP cross-polarization (ramp on the proton channel) with a contact time of 5 ms. High-power SPINAL 64 heteronuclear proton decoupling was applied during acquisition.

Thermal and mechanical properties of the material were measured using thermogravimetric analysis (TGA, 10-15 mg of the sample under synthetic air and nitrogen atmosphere with a TA Instruments Q50 TGA analyser at 10°C·min−1), differential scanning calorimetry (DSC, 10-15 mg of the sample under a nitrogen atmosphere with a TA Instruments Q200 DSC analyser at 20°C·min−1), and tensile properties analysis (5 × 9.44 × 0.122mm samples using a Shimadzu EZ Test Compact Table-Top Universal Tester at 1mm·min−1). The weight percentage of water taken up by the films upon soaking in pure water at 20°C until reaching equilibrium (water-swelling percentage, WSP) was obtained from the weight of a dry sample film (ω_d) and its water-swelled weight (ω_s) using the following expression: WSP=100×[(ω_s−ω_d)/ω_d].

High-resolution electron-impact mass spectrometry (EI-HRMS) was carried out on a Micromass AutoSpect Waters mass spectrometer (ionisation energy: 70 eV; mass resolving power: >10,000).

UV/Vis spectra were recorded using a Hitachi U-3900 UV/Vis spectrophotometer.

RAMAN spectra were recorded with a confocal AFM-RAMAN model Alpha300R – Alpha300A AFM from WITec, using a laser radiation of 532 nm, at magnifications of 100x. All spectra were taken at room temperature.

Chronic wounds were initially visually analysed by physicians. Then, all CWS were analysed by two methods: reference method based on Nielsen's method (see ESI section S6) and RGB_method explaining in this work [41]. All data obtained were analysed by statistical linear and non-linear methods for diagnosis and classification, such as Discriminant Analysis (DA) [47], Logistic Regression (LR) [48], or Support Vector Machine (SVM) [49–51].

2.3. Monomer synthesis

For the synthesis of a polymer with ninhydrin-based receptor units, the synthesis of a monomer with a reactive side moiety was performed following the same philosophy as in previous works [45,52,53]. Instead of carrying out the complete synthesis of the sensory monomer, we prepared a monomer which subsequent bulk radical initiated polymerization rendered a functional polymer film that was transformed into the sensory polymer containing ninhydrin-based receptors by straightforward solid phase synthesis. Compared to conventional monomer synthesis, this methodology is cost effective and greener, it reduces both the use of solvents and the time needed.

The preparation and characterization of the monomer with the reactive side moiety, which is a derivative of 6-aminoindanone, is described in the electronic supplementary information, ESI section S1, and shown schematically in Scheme 1.
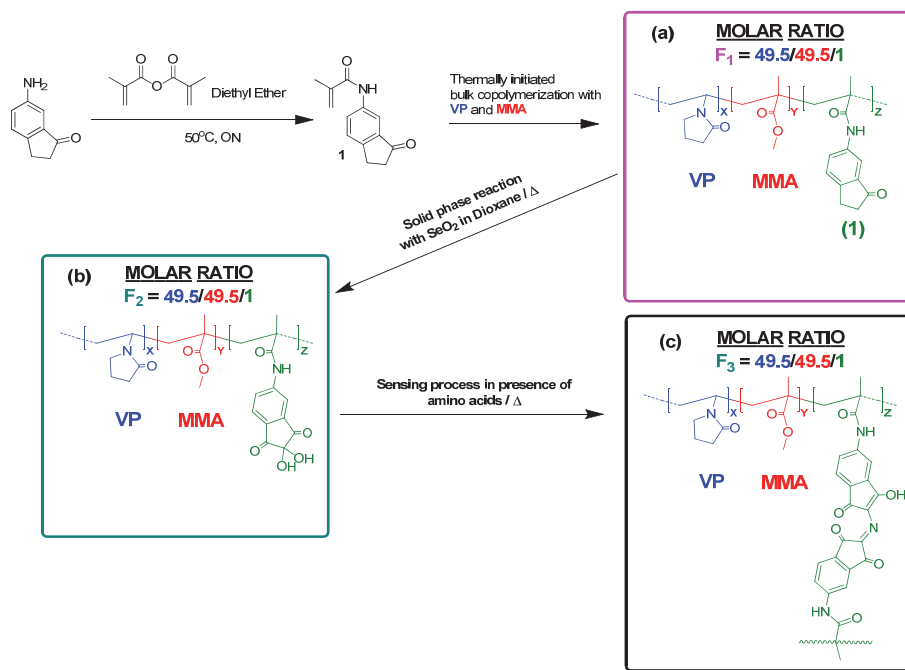
Scheme 1. Synthetic route for the sensory monomer **1** and sensory polymer **F$_2$.**

2.4. Polymer synthesis

Preparation of the sensory film

We obtained the starting material by thermally initiated radical copolymerisation of two main co-monomers, one hydrophilic (vinylpyrrolidone, VP) and the other hydrophobic (methylmethacrylate, MMA), and the monomer with the reactive side moiety, (1). The bulk radical polymerisation was carried out in a silanised glass mould (100 μm thick) in an oxygen-free atmosphere at 60°C overnight to obtain the membrane F1. Regarding the molar ratio of the monomers, this can be adjusted for different purposes. In our case, the colorimetric response of the material toward amino acid was modulated by controlling this molar ratio, i.e., 49.5/ 49.5/1 (VP/MMA/(1)). After the bulk radical polymerisation, a solid phase reaction was made in the solid membrane to obtain the final sensory material (F2). We chose solid-phase synthesis to synthesise the anchor monomer derived

from ninhydrin because, following the conventional route, the process would require several purifications per column with a high solvent expenditure. Also, this methodology has given us good results in works previous [45,52]. The reaction was carried out as previously depicted for the preparation of different ninhydrin derivates [54]. First, the membranes (4 membranes 13 cm wide and 9 cm long) were washed with 200 ml of dioxane in a pressured flask for one night at RT. Secondly, the dioxane was removed from the flask, and a solution of SeO2 in dioxane (1g in 200ml) was added. The flask was heated at 90oC for 24 hours, or until no colour evolution of the membrane observed in the presence of amino acid. Finally, the solution was removed from the flask, and the films were washed with acetone (2 times) and water (2 times).

The chemical structure of the films used to prepare the sensory materials is depicted in Scheme 1. Additionally, the thermally initiated bulk polymerisation procedure for polymers prepared with VP results in crosslinked materials [55], which limits conventional NMR or GPC analysis. Thus, we have developed a sensory film with a higher proportion of ninhydrin units for the characterisation of the materials by FT-IR spectroscopy, Raman spectroscopy and solid-state NMR (see ESI section S2, Figures S2-S4).

Ethical statement

All experiments with human subjects have been performed based on the use and ethics of the HUBU policy for trials with humans. This study (minute 13/2017, internal code: 2017.200) on November 16, 2017, has been approved by the ethics committee of clinical experimentation of the region of Burgos, Spain. According to Spanish Organic Law 15/199, December 13, related to Spanish Personal Data Protection Regulation and Royal Decree-Law 1720/2007, December 21, all participants of the study were informed and gave their consent.

3. Results and discussion

3.1. Water uptake of films

In this case, the water swelling percentage (WSP) was 56% for **F$_1$**, 101% for **F$_2$** and 38% for **F$_3$**, and envisaged appropriate diffusion of species, such as amino acids, inside the water-swelled sensory film. The increase in swelling between **F$_1$** and **F$_2$** is because the ninhydrin derivative present in **F$_2$** is more hydrophilic than the indanone derivative of **F$_1$**. The decrease of the water uptake in **F$_3$** is due to the crosslinking process that results after the reaction of ninhydrin motifs with an amino acid.

3.2. Thermal and mechanical characterisation

An essential property in sensory materials is their manageability. This is related with a good thermal behaviour, with thermal resistance above the higher-expected environmental temperatures, and also with good mechanical properties. Regarding the former, the 5 % (T_5) and 10 % (T_{10}) weight loss under nitrogen atmosphere, obtained by TGA, are 360 and 387ºC for **F$_1$**, 296 and 355ºC for **F$_2$**, and 332 and 370ºC for **F$_3$**. The thermal characterization was complemented with the determination of the glass transition temperatures (*Tg*) of the materials DSC. The *Tg* values were 177, 206 and 202°C for **F$_1$**, **F$_2$** and **F$_3$** respectively. The DSC and TGA patterns are shown in the **ESI section S3, Figure S5**. The mechanical properties for **F$_1$**, **F$_2$**, and **F$_3$** (Young's moduli of 48, 31, and 105 MPa, respectively) were obtained from strips of the water swelled films. These values are very similar for **F$_1$** and **F$_2$**, the small differences are due to the swelling in water, in **F$_2$** is higher, so the modulus decreases. In **F$_3$** Young's modulus is higher because of the crosslinking of the material.

3.3. Study of pH

Biological samples usually need specific conditions in terms of pH. Accordingly, we carried out a study of the behaviour of F_2 at different pHs. For it, 14 discs (8 mm diameter) of F_2 were immersed in a mixture of 1 mL of 0.1 M amino acid solution (ΣM) mimicking epidermis (**EPI**), and 1 mL of aqueous solutions with pH ranging from 1 to 14 (HCl:NaOH). The system was heated at 100oC for 60 min, and the discs were washed with water. Photographs of the discs were taken in the retro-illumination lightbox and were analysed by the RGB_method (**ESI-S4, Table S1**). The results shows (**Figure 1**) that the sensory material can be used from pH 3 to 11. In our case, 4.66 was chosen as the working pH.
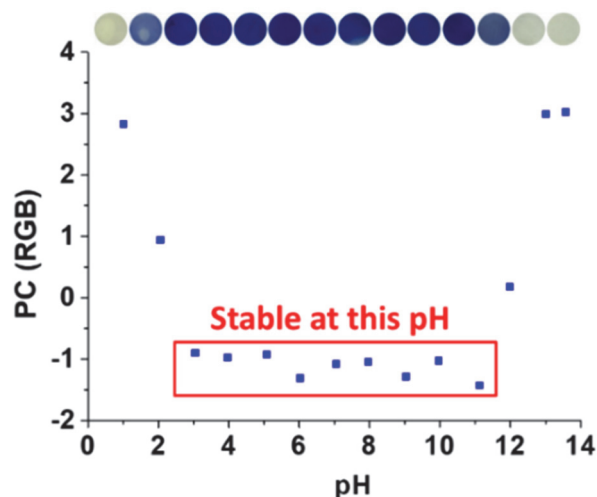
Figure 1. The pH study was performed using the RGB_method, by immersing 8 mm diameter discs of F_2 in a mixture of 1 mL of 0.1 M **EPI**, and 1 mL of aqueous solutions with pH ranging from 1 to 14 (HCl:NaOH), at 100ºC for 60 min. Then, the discs were washed several times with water, and photographed for the extraction of the RGB variables, which were simplified to a single variable (principal component, **PC**) through a multivariate analysis. Additional information in **ESI section S4, Table S1.**

3.4. Method for measuring amino acid concentrations with photographs taken to sensory films (RGB_method)

The 8mm discs of F2 changes their colour upon immersion in water solution of amino acids (pH 4.66) at 100oC for 60 min. The initial orange colour evolves to

blue in presence of varying amino acid concentrations (see ESI-S5, Figure S6). The sensing mechanism is depicted in Scheme 1. The sensing mechanism is based on the 'ninhydrin test' in which two molecules of ninhydrin react with a free α-amino acid to render the Ruhemann's purple [56]. Ninhydrin behaves as oxidizing agent causing the deamination and decarboxylation of the amino acids with the concomitant condensation between the reduced ninhydrin residue and the second molecule of ninhydrin with the release of ammonia, giving rise to a highly coloured diketohydrin complex.

In a first stage, we tested our sensory material with amino acid solutions mimicking collagen (COL), elastin (ELA) and epidermis (EPI), as we have depicted in previous works [57]. These are the main proteins conforming the skin, i.e., that are supposed to be related with the protease activity in chronic wounds. **Figure 2** shows the titration of F2 discs EPI, in sum of concentrations of all amino acids ranging from 5x10-4 to 1x10-2 M (ΣM). Further information related with the fitted curve, and equivalent experiments carried out with COL and ELA (**ESI-S5, Figure S7-S9**).
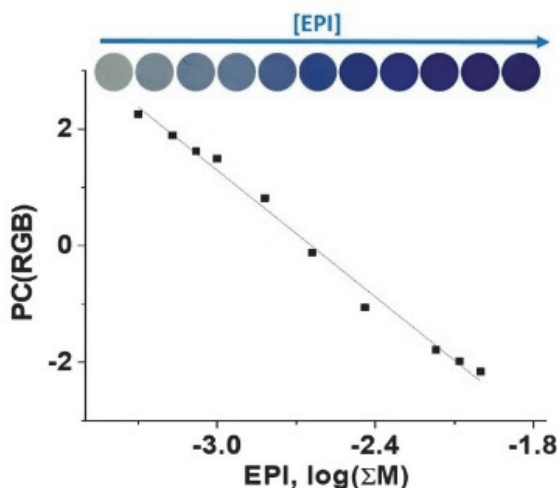
Figure 2. Titration of F_2 discs with solution mimicking epidermis (**EPI**) was performed with RGB_method. Discs of 8 mm diameter of F_2 were dipped in pH 4.66 buffered solutions of **EPI**, with a sum of concentrations of all amino concentrations ranging from $5x10^{-4}$ to $1x10^{-2}$ M ($\square$M). After reaction at 100oC for 60 min, the discs were washed several times with water, and photographed for the extraction of RGB data, which were simplified to a single variable (principal component, **PC**) through a multivariate analysis. Additional information can in **ESI section S5, Figure S6**.

3.5. Interference study

The study of interferences was carried out with a wide collection of anions and cations (**Figure 3**), by immersing an 8 mm diameter disc of F_2 in 1 mL of 4.66 buffer and 1 mL of an aqueous solution of the interferents at high concentration (10^{-2} M), at 100ºC for 60 min. The disc was photographed in the retro-illuminated lightbox. We observed no interferences concerning the application of the sensory material.
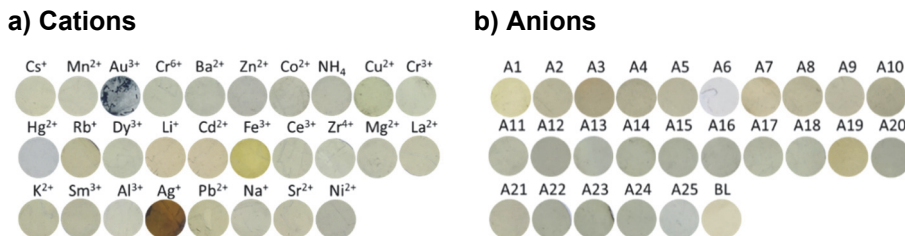
a) Cations   **b) Anions**

Figure 3. Discs of F2 were dipped for 60min at 100oC in a mixture of 1 mL of 4.66 buffer and 1 mL of an aqueous solution of the interferents (1x10-2 M). a) Cations of nitrate or chloride salt. b) Anions. A1=Cyanide, A2=acetate, A3=hydroxile, A4=fluoride, A5=perchlorate, A6=dodecyl sulfate, A7=nitrite, A8=ethoxide, A9=hydrogen phthalate, A10=pyrophosphate, A11=persulfate, A12=methanesulfonate, A13=pyrophosphate dibasic, A14=trifluoromethanesulfonate, A15=p-toluenesulfonate, A16=bromide, A17=thiocyanate, A18=oxalate, A19=carbonate, A20=benzoate, A21=dihydrogenphosphate, A22=sulfate, A23=chloroacetate, A24=trifluoroacetate, A25=periodate. See materials section

3.6. Testing the material with a real sample: food matrix, beef, loin cut.

After the test of the sensory material with **COL**, **ELA** and **EPI** solutions, and before the analysis with samples from human chronic wounds, we carried out a proof of concept with a beefsteak from the local market (see **ESI-S6, Figure S10**). The aim of this experiment was the detection of amino acids from the activity of the proteinase papain (papaya proteinase I) on the beefsteak by two different ways, the reference method and RGB_method. The degree of hydrolysis (DH%) produced by papain was measured at different times by reference method, as we explain thoroughly in **ESI section S6**. Additionally, at the same times, F_2 discs were immersed in a mixture of 1 ml from the beefsteak hydrolysis flask and 1 ml

of pH 4.66 buffer solution, and the system was heated for 60 min at 100°C. The discs were washed and photographed for the measurement of the RGB parameters and calculation of the principal component (PC). The results of both methods are shown in **Figure 4**, where we can see a good correlation between DH% obtained with the reference method, and PC obtained with RGB_method.
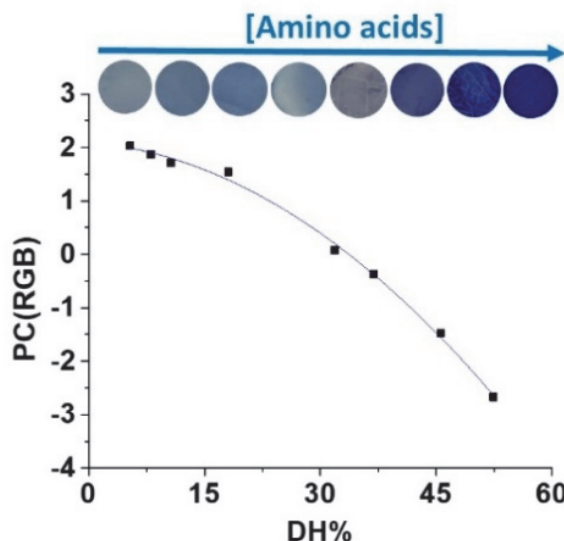
Figure 4. The figure shows the picture of F_2 discs after dipped for 60 min at 100°C in a mixture of 1 ml from the beefsteak hydrolysis flask and 1 ml of pH 4.66 buffer solution. After washed with water, the discs were photographed for measuring the RGB parameters and after that calculation of the principal component (PC). The graph shows the correlation of PC with the chosen reference method, which shows the amino acid concentration of the hydrolysis flask, expressed as the degree of hydrolysis (DH%), due to the proteinase activity of the enzyme papain (papaya proteinase I) on the beefsteak. Further information can be found in the **ESI section S6.**

3.7. Analysis of human chronic samples by data mining methods from data obtained with our methodology (RGB_method)

Once checked the response of the sensory discs to amino acids in the lab-prepared solutions (**COL**, **ELA** and **EPI**), and after the successful proof of concept following the proteinase activity of papain on a beef steak, we decided to initiate a study with 34 patients (all data can be found in **ESI section S7, Table S12**). The main objectives of this work are two: **1**) to replace the reference method used

so far for the quantification of amino acids, by the method that we propose in this work based on our sensory materials; **2)** to demonstrate that the amino acid concentration of a chronic wound is directly correlated with the state of the wound (according to the visual analysis of the medical personnel). For both, we have analysed five types of samples from each chronic human wound: swab (A), wound bed (B), edge (C), capsular tissue (D) and/or bone (E). Physicians at the HUBU collected the samples, according to the established protocols.

The study was carried out on a representative group of patients, taking into account variables such as age, and wound status. Two questions were stated:

1) *Is there a function f such that reference method = f(RGB_method) ?*

In this test, we try to establish if there is any kind of functional relationship between the variable obtained from reference method (absorbance at 330 nm, or ABS 330) and the variables R, G, B (which classically determine a colour depending on the values Red, Green and Blue from 0 to 255). The test was performed with a sample of n =35 cases, and three different models have been used: two linear models (Linear Regression, **LinR**, and Support Vector Regression, **SVR**) and a non-linear model (**SVR** with Gaussian Kernel, **SVR-GK**). For each test, we have analysed Mean Square Error (**MSE,** equation 1), Mean Absolute Error (**MAE,** equation 2) and Fit or R^2. Let's be O_i the observed value (each value of ABS 330) and E_i the value estimated for each model, in case i, i = 1…n:

$$MSE = \frac{1}{n} \cdot \left(\sum_{i=1}^{n} (O_i - E_i)^2 \right) \quad (1)$$

$$MAE = \frac{1}{n} \cdot \left(\sum_{i=1}^{n} |O_i - E_i| \right) \quad (2)$$

Fit = R^2 where R is Pearson's correlation between O_i y E_i.

The values of O_i have been standardised between 0 and 1. The results obtained are depicted in **Table 1**.

Table 1. Results of different models to adjust the values of ABS 330

	MSE	MAE	Adjustment (R^2)
LinR	0.0108585	0.0819458	0.6961003
SVR	0.0135306	0.0868035	0.6771253
SVR-GK	0.0085048	0.0599027	0.7700693

The results show great fits and low errors. Besides, Snedecor's F test to validate the **LinR** model gives a value of F = 23,669, with a probability queue $p <$ 0.001. Therefore, there is at least one significant linear functional relationship, and there could be a non-linear relationship because of the good results of SVR-KG. Thus, yes, our proposed RGB_method can replace the reference method.

2) *Is the concentration of amino acids in a chronic wound related to its condition?*

The state of the chronic wounds was determined by four parameters or pathologies: infectious appearance, bad evolution, necrosis and ischemia. Then, we compared these results with the amino acid concentration obtained by reference method and our proposed RGB_method. For this study, three linear classification methods were used: discriminant analysis (**DA**), logistic regression (**LR**) and support vector machine (**SVM**). With the observed data, a set of coefficients was determined (c_i) accompanying the explanatory variables, plus a free coefficient c_0. With these coefficients, the classification/diagnosis of a specific case was obtained by calculating the val parameter with Equation 3, where m is the number of explanatory variables and $v_1,\ldots, v_m$ are the values of these variables for this case. In this way, if $val > 0$, the case is diagnosed positive (YES) and otherwise negative (NO).

Table 2 depicts the results obtained by the three methods considered, using the absorbance at 330 nm in the case of reference method (m = 1), and RGB parameters in the case of the RGB_method (m = 3) as explanatory variables for all analysed medical parameters. The results include the number of successes (Sc, i.e. number of correctly diagnosed cases), the ratio (rat, from 0 to 1), and thenumber of positive and negative cases for each parameter.

Table 2. Results obtained by the diagnostic methods (discriminant analysis, **DA**, logistic regression, **LR**, and support vector machine, **SVM**) using both reference method and RGB_method as explanatory variables (absorbance at 330 nm and RGB parameters respectively).

Experimental Method	Medical parameter	Cases		Analysis Method		
		No	Yes	DA	LR	SVM
Reference Method	Infectious aspect	26	9	16 **(Sc)**	26	26
				0.4571 (rat)	*0.7429*	*0.7429*
	Bad evolution	21	14	20	**24**	21
				0.5714	*0.6857*	*0.6*
	Necrosis	26	9	24	25	26
				0.6857	*0.7143*	*0.7429*
	Ischemia	28	7	24	27	28
				0.6857	*0.7714*	*0.8*
RGB_method	Infectious aspect	25	9	19	23	25
				0.5588	*0.6765*	*0.7353*
	Bad evolution	21	13	19	**22**	21
				0.5588	*0.6471*	*0.6176*
	Necrosis	25	9	21	**31**	25
				0.6176	*0.9118*	*0.7353*
	Ischemia	27	7	22	26	27
				0.6471	*0.7647*	*0.7941*

$$val = c_0 + c_1 \cdot v_1 + \cdots + c_m \cdot v_m \qquad (3)$$

For reference method, apparently, there are several combinations parameter/method where an interesting rate of success is reached (in fact 12 of 16 over 68%). Still, we must be cautious about this: when the cases of each group are unbalanced as in this database, the classification methods can be limited to say that all are from the most numerous group and artificially get a good result. Therefore, initially, we only consider a number of successes higher than the largest group to be interesting. So that the diagnosis of the *bad evolution* explained by **LR** is an interesting result. For the RGB_method, we would consider as exciting the diagnosis of the *bad evolution* defined by LR and especially the 31 successes of 34 cases also achieved with **LR** in the diagnosis of *necrosis*. In short, the concentration of amino acids is directly correlated with the state of the wound, regardless of whether it was obtained using the reference method, or using the RGB_method. Even in the case of *necrosis*, the RGB_method combined with the **LR** method gives exciting results.

3.8. Figure of merits

There are many techniques/methods in the literature for detecting protease activity qualitatively or quantitatively. However, in most cases, these procedures need much time and/or their costs are very high because they require extensive instrumentation. **Table 3** shows a short study of the published detection methods for amino acid, in terms of the low-cost character, response time and naked-eye detection.

Table 3. Comparative table of analytical methods for amino acids.

Method name	Detection method	Low-cost[&]	Response time	Naked eye detection	Ref.
Reference method	UV-vis	no	15min	no	[41]
Spectrophotometric		no	1h	no	[58]
Quenched BODIPY	Fluorescence	no	1.5h	no	[59]
Fluorescence Polarisation		no	2h	no	[60]
SPR sensor		no	30min	no	[61]
Direct measurement		no	3.5h	no	[62]
Densitometry	Scanning densitometry	no	3h	no	[63]
In vivo	Metal-oxide-semiconductor imaging device	no	5h	no	[64]
Free porous silicon (PSi) photonic crystals	Optical Reflectivity	no	24h	no	[65]
Nanopore sensor	potentiometric	no	2h	no	[66]
RGB	Digital pictures (RGB parameters defining the digital colours)	yes	1h	yes	This work

[&] Low-cost: no need of equipment, maintenance and lab space for the equipment, and trained personal to carry on the measurements

4. Conclusions

We propose a new method and methodology for the control and diagnosis of chronic wounds based on pictures taken to discs cut from sensory films, which change their colour upon entering into contact with amino acids. The sensory polymeric material is inexpensively prepared by straightforward We propose a new method and methodology for the control and diagnosis of chronic wounds based on pictures taken to discs cut from sensory films, which change their colour upon entering into contact with amino acids. The sensory polymeric material is inexpensively prepared by straightforward procedures from 99% of commercially

available monomers. The experimental procedure is simple, neither reactants nor expensive equipment are needed, and can be straightforward carried out by untrained personnel by taking a photograph with a smartphone to the sensory material after immersing in the exudate. The sensor can be used in a broad pH range and has no interference with a vast number of anions and cations. Additionally, we have demonstrated that the state/evolution of the wound correlates with the concentration of amino acids. The chosen reference method for measuring amino acids (Nielsen method) [41] has shown to have good results in wound diagnosis. Mainly, in the case of *bad evolution*, the results are fascinating. In the other hand, it has been established that there is a functional relationship between the values of this reference method and the values of the digital colour of the photograph of the discs (R, G and B parameters). Even, the RGB values show to have a diagnostic capability of chronic wounds similar to the reference method, and better in the case of *necrosis*. We have used linear models, for data treatment and predictions, which are conceptually simple to understand and apply. However, more sophisticated models could significantly improve the quality of the results, and could be integrated into an easy to use software or smartphone app.

Acknowledgements

References

[1]   C.D. Hinman, H. Maibach, Effect of Air Exposure and Occlusion on Experimental Human Skin Wounds, Nature. 200 (1963) 377–378. https://doi.org/10.1038/200377a0.

[2]   G.C. Gurtner, S. Werner, Y. Barrandon, M.T. Longaker, Wound repair and regeneration, Nature. 453 (2008). https://doi.org/10.1038/nature07039.

[3]   G.M. Sundaram, J.E.A. Common, F.E. Gopal, S. Srikanta, K. Lakshman, D.P. Lunny, T.C. Lim, V. Tanavde, E.B. Lane, P. Sampath, 'See-saw' expression of microrna-198 and fstl1 from a single transcript in wound healing, Nature. 495 (2013) 103–106. https://doi.org/10.1038/nature11890.

[4]   P. Martin, J. Lewis, Actin cables and epidermal movement in embryonic wound healing, Nature. 360 (1992) 179–183. https://doi.org/10.1038/360179a0.

[5]   M. Zhao, B. Song, J. Pu, T. Wada, B. Reid, G. Tai, F. Wang, A. Guo, P. Walczysko, Y. Gu, T. Sasaki, A. Suzuki, J. V. Forrester, H.R. Bourne, P.N. Devreotes, C.D. McCaig, J.M. Penninger, Electrical signals control wound healing through phosphatidylinositol-3-OH kinase-γ and PTEN, Nature. 442 (2006) 457–460. https://doi.org/10.1038/nature04925.

[6]   M.C. Coles, C.D. Buckley, Ready-made cellular plugs heal skin wounds, Nature. 576 (2019) 215–216. https://doi.org/10.1038/d41586-019-03602-4.

[7]   S. Mahmoudi, E. Mancini, L. Xu, A. Moore, F. Jahanbani, K. Hebestreit, R. Srinivasan, X. Li, K. Devarajan, L. Prélot, C.E. Ang, Y. Shibuya, B.A. Benayoun, A.L.S. Chang, M. Wernig, J. Wysocka, M.T. Longaker, M.P. Snyder, A. Brunet, Heterogeneity in old fibroblasts is linked to variability in reprogramming and wound healing, Nature. 574 (2019) 553–558. https://doi.org/10.1038/s41586-019-1658-5.

[8]   P. Gómez Fernández, Revisión del tratamiento de las úlceras venosas: terapia compresiva, RqR Enfermería Comunitaria. 3 (2015) 43–54.

[9]   J. Posnett, F. Gottrup, H. Lundgren, G. Saal, The resource impact of wounds on health-care providers in Europe., J. Wound Care. 18 (2009) 154–161. https://doi.org/10.12968/jowc.2009.18.4.41607.

[10]   S.R. Nussbaum, M.J. Carter, C.E. Fife, J. DaVanzo, R. Haught, M. Nusgart, D. Cartwright, An Economic Evaluation of the Impact, Cost, and Medicare Policy Implications of Chronic Nonhealing Wounds, Value Heal. 21 (2018) 27–32. https://doi.org/10.1016/j.jval.2017.07.007.

[11]   L. MacGregor, K. Day, Principles of best practice: Diagnostics and wounds. A consensus document., Medical Education Partnership (MEP), London, 2008.

[12]   K. Day, Consenso internacional. Función de las proteasas en el diagnóstico de heridas. Revisión de un grupo de trabajo de expertos, Wounds International Enterprise House, London, 2011.

[13]   M.J. Westby, J.C. Dumville, N. Stubbs, G. Norman, N. Cullum, Protease-modulating matrix treatments for healing venous leg ulcers, Cochrane Database Syst. Rev. 2015 (2015). https://doi.org/10.1002/14651858.CD011918.

[14]   D.E. Kleiner, W.G. Stetlerstevenson, Quantitative zymography: Detection of picogram quantities of gelatinases, Anal. Biochem. 218 (1994) 325–329. https://doi.org/10.1006/abio.1994.1186.

[15]   Z.S. Calis, G.K. Sukhova, P. Libby, Microscopic localization of active proteases by in situ zymography: detection of matrix metalloproteinase activity in vascular tissue, FASEB J. 9 (1995) 974–980. https://doi.org/10.1096/fasebj.9.10.7615167.

[16]   M.F. Clark, A.N. Adams, Characteristics of the microplate method of enzyme linked immunosorbent assay for the detection of plant viruses, J. Gen. Virol. 34 (1977) 475–483. https://doi.org/10.1099/0022-1317-34-3-475.

[17]   M.T. Veledo, M. De Frutos, J.C. Diez-Masa, Amino acids determination using capillary electrophoresis with on-capillary derivatization and laser-induced fluorescence detection, J. Chromatogr. A. 1079 (2005) 335–343. https://doi.org/10.1016/j.chroma.2005.03.111.

[18]   A.E. Pasieka, M.E. Thomas, The detection of β-alanine in biological fluids, Clin. Biochem. 2 (1968) 423–429. https://doi.org/10.1016/s0009-9120(68)80101-8.

[19]   K. Mopper, P. Lindroth, Diel and depth variations in dissolved free amino acids and ammonium in the Baltic Sea determined by shipboard HPLC analysis, Limnol. Oceanogr. 27 (1982) 336–347. https://doi.org/10.4319/lo.1982.27.2.0336.

[20]   K. Petritis, C. Elfakir, M. Dreux, HPLC-CLND for the Analysis of Underivatized Amino Acids, LC GC Eur. 14 (2001) 389–395.

[21]   S. Katsikis, I. Marin-Montesinos, C. Ludwig, U.L. Günther, Detecting acetylated aminoacids in blood serum using hyperpolarized 13C-1H-2D-NMR, J. Magn. Reson. 305 (2019) 175–179. https://doi.org/10.1016/j.jmr.2019.07.003.

[22]   K. Adriaenssens, R. Vanheule, D. Karcher, Y. Hardens, A simple screening method for the study of amino acids in tissues using frozen slices, Clin. Chim. Acta. 18 (1967) 351–354. https://doi.org/10.1016/0009-8981(67)90030-7.

[23]   A. Saifer, Rapid screening methods for the detection of inherited and acquired aminoacidopathies, Adv. Clin. Chem. 14 (1971) 145–218. https://doi.org/10.1016/S0065-2423(08)60146-8.

[24]   A. Szeinberg, B. Szeinberg, B.E. Cohen, Screening method for detection of specific aminoacidemias, Clin. Chim. Acta. 23 (1969) 93–95. https://doi.org/10.1016/0009-8981(69)90015-1.

[25]   D. Kumar, M. Abdul Rub, M. Akram, Kabir-Ud-Din, Interaction of chromium(III) complex of glycylphenylalanine with ninhydrin in aqueous and cetyltrimethylammonium bromide (CTAB) micellar media, Tenside, Surfactants, Deterg. 51 (2014) 157–163. https://doi.org/10.3139/113.110296.

[26]   C.B. Bottom, S.S. Hanna, D.J. Siehr, Mechanism of the ninhydrin reaction, Biochem. Educ. 6 (1978) 4–5. https://doi.org/10.1016/0307-4412(78)90153-X.

[27]   S. Ruhemann, CXXXII. - Cyclic di- and tri-ketones, J. Chem. Soc. Trans. 97 (1910) 1438–1449. https://doi.org/10.1039/CT9109701438.

[28]   S. Ruhemann, LXXXIV. - Triketohydrindene hydrate. Part III. Its relation to alloxan, J. Chem. Soc. Trans. 99 (1911) 792–800. https://doi.org/10.1039/CT9119900792.

[29]   S. Ruhemann, CXLII. - Triketohydrindene hydrate. Part IV. Hydrindantin and its analogues, J. Chem. Soc. Trans. 99 (1911) 1306–1310. https://doi.org/10.1039/CT9119901306.

[30]   S. Ruhemann, CLXX. - Triketohydrindene hydrate. Part V. The analogues of uramil and purpuric acid, J. Chem. Soc. Trans. 99 (1911) 1486–1492. https://doi.org/10.1039/CT9119901486.

[31]   M. Friedman, Applications of the Ninhydrin Reaction for Analysis of Amino Acids, Peptides, and Proteins to Agricultural and Biomedical Sciences, J. Agric. Food Chem. 52 (2004) 385–406. https://doi.org/10.1021/jf030490p.

[32]   D.J. McCaldin, The chemistry of ninhydrin, Chem. Rev. 60 (1960) 39–51. https://doi.org/10.1021/cr60203a004.

[33]   J.H. Holtz, S.A. Asher, Polymerized colloidal crystal hydrogel films as intelligent chemical sensing materials, Nature. 389 (1997) 829–832. https://doi.org/10.1038/39834.

[34]   J. Xiao, Y. Tan, Y. Song, Q. Zheng, A flyweight and superelastic graphene aerogel as a high-capacity adsorbent and highly sensitive pressure sensor, J. Mater. Chem. A. 6 (2018) 9074–9080. https://doi.org/10.1039/c7ta11348j.

[35]   J. Hou, M. Liu, H. Zhang, Y. Song, X. Jiang, A. Yu, L. Jiang, B. Su, Healable green hydrogen bonded networks for circuit repair, wearable sensor and flexible electronic devices, J. Mater. Chem. A. 5 (2017) 13138–13144. https://doi.org/10.1039/c7ta03100a.

[36]   H.J. Salavagione, A.M. Díez-Pascual, E. Lázaro, S. Vera, M.A. Gómez-Fatou, Chemical sensors based on polymer composites with carbon nanotubes and graphene: The role of the polymer, J. Mater. Chem. A. 2 (2014) 14289–14328. https://doi.org/10.1039/c4ta02159b.

[37]   M. Guembe-García, P.D. Peredo-Guzmán, V. Santaolalla-García, N. Moradillo-Renuncio, S. Ibeas, A. Mendía, F.C. García, J.M. García, S. Vallejos, Why is the Sensory Response of Organic Probes within a Polymer Film Different in Solution and in the Solid-State? Evidence and Application to the Detection of Amino Acids in Human Chronic Wounds, Polymers (Basel). 12 (2020) 1249. https://doi.org/10.3390/polym12061249.

[38]   J.E. Eastoe, The amino acid composition of proteins from the oral tissues-II. The matrix proteins in dentine and enamel from developing human deciduous teeth, Arch. Oral Biol. 8 (1963) 633–652. https://doi.org/10.1016/0003-9969(63)90078-5.

[39]   F.W. Keeley, S.M. Partridge, Amino acid composition and calcification of human aortic elastin, Atherosclerosis. 19 (1974) 287–296. https://doi.org/10.1016/0021-9150(74)90063-X.

[40]   J.E. Eastoe, P. Martens, N.R. Thomas, The amino-acid composition of human hard tissue collagens in osteogenesis imperfecta and dentinogenesis imperfecta, Calcif. Tissue Res. 12

(1973) 91–100. https://doi.org/10.1007/BF02013724.

[41]   P.M. Nielsen, Improved Method for Determining Protein Hydrolysis, J. Food Sci. 66 (2001) 642–646.

[42]   S. Vallejos, D. Moreno, S. Ibeas, A. Muñoz, F.C. García, J.M. García, Polymeric chemosensor for the colorimetric determination of the total polyphenol index (TPI) in wines, Food Control. 106 (2019) 106684. https://doi.org/10.1016/j.foodcont.2019.06.010.

[43]   S. Vallejos, E. Hernando, M. Trigo, F.C. García, M. García-Valverde, D. Iturbe, M.J. Cabero, R. Quesada, J.M. García, Polymeric chemosensor for the detection and quantification of chloride in human sweat. Application to the diagnosis of cystic fibrosis, J. Mater. Chem. B. 6 (2018) 3735–3741. https://doi.org/10.1039/c8tb00682b.

[44]   S. Vallejos, A. Muñoz, S. Ibeas, F. Serna, F.C. García, J.M. García, Solid sensory polymer substrates for the quantification of iron in blood, wine and water by a scalable RGB technique, J. Mater. Chem. A. 1 (2013) 15435–15441. https://doi.org/10.1039/c3ta12703f.

[45]   S. Vallejos, J.A. Reglero, F.C. García, J.M. García, Direct visual detection and quantification of mercury in fresh fish meat using facilely prepared polymeric sensory labels, J. Mater. Chem. A. 5 (2017) 13710–13716. https://doi.org/10.1039/c7ta03902f.

[46]   S. Vallejos, P. Estévez, S. Ibeas, F.C. García, F. Serna, J.M. García, An organic/inorganic hybrid membrane as a solid "Turn-On" fluorescent chemosensor for coenzyme a (CoA), cysteine (Cys), and glutathione (GSH) in aqueous media, Sensors. 12 (2012) 2969–2982. https://doi.org/10.3390/s120302969.

[47]   A. Tharwat, Linear vs. quadratic discriminant analysis classifier: a tutorial, Int. J. Appl. Pattern Recognit. 3 (2016) 145. https://doi.org/10.1504/ijapr.2016.079050.

[48]   I.L. Lottes, M.A. Adler, A. DeMaris, Using and interpreting logistic regression: A guide for teachers and students, Teach. Sociol. 24 (1996) 284–298. https://doi.org/10.2307/1318743.

[49]   V. Vapnik, The Support Vector Method of Function Estimation, in: Nonlinear Model., Springer US, 1998: pp. 55–85. https://doi.org/10.1007/978-1-4615-5703-6_3.

[50]   G. Rozenberg, T. Back, J.N. Kok, Handbook of Natural Computing, 2012. https://doi.org/10.1007/978-3-540-92910-9.

[51]   H. Yu, S. Kim, SVM tutorial-classification, regression and ranking, Handb. Nat. Comput. 1– 4 (2012) 479–506. https://doi.org/10.1007/978-3-540-92910-9_15.

[52]   S. Vallejos, E. Hernando, M. Trigo, F.C. García, M. García-Valverde, D. Iturbe, M.J. Cabero, R. Quesada, J.M. García, Polymeric chemosensor for the detection and quantification of chloride in human sweat. Application to the diagnosis of cystic fibrosis, J. Mater. Chem. B. 6 (2018) 3735–3741. https://doi.org/10.1039/c8tb00682b.

[53]   S.E. Bustamante, S. Vallejos, B.S. Pascual-Portal, A. Muñoz, A. Mendia, B.L. Rivas, F.C. García, J.M. García, Polymer films containing chemically anchored diazonium salts with long-term stability as colorimetric sensors, J. Hazard. Mater. 365 (2019) 725–732. https://doi.org/10.1016/j.jhazmat.2018.11.066.

[54]   M.M. Joullié, T.R. Thompson, N.H. Nemeroff, Ninhydrin and ninhydrin analogs. Syntheses and applications, Tetrahedron. 47 (1991) 8791–8830. https://doi.org/10.1016/S0040-4020(01)80997-2.

[55]   M. Yin, Y. Ye, M. Sun, N. Kang, W. Yang, Facile one-pot synthesis of a polyvinylpyrrolidone-based self-crosslinked fluorescent film, Macromol. Rapid Commun. 34 (2013) 616–620. https://doi.org/10.1002/marc.201200750.

[56]   D.C. Wigfield, G.W. Buchanan, S.M. Croteau, On Ruhemann's Purple, Can. J. Chem. 58 (1980) 201–205. https://doi.org/10.1139/v80-032.

[57]   M. Guembe-García, P.D. Peredo-Guzmán, V. Santaolalla-García, N. Moradillo-Renuncio, S. Ibeas, A. Mendía, F.C. García, J.M. García, S. Vallejos, Why the sensory response of organic probes is different in solution and in the solid- state within a polymer film? Evidence and application to the detection of amino acids in human chronic wounds Marta Guembe-García, Unpubl. Work. (n.d.).

[58]   S. Stephan, H. Schwarz, A. Borchert, D. Bussfeld, E. Quak, B. Simshaeuser-Knaub, S. Teigelkamp, F. Behrens, F. Vitzthum, Tests for the measurement of factor VII-activating protease (FSAP) activity and antigen levels in citrated plasma, their correlation to PCR testing, and utility for the detection of the Marburg I-polymorphism of FSAP, Clin. Chem. Lab. Med. 46 (2008) 1109–1116. https://doi.org/10.1515/CCLM.2008.218.

[59]   L.J. Jones, R.H. Upson, R.P. Haugland, N. Panchuk-Voloshina, M. Zhou, R.P. Haugland, Quenched BODIPY dye-labeled casein substrates for the assay of protease activity by direct

fluorescence measurement, Anal. Biochem. 251 (1997) 144–152. https://doi.org/10.1006/abio.1997.2259.

[60]   L.M. Levine, M.L. Michener, M. V. Toth, B.C. Holwerda, Measurement of specific protease activity utilizing fluorescence polarization, Anal. Biochem. 247 (1997) 83–88. https://doi.org/10.1006/abio.1997.2047.

[61]   J. Park, G. Baik Kim, A. Lippitz, Y.M. Kim, D. Jung, W.E.S. Unger, Y.P. Kim, T.G. Lee, Plasma-polymerized antifouling biochips for label-free measurement of protease activity in cell culture media, Sensors Actuators, B Chem. 281 (2019) 527–534. https://doi.org/10.1016/j.snb.2018.10.123.

[62]   N. Safa, J.H. Pettigrew, T.J. Gauthier, A.T. Melvin, Direct measurement of deubiquitinating enzyme activity in intact cells using a protease-resistant, cell-permeable, peptide-based reporter, Biochem. Eng. J. 151 (2019) 107320. https://doi.org/10.1016/j.bej.2019.107320.

[63]   Y. Mori, H. Wada, E.C. Gabazza, N. Minami, T. Nobori, H. Shiku, H. Yagi, H. Ishizashi, M. Matsumoto, Y. Fujimura, Predicting response to plasma exchange in patients with thrombotic thrombocytopenic purpura with measurement of vWF-cleaving protease activity, Transfusion. 42 (2002) 572–580. https://doi.org/10.1046/j.1537-2995.2002.00100.x.

[64]   D.C. Ng, H. Tamura, T. Tokuda, A. Yamamoto, M. Matsuo, M. Nunoshita, Y. Ishikawa, S. Shiosaka, J. Ohta, Real time in vivo imaging and measurement of serine protease activity in the mouse hippocampus using a dedicated complementary metal-oxide semiconductor imaging device, J. Neurosci. Methods. 156 (2006) 23–30. https://doi.org/10.1016/j.jneumeth.2006.02.005.

[65]   B. Gupta, K. Mai, S.B. Lowe, D. Wakefield, N. Di Girolamo, K. Gaus, P.J. Reece, J.J. Gooding, Ultrasensitive and Specific Measurement of Protease Activity Using Functionalized Photonic Crystals, Anal. Chem. 87 (2015) 9946–9953. https://doi.org/10.1021/acs.analchem.5b02529.

[66]   L. Wang, Y. Han, S. Zhou, X. Guan, Real-time label-free measurement of HIV-1 protease activity by nanopore analysis, Biosens. Bioelectron. 62 (2014) 158–162. https://doi.org/10.1016/j.bios.2014.06.041.

CAPÍTULO 3

Polímeros sensores para la detección de zinc (II)

El Zinc (Zn(II)) es una especie química esencial a nivel biológico. Se trata del catión más abundante a nivel celular. Se encuentra en todo los tejidos y fluidos, y participa en un gran número de procesos biológicos, como por ejemplo en la síntesis de ADN o los procesos de cicatrización. Tanto su déficit como su exceso ocasionan problemas de salud. Por ello, su determinación y cuantificación es relevante a la hora de diagnosticar o evaluar ciertas enfermedades y trastornos. Aunque existen muchas técnicas analíticas para este fin, una de las maneras más comunes de determinarlo es a través de la formación de complejos fluorescentes entre el Zn(II) y moléculas receptoras, como el Zinquin y sus derivados.

3.1. Introducción

El Zn(II) es considerado un oligoelemento porque tiene un papel imprescindible en el organismo a pesar de su baja concentración. Se estima que el Zn(II) total en un adulto está entre 2.5 g en hombres y 1.5 g en mujeres.[78] En sangre solo podemos encontrar entre 70 y 125 µg/dl, ya que más del 95% es Zn(II) intracelular, y está presente en todo tipo de órganos y tejidos. También forma

---

[78] V. J. Temple and A. Masta, *P. N. G. Med. J.*, **2004**, 47, 146–158.

parte de más de 300 enzimas, e interviene en un gran número de procesos biológicos.[79,80]

Tanto su exceso como su defecto son perjudiciales y están asociados con distintitos trastornos y enfermedades. Por ejemplo, el exceso de Zn(II) es tóxico para el ser humano, y causa fallos en la función inmune, reducción de los niveles de colesterol HDL, vómitos, daños gástricos, cansancio y fatiga. Por el contrario, un defecto de Zn(II) afecta al sistema gastrointestinal, nervioso central, inmunitario, óseo y reproductor. Además, está relacionado con enfermedades como la diabetes de tipo II, el cáncer, el Alzheimer, trastornos hepáticos y el VIH, o con procesos biológicos como el envejecimiento celular, los procesos de cicatrización cutáneos y los procesos de oxidación a nivel celular.[78]

El papel que desempeña el Zn(II) en el medio biológico se puede clasificar en tres funciones claramente diferenciadas y esenciales:

1. *Catalítica***:** existe un gran número de enzimas conocidas como "Enzimas dependientes de Zn(II)", que contienen un átomo de Zn(II) sin el que no pueden llevar a cabo su función. Un ejemplo de este tipo de enzimas son algunas metaloproteasas (**Figura 3.1**), cuya función está asociada a los procesos de regeneración celular en las heridas crónicas.

2. *Estructural*: algunas proteínas necesitan Zn(II) para formar su estructura funcional, como es el caso de la metaloproteasa MMP-2 (**Figura 3.1**), que además de un átomo de Zn(II) catalítico también tiene otro estructural.

3. *Regulatoria*: Las proteínas comúnmente denominadas como "dedos de zinc" (**Figura 3.1**), son conocidas por su papel regulador en la síntesis de ADN, ya que activan los factores de transcripción y controlan la expresión genética.[2] Además, el Zn(II) también tiene un papel importante en la liberación hormonal y la transmisión del impulso nervioso.

---

[79] JC. Fleet. Zinc, Copper, and Manganese. In: Stipanuk MH , editor .Biochemical and Physiological aspects of Human Nutrition .New York; Saunders**: 2000**. p.741-759.

[80] JC. King, CL. Keen. Zinc. In. Shils ME, OlsonJA , Shike M, Ross CA, editors. Modern Nutrition in Health and Disease. 9th Ed. NewYork ; Lippinkott Williams& Wilkins: **2003**. p.223-239.

Actualmente se está estudiando se implicación junto con el Cu (II) en enfermedades neurodegenerativas como el Alzheimer.[81-83]
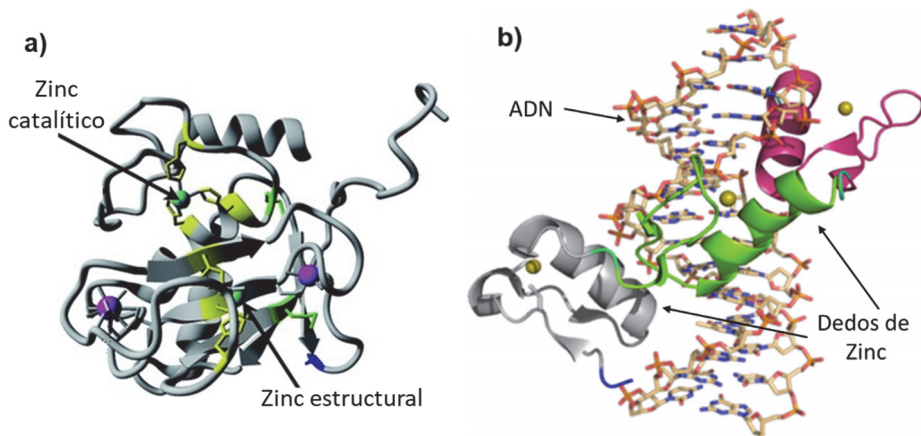
Figura 3.1. Estructuras cuaternarias de proteínas que contienen Zn(II): a) Estructura de la enzima MMP-2 con dos átomos de Zn(II), uno con función estructural y otro catalítico;[84] y b) estructura de la enzima "dedos de zinc" (α-hélices gris, verde y magenta), interactuando con el ADN.[85]

En una etapa del desarrollo de mi tesis se planteó la hipótesis de que el catión Zn(II) pudiera ser un marcador para la cuantificación directa de metaloproteasas, dado que está presente en muchas de las enzimas con función estructural y/o catalítica. Aunque en la bibliografía podemos encontrar una gran variedad de técnicas para la detección de Zn y Zn(II), ICP-masas ("*Inductively Coupled Plasma Mass Spectrometry),*[86] radiometría,[87,88] electroquímica,[89]

[81] K. Socha, K. Klimiuk, S. K. Naliwajko, J. Soroczyńska, A. Puścion-jakubik, R. Markiewicz-żukowska and J. Kochanowicz, Nutrients, **2021**, 13, 1–14.

[82] M. Scholefield, S. J. Church, J. Xu, S. Patassini, F. Roncaroli, N. M. Hooper, R. D. Unwin and G. J. S. Cooper, Front. Aging Neurosci., **2021**, 13, 1–16.

[83] S. Li and K. Kerman, Biosens. Bioelectron., **2021**, 179, 113035.

[84] G. Grasso and S. Bonnet, *Metallomics*, **2014**, 6, 1346–1357.

[85] K. S. Eom, J. S. Cheong and S. J. Lee, *J. Microbiol. Biotechnol.*, 2016, 26, 2019–2029.

[86] P. Arrowsmith, *Laser Ablation of Solids for Elemental Analysis by Inductively Coupled Plasma Mass Spectrometry*, **1987**, vol. 59.

[87] N. C. Lim, J. V. Schuster, M. C. Porto, M. A. Tanudra, L. Yao, H. C. Freake and C. Brückner, *Inorg. Chem.*, **2005**, 44, 2018–2030.

[88] Y. Lv, M. Cao, J. Li and J. Wang, *Sensors (Switzerland)*, **2013**, 13, 3131–3141.

[89] J. Kudr, H. V. Nguyen, J. Gumulec, L. Nejdl, I. Blazkova, B. Ruttkay-Nedecky, D. Hynek, J. Kynicky, V. Adam and R. Kizek, *Sensors (Switzerland)*, 2014, 15, 592–610.

potenciometria[90] o Fibra óptica (espectroscopia UV-vis),[91] las técnicas más utilizadas para la detección y/o cuantificación de Zn(II) son la espectroscopia UV-vis y la fluorimetría,[92,93] a través de la formación de complejos de coordinación.

Si bien es cierto que para poder detectar Zn(II) a través de la formación de un complejo organometálico el metal no puede estar coordinado a la proteína, también es cierto que las constantes de complejación de este tipo de metales con receptores basados en quinolinas son extremadamente altas, incluso mayores que las constantes que presenta con la propia enzima.[24,94,95] Esto supone una gran ventaja, ya que hace posible la detección de Zn(II) estructural y/o catalítico de enzimas como las metaloproteasas con este tipo de receptores. Los complejos de Zn(II) con cumarinas o quinolinas se caracterizan por tener altos rendimientos cuánticos, de manera que, en presencia de estos compuestos, la fluorescencia aumenta de manera directamente proporcional a la concentración de Zn(II). Dado que el compuesto más utilizado para este tipo de medidas es el "Zinquin" (derivado de quinolina, CAS 151606-29-0), se decidió sintetizar un monómero sensor (receptor) inspirado en ese tipo de estructura, preparado a través de la ruta sintética que se muestra en la **Figura 3.2.**

Con estos monómeros sensores, en este estudio se propone la preparación y utilización de polímeros sensores para la detección de Zn(II) en muestras biológicas procedentes de exudados de heridas crónicas. Se trata de un proceso de encendido de la fluorescencia, *Off-On*, que además de registrarse con un fluorímetro, también se caracterizó a través de los parámetros RGB que definen el color del sensor en una fotografía digital hecha con un teléfono

[90] M. A. Abbasi, Z. H. Ibupoto, M. Hussain, Y. Khan, A. Khan, O. Nur and M. Willander, *Sensors (Switzerland)*, **2012**, 12, 15424–1543.
[91] S. Kopitzke and P. Geissinger, *Sensors (Switzerland)*, **2014**, 14, 3077–3094.
[92] F. Zhou, C. Li, H. Zhu and Y. Li, *Optik (Stuttg).*, **2019**, 182, 58–64.
[93] R. Pandey, A. Kumar, Q. Xu and D. S. Pandey, *Dalt. Trans.*, **2020**, 49, 542–568.
[94] G. K. Walkup and B. Imperiali, *J. Am. Chem. Soc.*, **1997**, 119, 3443–3450.
[95] A. B. Nowakowski, J. W. Meeusen, H. Menden, H. Tomasiewicz and D. H. Petering, Inorg. Chem, **2015**, 54, 11637–11647.

inteligente. El estudio completo se publicó en la revista *Reactive and Functional Polymers.*[96]

a)   **b)**

c)
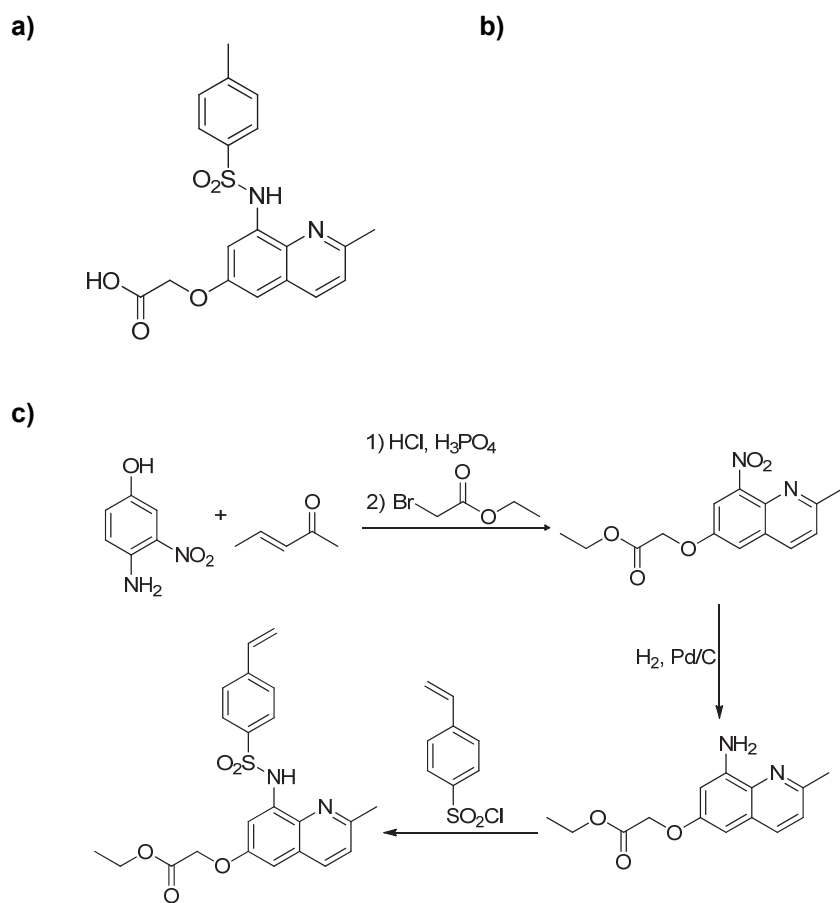
Figura 3.2. Sistema sensor basado en Zinquin: a) Estructura Zinquin; b) Sistema sensor polimérico con Zinquin modificado; c) Ruta sintética.

3.2. Resultados

A continuación, se describen los resultados obtenidos a través de la transcripción íntegra del trabajo publicado:

- *Zn(II) detection in biological samples with a smart sensory polymer.*

---

[96] M. Guembe-García, S. Vallejos, I. Carreira-Barral, S. Ibeas, F. C. García, V. Santaolalla-García, N. Moradillo-Renuncio and J. M. García, *React. Funct. Polym.*, **2020**, 154, 104685.

Zn(II) detection in biological samples with a smart sensory polymer

Zn(II) detection in biological samples with a smart sensory polymer

Marta Guembe-García,[1] Saúl Vallejos,[1,*] Israel Carreira-Barral,[1] Saturnino Ibeas,[1] Félix C. García,[1] Victoria Santaolalla-García,[2] Natalia Moradillo-Renuncio,[2] José M. García[1,*]

[1] Departamento de Química, Facultad de Ciencias, Universidad de Burgos, Plaza de Misael Bañuelos s/n, 09001 Burgos, Spain. E-mail: jmiguel@ubu.es (J.M.G.), svallejos@ubu.es (S.V.)
[2] Complejo Asistencial Universitario de Burgos, Burgos, Spain
* Correspondence: svallejos@ubu.es (S.V.); jmiguel@ubu.es (J.M.G.)

Abstract

We have developed a new sensory material for the rapid and inexpensive determination of Zn(II), and we have carried out a proof of concept for the determination of Zn(II) in biological samples. The interaction with Zn(II) generates an OFF-ON fluorescence process on the material, which can be recorded both with a fluorimeter and with a smartphone by analyzing the RGB components of the taken photographs. This sensory material is prepared with 99.75% of commercially available monomers and contains 0.25% of a sensory monomer based on a quinoline structure. The sensory motifs are chemically anchored to the polymeric structure, and, accordingly, no migration of organic substances from the material occurs during the sensing process. Our method has been tested with freshly prepared Zn(II) aqueous solutions, but also with biological samples from exudates of chronic wounds. The proposed methodology provides limits of detection (LOD) of 13 and 27 ppb when employing a water-soluble polymer (WsP) and a hydrophilic polymeric film (HP), respectively, using emission spectroscopy. The measurements have been contrasted with ICP-MS as the reference method, obtaining reliable data. This study is the starting point towards a larger investigation with patients, which will address the challenge of establishing a direct relationship between the concentration of zinc(II), other cations and also of amino acids, with the protease activity and, finally, with the state/evolution of chronic wounds. In this context, the proposed sensory material and others we are now working with will act as a simple and cheap method for this purpose.

Keywords: smart materials; sensory polymers; zinc(II) detection; biological samples; chronic wounds.

1. Introduction

Zn(II) is an essential element for human body. It is found in secretions such as urine, sweat, semen, and hair, but it is mostly located in muscles and bones [1]. The concentration of Zn(II) can be especially high in some organs, such as liver or skin, where up to 5% of all the Zn(II) present in the human body can be found. Regarding cells, Zn(II) can reach pico- to nanomolar concentrations inside, and micromolar concentrations in the extracellular space [2].

Also, Zn(II) is part of more than 300 enzymes with different functions, in which it is present as a structural, catalytic and/or regulatory component [3,4]. Given this multifunctionality of Zn(II), the deficiency of this ion has a great impact on the organism, and it is related to gastrointestinal disorders,[5] kidney and liver diseases [6], dermatitis [7], hypogonadism [8], or impartial wound healing [9,10]. In fact, the relationship between Zn(II) deficiency and impaired wound healing has been a research topic in recent years [11,12].

Other authors have studied the relationship between Zn(II) and prostate cancer, developing specific markers of Zn(II) to monitor the disease [13]. To assess the Zn(II) status in the body, serum, plasma, and erythrocyte levels are used as biomarkers [14–19]. In day to day, hospital laboratories analyze serum zinc(II) by UV-Vis spectrophotometry, especially to adjust the Zn(II) percentage in parenteral nutrition, but this methodology requires expensive equipment and skilled people.

Smart sensory polymers are a really hot topic [20–24], and have provided good results with easy procedures [25], so we propose a rapid, inexpensive and easy-to-use sensory material, which generates a visual fluorescent response

measurable with a simple smartphone. Our material will provide rapid information about the Zn(II) concentration of the biological sample; corrective personalized treatments could be applied by the medical staff. The main objective of this study is to prepare a polymeric sensory material for the easy and rapid detection of Zn(II), taking into consideration that not all Zn(II) is accessible; for example, when coordinated as a structural or catalytic component in different enzymes. Thus, we have designed a sensory material with quinoline-based receptors for the recognition of this metal ion, the complex formation being highly favorable from the thermodynamic point of view [26–29]. Our quinoline derivative is based on the 'Zinquin' (CAS number: 151606-29-0) structure, a commercially available reagent [30], which behaves as a membrane-permeable fluorophore and is commonly used to detect Zn(II) in cells [31] and to control the change in intracellular Zn(II) concentrations in thymocytes and hepatocytes [32].

Our sensory material has been tested with freshly prepared Zn(II) aqueous solutions and, most importantly, with real samples obtained from exudates of chronic wounds, following procedures established by the Vascular Surgery Unit at Burgos University Hospital (HUBU). This is the first of a set of studies devoted to prepare a sensory material which will act as a simple and cheap method to analyze relationships between the concentration of zinc(II), other cations and amino acids, and the protease activity of chronic wounds as well as the state/evolution of these wounds.

2. Experimental

2.1. Materials

Materials and solvents are commercially available and were used as received unless otherwise indicated. The following materials and solvents were employed: *trans*-crotonaldehyde (≥99%, Sigma-Aldrich), 3,4-dinitrophenol (98%, Acros Organics), palladium on carbon (10%, Sigma-Aldrich), ethanol absolute (100%, VWR), methanol (100%, VWR), dichloromethane (100%, VWR), hexane (95%,

VWR), ethyl acetate (99.9%, VWR), thionyl chloride (99%, VWR), sodium 4-vinylbenzenesulfonate (≥90%, Sigma-Aldrich), dimethylformamide (99%, VWR), diethyl ether (99.7%, VWR), sodium sulfate (≥99%, VWR), pyridine (99.5%, Merck), 2,2′-azobis(2-methylpropionitrile) (AIBN) (98%, Aldrich), 1-vinyl-2-pyrrolidone (**VP**) (99%, Acros Organics), methylmethacrylate (**MMA**) (99%, Merck), pH 4.66 buffer (VWR), zinc(II) nitrate hexahydrate (98%, Sigma-Aldrich), quinine sulfate (99%, Sigma-Aldrich), cesium nitrate (≥99%, Fluka), manganese(II) nitrate hexahydrate (98+%, Alfa Aesar), tetrachloroauric(III) acid trihydrate (99.9+%, Sigma-Aldrich), potassium dichromate (≥99.5%, Sigma-Aldrich), barium chloride dihydrate (99%, Labkem), cobalt(II) nitrate hexahydrate (≥99%, Labkem), ammonium nitrate (≥98%, Sigma-Aldrich), calcium nitrate tetrahydrate (≥99%, Sigma-Aldrich), chromium(III) nitrate nonahydrate (98.5%, Alfa Aesar), mercury(II) nitrate (98%, Alfa Aesar), rubidium nitrate (99.95%, Sigma-Aldrich), dysprosium(III) nitrate (99.9%, Alfa Aesar), lithium chloride (≥99%, Sigma-Aldrich), cadmium nitrate tetrahydrate (98.5%, Alfa Aesar), iron(III) nitrate nonahydrate (VWR-Prolabo), cerium(III) chloride tetrahydrate (≥99.99%, Sigma-Aldrich), zirconium(IV) chloride (98%, Alfa Aesar), lanthanum(III) nitrate hexahydrate (99.9%, Alfa Aesar), potassium nitrate (99+%, Sigma-Aldrich), samarium(III) nitrate (99.9%, Alfa Aesar), magnesium nitrate hexahydrate (≥99%, Labkem), aluminum nitrate nonahydrate (≥98.9%, Sigma-Aldrich), silver nitrate (≥99.9%, Sigma-Aldrich), neodymium(III) nitrate (99.9%, Alfa Aesar), lead(II) nitrate (≥99%, Fluka), strontium nitrate (99+%, Sigma-Aldrich), copper(II) nitrate trihydrate (98%, Sigma-Aldrich), nickel(II) nitrate hexahydrate (98.5%, Sigma-Aldrich), sodium nitrate (99%, LabKem), tin(II) chloride (98%, Sigma-Aldrich) and zinc(II) chloride (≥98%, Sigma-Aldrich).

Real biological samples (exudates) were removed from chronic wounds in patients admitted at the Vascular Surgery Unit in HUBU. According to the status of the patient and considering the needs of each particular wound, a swab was carefully and exhaustively scraped all over the clean loss of substance, under strict aseptic and antiseptic conditions.

2.2. Measurements and instrumentation

The color of each pixel in the RGB color model is expressed indicating how much of the three variables red (R), green (G) and blue (B) define it. The R, G and B triplet defining a digital color in the model can vary from zero to a maximum, typically integers from 0 to 255 in digital cameras of smartphones and computers. In this work we analyze the color of the sensory polymers was using this model, thus considering the digital red (R), green (G) and blue (B) color parameters (RGB) of the material (from now on the RGB method). Digital pictures were taken to the sensory discs (12 mm diameter; this is the inside distance from one corner to the opposite one –diagonal– of a standard 1 x 1 cm fluorescence cuvette) with a Huawei Mate 20 X smartphone after their immersion in aqueous media with different Zn(II) concentrations. To obtain a good reproducibility of the results, and to avoid external influences in the photographs, these were taken in a dark room. The digital photographs were analyzed with a generic image software to obtain the RGB parameters of the complete surface of the sensory disc. Photographs were taken six-fold for error calculations, for each the RGB parameters were overaged from the pixels of the overall disc within the picture, and then the six triplet defining the color of the disc (R, G and B variables) were again averaged. For this system, the simple study of each component versus the logarithm of Zn(II) molarity shows that the green component varies linearly with Zn(II) concentration. This easy and cheap method allows the quantification of Zn(II) in aqueous media, by only taking a photo, and we have widely used it in previous works [33,34].

Fluorescence spectra were recorded by triplicate using a F-7000 Hitachi Fluorescence spectrophotometer. Measurements with the water-soluble polymer (**WsP**) were carried out in a conventional cuvette, with no special procedures. However, measurements with the hydrophilic polymeric film (**HP**) were conducted by positioning the membrane vertically in the spectrofluorimeter and at 45° regarding the light source and the detector, as we describe in a previous article [35]. The reflection of light on the film surface was prevented from reaching the

detector by placing the discs in a position such that the light source would hit the discs on one side; the other side would emit the detected light, with the reflected one going in the opposite direction.·

The starting material was thermally and mechanically characterized using thermogravimetric analysis (TGA, 10–15 mg of a sample under synthetic air and nitrogen atmosphere with a TA Instruments Q50 TGA analyzer at 10 °C·min^{-1}), differential scanning calorimetry (DSC, 10–15 mg of a sample under a nitrogen atmosphere with a TA Instruments Q200 DSC analyzer at 20 °C·min^{-1}), and tensile properties analysis (5 × 9.44 × 0.122 mm samples using a Shimadzu EZ Test Compact Table-Top Universal Tester at 1 mm·min^{-1}). The infrared spectra (FT-IR) of the synthesized compounds and prepared sensory films were recorded using a JASCO FT-IR 4200 (4000-400 cm^{-1}) spectrometer.

High-resolution electron-impact mass spectrometry (EI-HRMS) was carried out on a Micromass AutoSpect Waters mass spectrometer (ionization energy: 70 eV; mass resolving power: >10,000). Inductively coupled plasma mass spectrometry (ICP-MS) measurements were recorded on an Agilent 7500 ICP-MS spectrometer. ^{1}H and ^{13}C NMR spectra were recorded with a Varian Inova 400 spectrometer operating at 399.92 and 100.57 MHz, respectively, with deuterated dimethyl sulfoxide as the solvent. The weight percentage of water taken up by the films upon soaking in pure water at 20 °C until reaching equilibrium (water-swelling percentage, WSP) was obtained from the weight of a dry sample film (ω_d) and its water-swelled weight (ω_s) using the following expression: WSP=100×[(ω_s−ω_d)/ω_d].

Three-dimensional X-ray data were collected on a Bruker D8 VENTURE diffractometer, and the powder X-ray diffraction (PXRD) patterns were obtained using a Bruker D8 Discover (Davinci design) operating at 40 kV, using Cu(Ka) as the radiation source, a scan step size of 0.02º, and a scan step time of 2 s.

Quantum yields (F) were measured in *N,N*-dimethylacetamide (DMA) using quinine sulfate in sulfuric acid (0.05 M) as a reference standard [36].

2.3. Sensory monomer synthesis

The sensory monomer derived from 8-aminoquinoline was prepared and characterized according to the experimental procedure described in the electronic supplementary information, **ESI (Section S1)**, and shown schematically in **Figure 1**.
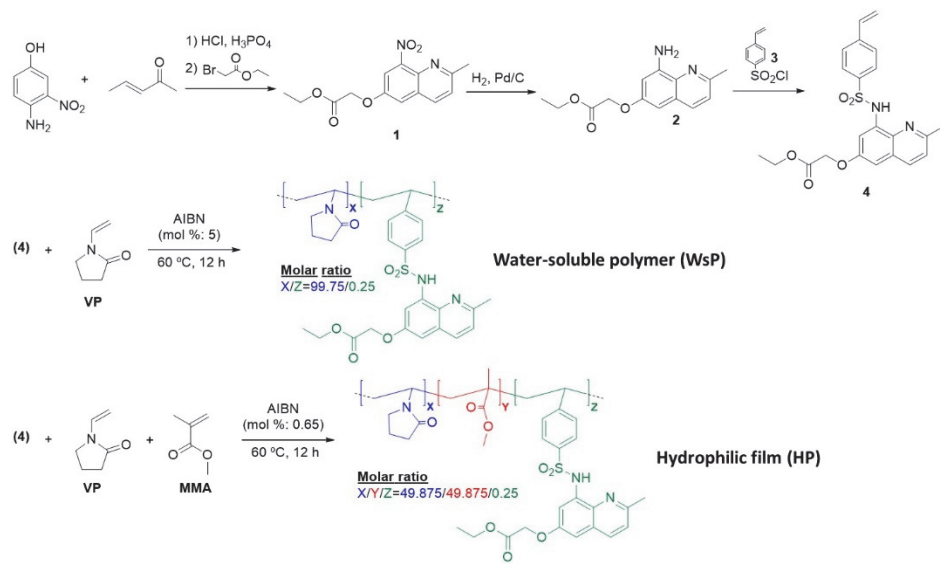
Figure 1. Synthetic route for sensory monomer **4** and its copolymerization with different commercial monomers (**VP** and **MMA**).

2.4. Polymer synthesis

*Water-soluble polymer (**WsP**)*

The linear copolymer (**WsP**) was prepared by radical polymerization of hydrophilic monomer **VP** and sensory monomer **4** in a 99.75/0.25 molar ratio, respectively (**Figure 1**). 0.11 mmol (48 mg) of **4** and 45 mmol (5 g) of **VP** were dissolved in DMF (22 mL) and the solution added to a round-bottom pressure

flask. Subsequently, radical thermal initiator AIBN (370 mg, 2.25 mmol, 5% of the total mol amount) was added and the solution sonicated for 10 min; then, it was heated at 60 °C overnight, under a nitrogen atmosphere and without stirring. The relative high amount of AIBN provides small polymers, or even oligomers, with a molecular mass of around 1000 (measured by ESI-TOF), which favors solubility and does not increase viscosity excessively. After that, the solution was cooled down and added in a dropwise manner to diethyl ether (300 mL) with vigorous stirring, yielding the desired product as a white precipitate. The water-soluble polymer was purified in a Soxhlet apparatus with diethyl ether as the washing solvent. The final product was dried overnight in a vacuum oven at 60 ^{0}C. Yield: 85%.

*Hydrophilic Film (**HP**)*

The starting material was obtained by radical copolymerization of the different monomers: **VP** as the hydrophilic monomer, **MMA** as the hydrophobic monomer, and **4** as the sensory monomer (**Figure 1**). The bulk radical polymerization was carried out in a silanized glass mold (100 µm thick) in an oxygen-free atmosphere at 60 °C overnight to obtain the hydrophilic film. Regarding the molar ratio of the monomers, this can be adjusted for different purposes. In our case, the fluorimetric response of the material toward Zn(II) was modulated by adjusting the molar feed ratio of monomers to 49.875/49.875/0.25 (**VP/MMA/4**), using 0.65% mol of AIBN. The relatively small amount of AIBN renders a high molecular mass polymer of around 1×10^6 (measured by GPC), which gives good mechanical properties to the film.

3. Results and discussion

3.1. Water uptake of the hydrophilic film

The swelling percentage of the hydrophilic film is a critical parameter to obtain a sensory material with good manageability and reasonable response times. This

is achieved by reaching the optimum ratio between the hydrophilic co-monomer (**VP**) and the hydrophobic co-monomer (**MMA**), since, if the material swells a lot (above 100%), response times will lower, but manageability will be bad. With swellings below 50%, the workability of the material may be high, but response times will be long. Therefore, given our experience in this area, we propose a material with 60% swelling for this work, which is achieved with a molar percentage of both **VP** and **MMA** of 49.875%. In this case, the molar ratio of the sensory monomer was set at 0.25%, to modulate the fluorescent signal according to the fluorimeter.

The three-dimensional hydrophilic film network generates a protective environment for the detection of targets, as we will report, since it reduces the interactions between the sensory monomer receptors and the solvent (water) [37]. This, together with its ability to anchor organic molecules (insoluble in water) in a hydrophilic polymer, favors the Zn(II) detection process within the hydrophilic film.

3.2. Thermal and mechanical characterization

We consider that a material has good manageability when it presents some technical features regarding its thermal and mechanical stability. In this case, the hydrophilic film displays good manageability. TGA analysis shows that T_5 and T_{10} (temperatures at which 5% and 10% weight loss, respectively, was observed) possess values of 345 ºC and 358 ºC, respectively. The material was also characterized by analyzing its glass transition temperature (Tg) by DSC, obtaining a value of 142 ºC. Both TGA and DSC patterns are shown in **ESI (Section S2)**.

Mechanical properties were tested with testing strips cut from the hydrophilic film and dried at 60 ºC for 1 hour. Strips were 0.5 mm wide, 3 cm long, and 0.1 mm thick, and the resulting Young's modulus was 986 MPa. These data confirm the manageability visually observed upon film handling.

### 3.3. CIE chromaticity coordinates and quantum yield

CIE chromaticity coordinates were calculated from the fluorescence spectra for the determination of the perceived color of **WsP** in the presence of Zn(II) upon irradiation in terms of the corresponding CIE 1931 color matching functions [38]. The results show values for X and Y coordinates of 0.15 and 0.25, respectively, according to the observed blue color. **Figure S4** of **ESI**, **Section S3** displays the CIE chromaticity coordinates (x and y) drawn on the CIE 1931 xy chromaticity diagram. The quantum yield was calculated from a solution of **4** in THF in the presence of one equivalent of Zn(II); quinine sulfate was used as a fluorescence reference in acidic media (0.05 M sulfuric acid) as depicted in previous works [35]. The results show that the Zn(II):**4** complex has a high quantum yield (F = 0.27), a datum similar to that of the reference, quinine sulfate (F = 0.53).

3.4. X-ray diffraction analyses

The solid-state structures of compounds **4** and Zn(II):**4** were determined by using single-crystal X-ray diffraction analyses (see **Figure S5** in **ESI**, **Section S4**, and **Figure 2,** respectively). Crystals of Zn(II):**4** contain the $[Zn(\mathbf{4})Cl_2]^-$ anion, a $(\mathbf{4}\text{-H})^+$ cation and a crystallization water molecule; the presence of both the anionic complex, coming from the deprotonation of the N-H fragment of the sulfonamide group, and the quinolinium cation accounts for the amphoteric nature of the monomer. The metal coordination environment can be described as distorted tetrahedral, with the nitrogen atoms of the sulfonamide and quinoline moieties [N(1) and N(2), respectively] and the two chloride anions [Cl(1) and Cl(2)] occupying the four coordination positions. The average Zn-N and Zn-Cl distances are 2.03 Å and 2.24 Å, respectively, similar to those reported in the literature for other Zn(II) complexes with a tetrahedral environment around the metal centre [39–41]. The distortion of the coordination polyhedron is mainly provoked by the small bite angle of **4** [N(1)-Zn(1)-N(2) 81.2°], which deviates remarkably from the ideal tetrahedral angle (109.5°). This structure is stabilized by slipped π-π stacking interactions involving the quinoline moiety of the protonated monomer

and that of the complex (mean centroid···centroid: 3.66 Å), as well as by an array of hydrogen-bonding interactions: among those of moderate strength [42,43], that in which the N-H fragment of the protonated ligand's sulfonamide group and one of the chloride anions are implied [N(4)···Cl(1) 3.17 Å, N(4)-H(4)···Cl(1) 169°] and those involving the water molecule [N(3)···O(11) 2.73 Å, N(3)-H(3)···O(11) 161°; O(11)···O(2) 2.81 Å, O(11)-H(11B)···O(2) 155°]; several weaker contacts are also observed (see **Figure 2**). Overall, this structure shows that, in the solid state, the metal to ligand stoichiometry is 1:1. Crystal data/refinement details and bond distances/angles of **4** and Zn(II):**4** can be found in **Tables S1** and **S2** of **ESI (Section 4)**, respectively.
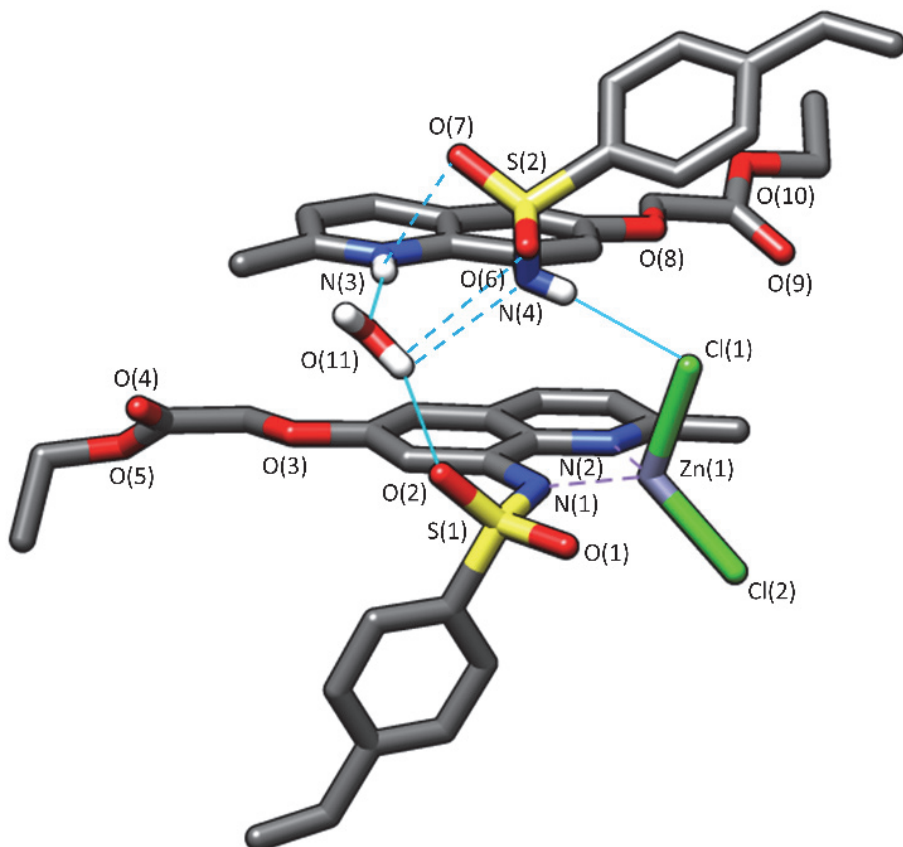
Figure 2. Solid-state X-ray structure of compound Zn(II):**4**. Hydrogen atoms, except those involved in hydrogen-bonding interactions (the moderate ones are represented by continuous light blue lines and the weaker ones by dotted light blue lines), have been omitted for the sake of simplicity.

3.5. Determination of Zn(II) by fluorimetry

*Using the water-soluble polymer (**WsP**)*

The titration with Zn(II) was carried out by increasing the Zn(II) concentration (from 2.5×10^{-7} to 2.7×10^{-3} M) in an aqueous solution of **WsP** (2.02 g/L, which corresponded to 4.52×10^{-2} milliequivalents of **4** per litre) buffered at pH 4.66 and recording the fluorescence spectra. **Figure 3** depicts the formation of a fluorescence band centered at 460 nm when the sample is irradiated at 370 nm. The Job´s plot diagram (**ESI**, **Section S5**, **Figure S6**) shows that the stoichiometry of the complex formed between the receptors of the polymer (**4**) and the Zn(II) ion is 1:1. The complex formation constant between Zn(II) and **4** amounts to 1.5×10^5, a value that was obtained from the representation of the recorded fluorescence at 460 nm versus the Zn(II) concentration; the fitted curve is shown in **ESI**, **Section S6** and **Figure S8**. The limit of detection (LOD) of this system was 13 ppb. Note that an ICP-MS of **WsP** was necessary for the calculation of the real amount of **4** motifs anchored to the polymer chain (see **ESI**, **Section S7**). Although the polymer was designed with 0.25% mol of **4**, the real concentration obtained from ICP-MS was 0.23%.
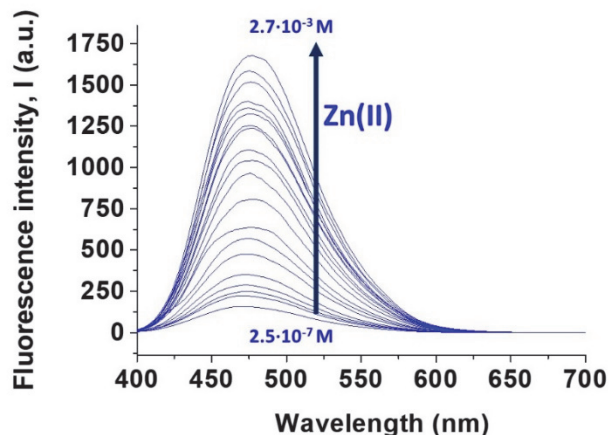
Figure 3. Titration of **WsP** with Zn(II) in an aqueous solution buffered at pH 4.66. The initial concentration of **WsP** in the cuvette was 2.02 g/L, which corresponded to 4.52×10^{-2} milliequivalents of **4** per litre. For this titration, Zn(II) concentrations ranged from 2.5×10^{-7} to 2.7×10^{-3} M. LOD: 13 ppb.

*Using the hydrophilic film (**HP**)*

12 mm diameter discs were cut from **HP** and immersed for 12 hours in solutions with different Zn(II) concentrations (from 1×10^{-11} to 1×10^{-3} M) buffered at pH 4.66, to reach the complete equilibrium of the system. After that, discs were washed with the same buffer solution and measured in the fluorimeter. **Figure 4** shows the linear evolution of fluorescence intensity at 460 nm (excitation at 370 nm) when represented versus the logarithm of Zn(II) molarity, for concentrations ranging from 1×10^{-5} to 1×10^{-1} M and with error bars. The calculated limit of detection (LOD) of this system was 27 ppb.
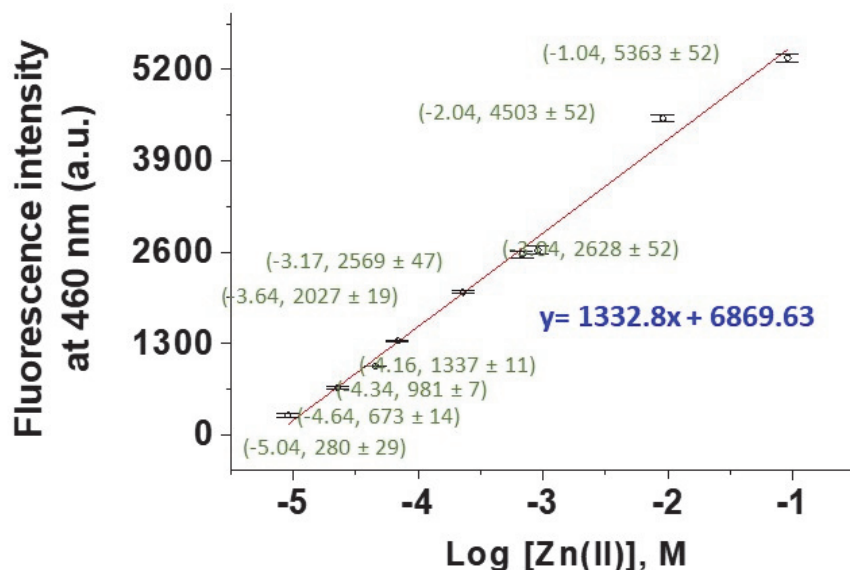
Figure 4. Titration of **HP** with Zn(II) in an aqueous solution buffered at pH 4.66. The 12 mm diameter discs were immersed in solutions with different Zn(II) concentrations (from 1×10^{-11} to 1×10^{-3} M). The graph shows the linear fitting of fluorescence intensity versus the logarithm of Zn(II) molarity between 1×10^{-5} and 1×10^{-1} M of Zn(II), with error bars. LOD: 27 ppb.

On the other hand, the Job´s plot calculations confirm the observed stoichiometry with **WsP**, i.e., 1:1 (see **ESI**, **Section S5**, **Figure S7**). The complex formation constant between Zn(II) and **4** motifs was calculated from fitting the

curve of fluorescence intensity versus Zn(II) concentration, yielding a value of 5.13×10^4 (see **ESI**, **Section S6**, **Figure S9**). To carry out these calculations, an estimation of the number of **4** motifs inside each 12 mm diameter disc was necessary. This was calculated from ICP-MS results (see **ESI**, **Section S7**), and the resulting data was 2.97×10^{-7} mol/disc, which represents a molar ratio of 0.20%. This result was confirmed with an additional ICP-MS analysis for Zn(II) after saturation of all **4** motifs in **HP** (see **ESI**, **Table S4**).

Regarding response times, at high concentrations (100 mM) the response time of the sensory material was less than 10 min. However, the aim is to measure Zn(II) in biological media, where it can reach concentrations as high as 7-10 μM. Preliminary studies show that the response time with these concentrations could be around 4-5 hours. However, it is necessary to make even less concentrated points to build the calibration curve, and given the point of "proof of concept" of the research, the sensory discs were immersed overnight (12 hours) to make sure that the equilibrium was reached.

3.6. Determination of Zn(II) by the RGB method

12 mm diameter discs were cut from **HP** and immersed for 12 hours in solutions with different Zn(II) concentrations (from 1×10^{-7} to 1×10^{-1} M) buffered at pH 4.66, to reach the complete equilibrium of the system. After that, discs were washed with the same buffer solution and photographed in a retro-illumination lightbox for the extraction of RGB parameters. The graphical representation of the green component versus the logarithm of Zn(II) molarity results in a parabolic trend for concentrations ranging from 4.5×10^{-6} to 1×10^{-4} M, as displayed in **Figure 5**. We have taken into consideration only the green component because the red and blue components provide no relevant information.
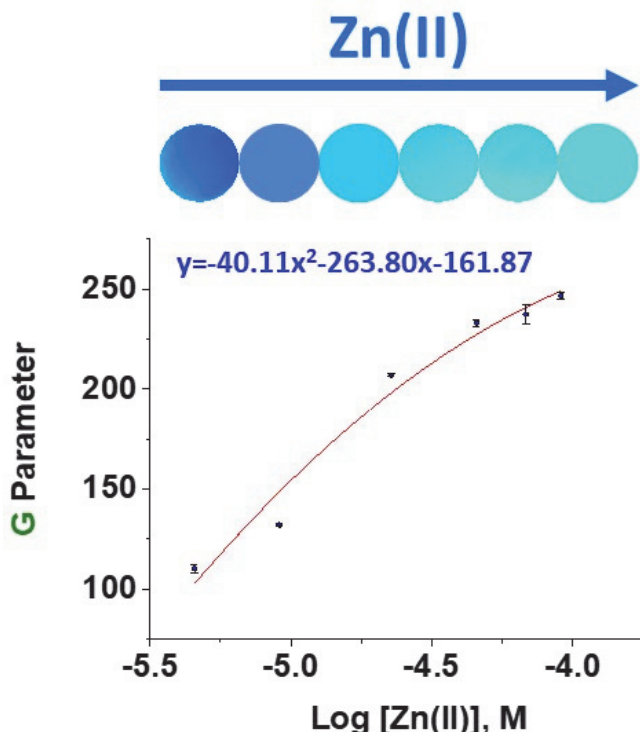
Figure 5. Graphical representation of the green component (**G**) of RGB parameters of the discs photographs versus the logarithm of Zn(II) molarity with error bars. Fitted curve for concentrations ranging from 4.5×10^{-6} to 1×10^{-4} M. RGB data can be found in **ESI**, **Section S8** and **Figure S10**.

3.7. pH study

A pH study was carried out with **HP** using the RGB method. A 12 mm diameter disc of **HP** was dipped in 250 ml of a 0.01 M Zn(II) solution. The pH of the solution was adjusted to 1 using HCl 0.1 M. The disc was photographed in the retro-illumination lightbox and pH was increased to 2 using NaOH 0.1 M. The procedure was repeated at 10 different pH values and, finally, the green parameter was graphically represented versus pH, as shown in **Figure 6**. The Zn(II):**4** complex is stable between pH 4 and pH 12, but very unstable at very acidic pHs. This behavior at pH below 3, allows the reusability of the material in a simple way, without using chelating reagents, by only dipping the films charged with Zn(II) in aqueous HCl.
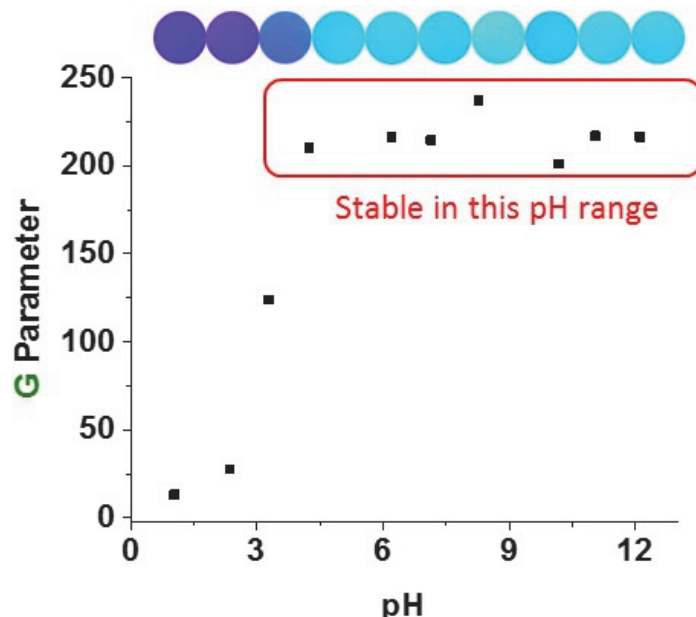
Figure 6. pH study carried out with the RGB method, by dipping a 12 mm diameter disc of **HP** in a 0.01 M Zn(II) solution and varying the pH. Graphical representation of the green parameter obtained from the photographs versus the pH of the solutions. RGB data can be found in **ESI**, **Section S9** and **Figure S11.**

3.8. Interference study

In this section we have considered several cations as possible interferents, regarding them as interferents if they can cause systematic errors (the definition of IUPAC is much centered on the magnitude of the systematic error caused in relation with the standard deviation of an unequivocally defined set of results) [44]. The study of possible interferents was performed in an aqueous solution buffered at pH 4.66, using 2 ml of a **WsP** solution (2.02 g/L, which corresponded to 4.52×10^{-2} milliequivalents of **4** per litre). The initial fluorescence of the solution was recorded in all cases. Then, 180 µl of an aqueous solution containing Zn(II) (5×10^{-4} M) and interferent (5×10^{-4} M) was added to the cuvette, and the fluorescence was recorded again. **Figure 7** shows the graphical representation of the normalized fluorescence intensity for all the measured interferents.
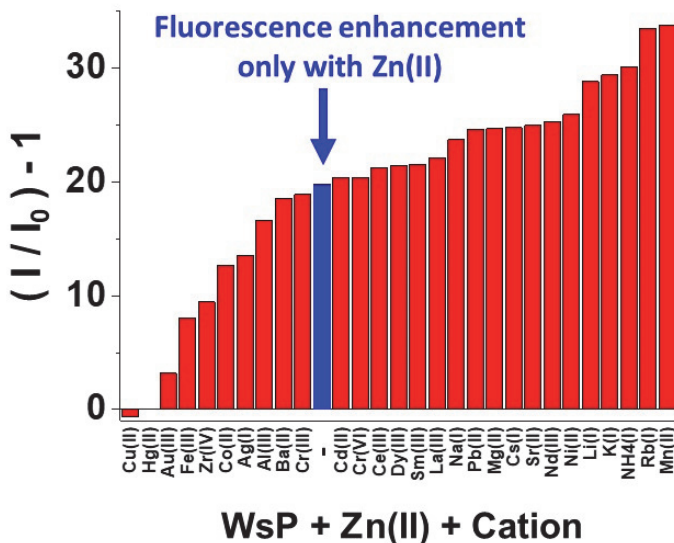
Figure 7. Interference study with 28 cations. Emission intensity enhancement (**(I/I$_0$)-1**) of a buffered aqueous solution of **WsP** (pH: 4.66, volume: 2 ml, concentration: 2.02 g/L, which corresponded to 4.52x10^{-2} milliequivalents of **4** per litre) after adding 180 µl of an aqueous solution containing Zn(II) (5x10^{-4} M) (blue bar), or Zn(II) (5x10^{-4} M) and interferent (5x10^{-4} M) (red bars). **I$_0$** is the emission intensity of the **WsP** buffered solution, and **I** the emission intensity after adding the cations.

As shown in **Figure 7**, cations as Cu(II) or Hg(II) are interferents of the detection system and switch off fluorescence. On the other hand, cations as Mn(II) or Rb(I) increase the fluorescence of the system significantly, so they are also interferents. However, they are not important interferents in the proposed real application of this sensor, i.e., the detection of Zn(II) in biological samples. In fact, our sensory material displays a behavior similar to that exhibited by 'Zinquin' (CAS number: 151606-29-0), a commercially available probe [30], that has been commonly used to detect zinc(II) in solution in biological media [31,32].

3.9. Proof of concept. Determination of Zn(II) in real biological samples

A real sample from chronic wounds was obtained from a human patient, following procedures established at Burgos University Hospital (HUBU) as described before. A swab was used to collect exudates from the chronic wounds, and then

the swab was boiled for 10 minutes in a pH 4.66 buffer solution. The solution was filtered off, and each sample was measured fivefold with the reference method (ICP-MS). Additionally, a 12 mm diameter disc of **HP** was dipped in the solution for 24 hours. Finally, the disc was measured in a fluorimeter, and by the RGB method as previously depicted. The Zn(II) concentration in the solution was calculated from the calibration equations (sections 3.6 and 3.7), and the results are shown in **Figure 8**.

a)

b)
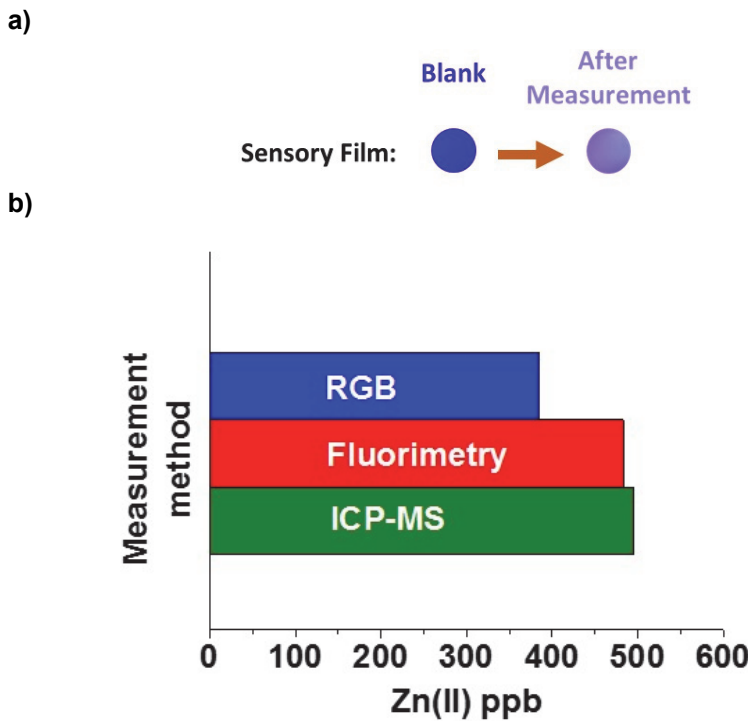
Figure 8. Results for the determination of Zn(II) in biological samples. **a)** Photos of an **HP** disc before and after dipping it in the biological solution. **b)** Zn(II) concentration data obtained from ICP-MS, fluorimetry and RGB method measurements.

As displayed in **Figure 8**, our material supposes a real alternative to the reference method (ICP-MS), both by using a fluorimeter and a smartphone to check the fluorescence change in the material. The results obtained using the proposed RGB method are relevant, even considering that the procedure is less accurate, because the overall procedure can be easily carried out by unskilled

personnel, by using a smartphone to take a photo of the sensory material after dipping it in the exudate.

3.10. Comparative study of the sensor

Table 1 shows a study of the published detection methods for Zn(II), in terms of low-cost philosophy, naked-eye detection and the possibility of a hypothetical use in biological applications.

Table 1. Comparative table of different Zn(II) analytical methods.

Detection method	Low-cost	Biological applications	Naked-eye detection	Ref.
ICP-Mass & Laser Ablation	no	-	no	[45]
Fluorimetry-Probes in Solution	no	no	no	[46], [47], [48], [49]
	no	yes	no	[50], [51], [52], [53]
	no	yes	yes	[54], [55], [56], [57], [58], [59], [60], [61]
Fluorimetry -CHEF-type and ratiometric probes	no	yes	no	[62], [63]
Fluorimetry-Review	no	yes	no	[64]
Stopped-flow fluorescence study	no	yes	no	[65]
Potentiometric sensors	no	no	no	[66]
Electrochemical sensors	no	yes	no	[67]
Optical Fiber-Based UV-Vis spectrophotometry	no	no	no	[68]
Fluorimetry film-based sensor	no	yes	no	This work
Digital pictures (RGB parameters defining digital colors)	yes	yes	yes	This work

4. Conclusions

We have developed a new sensory method for the determination of Zn(II) in biological samples. The method is based on a polymeric material made of 99.75% of commercially available monomers. The material response can be measured by typical fluorimetry analysis, but also with our proposed RGB method. This method requires no reactants, no expensive equipment and the measurements can be easily carried out by unskilled personnel with a smartphone, by taking a picture of the material after dipping it in the exudate. This sensor works in a wide range of pH, and some characteristics of the material, such as response times or hydrophilicity, could be adapted "a la carte". The study, results, and conclusions presented here encourage us to deepen in the challenge of establishing a direct relationship between the Zn(II) concentration and the state/evolution of chronic wounds, a work that is now being carried out by our research team, involving many patients with to provide a reliable sensory material to be used as a simple and cheap method to follow the evolution of these wounds.

Conflicts of interest

There are no conflicts to declare.

Supplementary Materials

Synthesis and characterization of monomer and polymers, calculation of the stoichiometry of the Zn(II):**4** complex and complex formation constants of **WsP** and **HP** with Zn(II), RGB data, CIE 1931 xy chromaticity diagram, and X-ray crystallographic files in CIF format for **4** (CCDC 1992454) and Zn(II):**4** (CCDC 1992455).

Acknowledgements

Data availability

The raw/processed data required to reproduce these findings cannot be shared at this time due to technical or time limitations. The data are available on request.

References

[1]   V.J. Temple, A. Masta, Zinc in human health., P. N. G. Med. J. 47 (2004) 146–158. https://doi.org/10.9790/0853-13721823.

[2]   R.A. Bozym, F. Chimienti, L.J. Giblin, G.W. Gross, I. Korichneva, Y. Li, S. Libert, W. Maret, M. Parviz, C.J. Frederickson, R.B. Thompson, Free zinc ions outside a narrow concentration range are toxic to a variety of cells in vitro, Exp. Biol. Med. 235 (2010) 741–750. https://doi.org/10.1258/ebm.2010.009258.

[3]   C. Rica Mora Solera, M. Conte, A. Javier, R. Mora, H. Flores, D. Silva, Papel de las Metaloproteinasas de la Matriz en la Degradación del Tejido Pulpar: Una revisión literaria, Rev. Científica Odontológica. 1 (2005) 20–26. www.merops.ac.uk (accessed April 28, 2020).

[4]   A. Tezvergil-Mutluay, K.A. Agee, T. Hoshika, M. Carrilho, L. Breschi, L. Tjäderhane, Y. Nishitani, R.M. Carvalho, S. Looney, F.R. Tay, D.H. Pashley, The requirement of zinc and calcium ions for functional MMP activity in demineralized dentin matrices, Dent. Mater. 26 (2010) 1059–1067. https://doi.org/10.1016/j.dental.2010.07.006.

[5]   C.D. Tran, R. Katsikeros, N. Manton, N.F. Krebs, K.M. Hambidge, R.N. Butler, G.P. Davidson, Zinc homeostasis and gut function in children with celiac disease, Am. J. Clin. Nutr. 94 (2011) 1026–1032. https://doi.org/10.3945/ajcn.111.018093.

[6]   S.S. Martinez, A. Campa, Y. Li, C. Fleetwood, T. Stewart, V. Ramamoorthy, M.K. Baum, Low Plasma Zinc Is Associated with Higher Mitochondrial Oxidative Stress and Faster Liver Fibrosis Development in the Miami Adult Studies in HIV Cohort, J. Nutr. 147 (2017) 556–562. https://doi.org/10.3945/jn.116.243832.

[7]   J. Mohammed, S. Mehrotra, H. Schulz, R. Lim, Severe Infant Rash Resistant to Therapy Due to Zinc Deficiency, Pediatr. Emerg. Care. 33 (2017) 582–584. https://doi.org/10.1097/PEC.0000000000001218.

[8]   I. Rotter, D.I. Kosik-Bogacka, B. Dołęgowska, K. Safranow, M. Kuczyńska, M. Laszczyńska, Analysis of the relationship between the blood concentration of several metals, macro- and micronutrients and endocrine disorders associated with male aging, Environ. Geochem. Health. 38 (2016) 749–761. https://doi.org/10.1007/s10653-015-9758-0.

[9]   P. Zorrilla, L.A. Gómez, J.A. Salido, A. Silva, A. López-Alonso, Low serum zinc level as a predictive factor of delayed wound healing in total hip replacement, Wound Repair Regen. 14 (2006) 119–122. https://doi.org/10.1111/j.1743-6109.2006.00100.x.

[10]   P.H. Lin, M. Sermersheim, H. Li, P.H.U. Lee, S.M. Steinberg, J. Ma, Zinc in wound healing modulation, Nutrients. 10 (2018) 16. https://doi.org/10.3390/nu10010016.

[11]   S. Kogan, A. Sood, M.S. Garnick, Zinc and Wound Healing: A Review of Zinc Physiology and Clinical Applications, Wounds a Compend. Clin. Res. Pract. 29 (2017) 102–106. https://doi.org/102-106 PMID: 28448263.

[12]   A.B.G. Lansdown, U. Mirastschijski, N. Stubbs, E. Scanlon, M.S. Ågren, Zinc in wound healing: Theoretical, experimental, and clinical aspects, Wound Repair Regen. 15 (2007) 2–16. https://doi.org/10.1111/j.1524-475X.2006.00179.x.

[13]   S.K. Ghosh, P. Kim, X.A. Zhang, S.H. Yun, A. Moore, S.J. Lippard, Z. Medarova, A novel imaging approach for early detection of prostate cancer based on endogenous zinc sensing, Cancer Res. 70 (2010) 6119–6127. https://doi.org/10.1158/0008-5472.CAN-10-1008.

[14]   R.M. Atwater, The Merck Manual of Diagnosis and Therapy, Merck Sharpe & Dohme Research Laboratories, 1950. https://doi.org/10.2105/ajph.40.11.1454.

[15]   K. T, T. I, H. R, Y. H, I. M, Y. Y, N. K, Selenium, zinc, copper and cadmium concentration in livers and kidneys of people exposed to environmental cadmium., J. Trace Elem. Electrolytes Health Dis. 2 (1988) 101–104.

[16]   R. Cornelis, F. Borguet, J. De Kimpe, Trace elements in medicine. Speciation: the new frontier, Anal. Chim. Acta. 283 (1993) 183–189. https://doi.org/10.1016/0003-2670(93)85221-5.

[17]   N. Fabris, E. Mocchegiani, Zinc, human diseases and aging, Aging Clin. Exp. Res. 7 (1995) 77–93. https://doi.org/10.1007/BF03324297.

[18]   S. Chan, B. Gerson, S. Subramaniam, The role of copper, molybdenum, selenium, and zinc in nutrition and health, Clin. Lab. Med. 18 (1998) 673–685. https://doi.org/10.1016/s0272-2712(18)30143-4.

[19]   K.P. Carter, A.M. Young, A.E. Palmer, Fluorescent sensors for measuring metal ions in living systems, Chem. Rev. 114 (2014) 4564–4601. https://doi.org/10.1021/cr400546e.

[20]   B. Wang, Y. Hu, Z. Su, Synthesis and photophysical behaviors of a blue fluorescent copolymer as chemosensor for protons and Ni2+ ion in aqueous solution, React. Funct. Polym. 68 (2008) 1137–1143. https://doi.org/10.1016/j.reactfunctpolym.2008.03.005.

[21]   D. Zeng, J. Cheng, S. Ren, J. Sun, H. Zhong, E. Xu, J. Du, Q. Fang, A new sensor for copper(II) ion based on carboxyl acid groups substituted polyfluoreneethynylene, React. Funct. Polym. 68 (2008) 1715–1721. https://doi.org/10.1016/j.reactfunctpolym.2008.10.001.

[22]   J.L. Pablos, S. Ibeas, A. Muñoz, F. Serna, F.C. García, J.M. García, Solid polymer and metallogel networks based on a fluorene derivative as fluorescent and colourimetric chemosensors for Hg(II), React. Funct. Polym. 79 (2014) 14–23. https://doi.org/10.1016/j.reactfunctpolym.2014.02.009.

[23]   R.S. Juang, P.C. Yang, H.W. Wen, C.Y. Lin, S.C. Lee, T.W. Chang, Synthesis and chemosensory properties of terpyridine-containing diblock polycarbazole through RAFT polymerization, React. Funct. Polym. 93 (2015) 130–137. https://doi.org/10.1016/j.reactfunctpolym.2015.06.008.

[24]   A.M. Sanjuán, J.A. Reglero Ruiz, F.C. García, J.M. García, Recent developments in sensing devices based on polymeric systems, React. Funct. Polym. 133 (2018) 103–125. https://doi.org/10.1016/j.reactfunctpolym.2018.10.007.

[25]   J.A.R. Ruiz, A.M. Sanjuán, S. Vallejos, F.C. García, J.M. García, Smart polymers in micro and nano sensory devices, Chemosensors. 6 (2018) 12. https://doi.org/10.3390/chemosensors6020012.

[26]   K. Boonkitpatarakul, A. Smata, K. Kongnukool, S. Srisurichan, K. Chainok, M. Sukwattanasinitt, An 8-aminoquinoline derivative as a molecular platform for fluorescent sensors for Zn(II) and Cd(II) ions, J. Lumin. 198 (2018) 59–67. https://doi.org/10.1016/j.jlumin.2018.01.048.

[27]   C.J. Fahrni, T. V. O'Halloran, Aqueous coordination chemistry of quinoline-based fluorescence probes for the biological chemistry of zinc, J. Am. Chem. Soc. 121 (1999) 11448–11458. https://doi.org/10.1021/ja992709f.

[28]   M.R. Karim, D.H. Petering, Newport Green, a fluorescent sensor of weakly bound cellular Zn2+: Competition with proteome for Zn2+, Metallomics. 8 (2016) 201–210. https://doi.org/10.1039/c5mt00167f.

[29]   S. Mukherjee, S. Talukder, A reversible luminescent quinoline based chemosensor for recognition of Zn2+ ions in aqueous methanol medium and its logic gate behavior, J. Lumin. 177 (2016) 40–47. https://doi.org/10.1016/j.jlumin.2016.04.016.

[30]   Zinquin, ≥95% (HPLC), solid | C19H18N2O5S | Sigma-Aldrich, (n.d.). https://www.sigmaaldrich.com/catalog/product/sial/z2376?lang=es&region=ES (accessed April 28, 2020).

[31]   P.D. Zalewski, I.J. Forbes, W.H. Betts, Correlation of apoptosis with change in intracellular labile Zn(II) using Zinquin [(2-methyl-8-p-toluenesulphonamido-6-quinolyloxy)acetic acid], a new specific fluorescent probe for Zn(II), Biochem. J. 296 (1993) 403–408. https://doi.org/10.1042/bj2960403.

[32]   C.D. Geddes (editor), Reviews in Fluorescence 2004, Springer, 2004. https://doi.org/10.1007/978-0-306-48672-2.

[33]   S. Vallejos, A. Muñoz, S. Ibeas, F. Serna, F.C. García, J.M. García, Solid sensory polymer

substrates for the quantification of iron in blood, wine and water by a scalable RGB technique, J. Mater. Chem. A. 1 (2013) 15435–15441. https://doi.org/10.1039/c3ta12703f.

[34] S. Vallejos, J.A. Reglero, F.C. García, J.M. García, Direct visual detection and quantification of mercury in fresh fish meat using facilely prepared polymeric sensory labels, J. Mater. Chem. A. 5 (2017) 13710–13716. https://doi.org/10.1039/c7ta03902f.

[35] S. Vallejos, A. Muñoz, S. Ibeas, F. Serna, F.C. García, J.M. García, Forced solid-state interactions for the selective Turn-On fluorescence sensing of aluminum ions in water using a sensory polymer substrate, ACS Appl. Mater. Interfaces. 7 (2015) 921–928. https://doi.org/10.1021/am507458k.

[36] A.M. Brouwer, Standards for photoluminescence quantum yield measurements in solution (IUPAC technical report), Pure Appl. Chem. 83 (2011) 2213–2228. https://doi.org/10.1351/PAC-REP-10-09-31.

[37] M. Guembe-García, P.D. Peredo-Guzmán, V. Santaolalla-García, N. Moradillo-Renuncio, S. Ibeas, A. Mendía, F.C. García, J.M. García, S. Vallejos, Why the sensory response of organic probes is different in solution and in the solid- state within a polymer film? Evidence and application to the detection of amino acids in human chronic wounds Marta Guembe-García, Unpubl. Work. (n.d.).

[38] L.O.I.I. Cie, P. Cie, Commission Internationale De L ' Éclairage International Commission on Illumination Internationale Beleuchtungskomm, 1931 (1993). http://files.cie.co.at/204.xls (accessed April 28, 2020).

[39] M.K. Chun, J. Cho, A.R. Jeong, K.S. Min, J.H. Jeong, Tetrahedral Zinc(II) Complexes with Chiral Diamine Ligands: Synthesis, Characterization, and Photoluminescence, Bull. Korean Chem. Soc. 40 (2019) 921–924. https://doi.org/10.1002/bkcs.11845.

[40] A. Ayadi, M.A. Benmensour, Y. Cheret, A. Boucekkine, A. El-Ghayoury, Zinc and copper complexes of stilbene iminopyridine ligands with η2-Olefin binding mode, J. Organomet. Chem. 858 (2018) 14–22. https://doi.org/10.1016/j.jorganchem.2018.01.002.

[41] T.M. Chang, S. Sinharay, A. V. Astashkin, E. Tomat, Prodigiosin analogue designed for metal coordination: Stable zinc and copper pyrrolyldipyrrins, Inorg. Chem. 53 (2014) 7518–7526. https://doi.org/10.1021/ic5008439.

[42] M.J. Minch, An Introduction to Hydrogen Bonding (Jeffrey, George A.), Oxford University Press, 1999. https://doi.org/10.1021/ed076p759.1.

[43] T. Steiner, The hydrogen bond in the solid state, Angew. Chemie - Int. Ed. 41 (2002) 48–76. https://doi.org/10.1002/1521-3773(20020104)41:1<48::AID-ANIE48>3.0.CO;2-U.

[44] J. Bartos, M.P. Roussel-Uclaf, International union of pure and applied chemistry analytical chemistry division commission on analytical reactions and reagents spectrophotometric and fluorimetric determination of amines, Pure Appl. Chem. 56 (1984) 467–477. https://doi.org/10.1351/pac198456040467.

[45] P. Arrowsmith, Laser Ablation of Solids for Elemental Analysis by Inductively Coupled Plasma Mass Spectrometry, 1987. https://doi.org/10.1021/ac00137a014.

[46] M. Ui, Y. Tanaka, Y. Araki, T. Wada, T. Takei, K. Tsumoto, S. Endo, K. Kinbara, Application of photoactive yellow protein as a photoresponsive module for controlling hemolytic activity of staphylococcal α-hemolysin, Chem. Commun. 48 (2012) 4764–4766. https://doi.org/10.1039/c2cc30963g.

[47] Y. Ding, Y. Xie, X. Li, J.P. Hill, W. Zhang, W. Zhu, Selective and sensitive "turn-on" fluorescent Zn2+ sensors based on di- and tripyrrins with readily modulated emission wavelengths, Chem. Commun. 47 (2011) 5431–5433. https://doi.org/10.1039/c1cc11493j.

[48] F. Wang, R. Peng, Y. Sha, Selective dendritic fluorescent sensors for Zn(II), Molecules. 13 (2008) 922–930. https://doi.org/10.3390/molecules13040922.

[49] Z. Wu, Q. Chen, G. Yang, C. Xiao, J. Liu, S. Yang, J.S. Ma, Novel fluorescent sensor for Zn(II) based on bis(pyrrol-2-yl- methyleneamine) ligands, Sensors Actuators, B Chem. 99 (2004) 511–515. https://doi.org/10.1016/j.snb.2003.12.070.

[50] S. Erdemir, S. Malkondu, Calix[4]arene based a NIR-fluorescent sensor with an enhanced stokes shift for the real-time visualization of Zn(II) in living cells, Sensors Actuators, B Chem. 306 (2020) 127574. https://doi.org/10.1016/j.snb.2019.127574.

[51] G. Ambrosi, M. Micheloni, D. Paderni, M. Formica, L. Giorgi, V. Fusi, Fluorescent macrocyclic chemosensor for Zn(II) detection at alkaline pH values, Supramol. Chem. 32 (2020) 139–149. https://doi.org/10.1080/10610278.2020.1713324.

[52] E. Tamanini, K. Flavin, M. Motevalli, S. Piperno, L.A. Gheber, M.H. Todd, M. Watkinson,

   Cyclam-based "clickates": Homogeneous and heterogeneous fluorescent sensors for Zn(II), Inorg. Chem. 49 (2010) 3789–3800. https://doi.org/10.1021/ic901939x.

[53] M. Hagimori, M. Taniura, N. Mizuyama, Y. Karimine, S. Kawakami, H. Saji, T. Mukai, Synthesis of a novel pyrazine-pyridone biheteroaryl-based fluorescence sensor and detection of endogenous labile zinc ions in lung cancer cells, Sensors (Switzerland). 19 (2019) 2049. https://doi.org/10.3390/s19092049.

[54] Y. Upadhyay, T. Anand, L.T. Babu, P. Paira, G. Crisponi, A.K. Sk, R. Kumar, S.K. Sahoo, Three-in-one type fluorescent sensor based on a pyrene pyridoxal cascade for the selective detection of Zn(II), hydrogen phosphate and cysteine, Dalt. Trans. 47 (2018) 742–749. https://doi.org/10.1039/c7dt04234e.

[55] T. Anand, A.S.K. Kumar, S.K. Sahoo, A novel Schiff base derivative of pyridoxal for the optical sensing of Zn2+ and cysteine, Photochem. Photobiol. Sci. 17 (2018) 414–422. https://doi.org/10.1039/c7pp00391a.

[56] T. Anand, A. Kumar SK, S.K. Sahoo, Vitamin B$_6$ Cofactor Derivative: A Dual Fluorescent Turn-On Sensor to Detect Zn^{2+} and CN$^-$ Ions and Its Application in Live Cell Imaging, ChemistrySelect. 2 (2017) 7570–7579. https://doi.org/10.1002/slct.201701024.

[57] K. Tayade, S.K. Sahoo, B. Bondhopadhyay, V.K. Bhardwaj, N. Singh, A. Basu, R. Bendre, A. Kuwar, Highly selective turn-on fluorescent sensor for nanomolar detection of biologically important Zn2+ based on isonicotinohydrazide derivative: APPLICATION in cellular imaging, Biosens. Bioelectron. 61 (2014) 429–433. https://doi.org/10.1016/j.bios.2014.05.053.

[58] U.A. Fegade, S.K. Sahoo, A. Singh, N. Singh, S.B. Attarde, A.S. Kuwar, A chemosensor showing discriminating fluorescent response for highly selective and nanomolar detection of Cu2+ and Zn2+ and its application in molecular logic gate, Anal. Chim. Acta. 872 (2015) 63–69. https://doi.org/10.1016/j.aca.2015.02.051.

[59] R. Selva Kumar, S.K. Ashok Kumar, K. Vijayakrishna, A. Sivaramakrishna, P. Paira, C.V.S. Brahmmananada Rao, N. Sivaraman, S.K. Sahoo, Bipyridine bisphosphonate-based fluorescent optical sensor and optode for selective detection of Zn2+ ions and its applications, New J. Chem. 42 (2018) 8494–8502. https://doi.org/10.1039/c8nj00158h.

[60] K. Tayade, B. Bondhopadhyay, K. Keshav, S.K. Sahoo, A. Basu, J. Singh, N. Singh, D.T. Nehete, A. Kuwar, A novel zinc(II) and hydrogen sulphate selective fluorescent "turn-on" chemosensor based on isonicotiamide: INHIBIT type's logic gate and application in cancer cell imaging, Analyst. 141 (2016) 1814–1821. https://doi.org/10.1039/c5an02295a.

[61] N. Khairnar, K. Tayade, S.K. Sahoo, B. Bondhopadhyay, A. Basu, J. Singh, N. Singh, V. Gite, A. Kuwar, A highly selective fluorescent "turn-on" chemosensor for Zn2+ based on a benzothiazole conjugate: Their applicability in live cell imaging and use of the resultant complex as a secondary sensor of CN-, Dalt. Trans. 44 (2015) 2097–2102. https://doi.org/10.1039/c4dt03247k.

[62] N.C. Lim, J. V. Schuster, M.C. Porto, M.A. Tanudra, L. Yao, H.C. Freake, C. Brückner, Coumarin-based chemosensors for zinc(II): Toward the determination of the design algorithm for CHEF-type and ratiometric probes, Inorg. Chem. 44 (2005) 2018–2030. https://doi.org/10.1021/ic048905r.

[63] Y. Lv, M. Cao, J. Li, J. Wang, A sensitive ratiometric fluorescent sensor for zinc(II) with high selectivity, Sensors (Switzerland). 13 (2013) 3131–3141. https://doi.org/10.3390/s130303131.

[64] R. Pandey, A. Kumar, Q. Xu, D.S. Pandey, Zinc(ii), copper(ii) and cadmium(ii) complexes as fluorescent chemosensors for cations, Dalt. Trans. 49 (2020) 542–568. https://doi.org/10.1039/c9dt03017d.

[65] E.M. Nolan, S.J. Lippard, Small-molecule fluorescent sensors for investigating zinc metalloneurochemistry, Acc. Chem. Res. 42 (2009) 193–203. https://doi.org/10.1021/ar8001409.

[66] M.A. Abbasi, Z.H. Ibupoto, M. Hussain, Y. Khan, A. Khan, O. Nur, M. Willander, Potentiometric zinc ion sensor based on honeycomb-Like NiO nanostructures, Sensors (Switzerland). 12 (2012) 15424–15437. https://doi.org/10.3390/s121115424.

[67] J. Kudr, H.V. Nguyen, J. Gumulec, L. Nejdl, I. Blazkova, B. Ruttkay-Nedecky, D. Hynek, J. Kynicky, V. Adam, R. Kizek, Simultaneous automatic electrochemical detection of zinc, cadmium, copper and lead ions in environmental samples using a thin-film mercury electrode and an artificial neural network, Sensors (Switzerland). 15 (2014) 592–610. https://doi.org/10.3390/s150100592.

[68]   S. Kopitzke, P. Geissinger, An optical fiber-based sensor array for the monitoring of zinc and copper ions in aqueous environments, Sensors (Switzerland). 14 (2014) 3077–3094. https://doi.org/10.3390/s140203077.

CAPÍTULO 4

Colorimetric Titration. Aplicación para teléfonos inteligentes como complemento de los polímeros sensores para la cuantificación de especies de interés

El método RGB (Red, Green, Blue) nos permite analizar los cambios visuales que ocurren en los polímeros sensores a través de una fotografía digital. Es un método muy eficaz y ampliamente estudiado, pero que maneja un gran volumen de datos que es necesario gestionar de forma adecuada. Para agilizar y mejorar este proceso, y con ello el uso y el manejo de los sensores poliméricos colorimétricos y fluorimétricos, en este trabajo se ha desarrollado una aplicación para teléfonos inteligentes con sistemas operativos basados en *Android* y *iOS* que permite llevar a cabo este análisis de resultados en poco tiempo y de manera eficaz.

4.1. Introducción

Desde el diseño inicial del Trabajo de esta Tesis siempre he tenido en el punto de mira la preparación de sensores que fueran fáciles de utilizar, intuitivos, y adaptados al uso por parte del ciudadano de a pie. Efectivamente, los polímeros sensores que se han desarrollado durante este trabajo cambian de color en función de la concentración de la especie diana, y ese mero cambio de color a simple vista es suficiente para un análisis cualitativo, o incluso semicuantitativo, utilizando una carta de colores. Sin embargo, si se requiere de un análisis cuantitativo es necesario emplear un equipo para registrar el cambio de color de forma objetiva y reproducible. En el caso del color, la técnica por excelencia que permite analizar estos cambios y correlacionarlos con la concentración es la espectroscopia ultravioleta-visible, y en el caso de la fluorescencia la fluorimetría. La primera, por ejemplo, mide la absorbancia de los sistemas coloreados, que se puede correlacionar con la concentración de la especie diana. Esto se consigue gracias a un calibrado previo en el que es necesario preparar una serie de disoluciones con concentraciones crecientes de la sustancia de interés. Un proceso tedioso que suele llevar a cabo personal especializado, y tras el cual se puede conocer la concentración de la especie diana en una muestra problema. Aunque es una técnica muy precisa, presenta tres grandes desventajas: el uso de equipamiento avanzado; un laborioso calibrado previo; y personal especializado para llevar a cabo todas las medidas.

Como alternativa a esta técnica, el Grupo de Polímeros lleva años utilizando lo que ha denominado como "el método RBG". Este método utiliza fotografías digitales para llevar a cabo un análisis del color, que se ha postulado como una digna alternativa a los métodos tradicionales.[25,27,37,38,28,29,97,98] Además, las ventajas son considerables, ya que en cada medida se realiza un auto calibrado con una referencia de color, por lo que cualquier persona puede llevar

---

[97] S. Vallejos, J. A. Reglero, F. C. García and J. M. García, *J. Mater. Chem. A*, **2017**, 5, 13710–13716

[98] S. Vallejos, A. Muñoz, S. Ibeas, F. Serna, F. C. García and J. M. García, *ACS Appl. Mater. Interfaces*, **2015**, 7, 921–928.

a cabo las medidas de manera rápida y sencilla, valiéndose únicamente de un teléfono.

Con el fin de mejorar aún más el método RGB, en este trabajo se ha desarrollado una aplicación para teléfonos inteligentes (con sistemas operativos tanto Android como iOS) que con tan solo una fotografía puede llevar a cabo el análisis completo, de manera rápida y sencilla.

4.2. Método RBG.

La definición digital de color se lleva a cabo dentro de un espacio de color, como puede ser RGB.[99] Pese a ser el más utilizado, el espacio de color RGB (Rojo, Verde, Azul. Del inglés *Red, Green, Blue*) no es el único, y existen otros similares como por ejemplo el espacio de color HSV (Matiz, Saturación y Brillo. Del inglés *Hue, Saturation* y *Value*), el espacio de color CIELAB (Comisión Internacional de la Iluminación. Del francés *Commission Internationale d'Éclairage LAB)* o el espacio de color CMYK (Cian, Magenta, Amarillo, Negro. Del inglés *Cyan, Magenta, Yellow, Key*).

Inicialmente, nuestro método se basaba en los parámetros RGB que definen el color de una fotografía digital en código HTML. Es decir, cada uno de los colores que vemos en una imagen digital se puede definir con una combinación de tres números, uno para cada parámetro. Cada uno de esos valores puede estar comprendido entre 0 y 255, de tal forma que mediante su combinación permiten definir más 16 millones de colores.

En la **Tabla 4.1.** se pueden ver algunos ejemplos de colores y sus correspondientes parámetros RGB.

---

[99] Y. Fan, J. Li, Y. Guo, L. Xie and G. Zhang, *Meas. J. Int. Meas. Confed.*, **2021**, 171, 108829.

Tabla 4.1. Colores según sus parámetros RGB.

R	**255**	255	255	125	**0**	0	0	0	**0**	125	255	255
G	**0**	125	255	255	**255**	255	255	125	**0**	0	0	0
B	**0**	0	0	0	**0**	125	255	255	**255**	255	255	125

El método RGB permite asociar valores numéricos a los colores y correlacionarlos con otras magnitudes, como la concentración. Usar este método para determinar concentraciones a partir de cambios visuales requiere la construcción de una carta de colores, que hace las veces de recta de calibrado. Esta carta se puede plastificar para que pueda ser reutilizada todas las veces que sea necesario. Suele estar compuesta de un mínimo de puntos, por ejemplo, por 5 discos de 8-10 mm de diámetro del polímero sensor, que se sumergen en disoluciones de concentraciones diferentes de la especie diana antes de su plastificación.

Una vez preparada la carta de colores, se toma una fotografía conjunta de los polímeros sensores con los que se han analizado las muestras problema y de la carta de colores. Este paso es de gran relevancia, ya que el hecho de trabajar con una única fotografía asegura que las condiciones de iluminación sean iguales para todos los puntos, haciendo del sistema un sensor auto-calibrable en cada medida y, además, altamente reproducible. Inicialmente, los puntos de la carta de colores se fotografiaban de forma independiente, complicando el proceso y alargándolo en el tiempo, debido a la necesidad de tomar las fotografías en ambientes de iluminación controlada.[23,25,27,37,38,28,29,98,96]

El proceso que nosotros realizábamos originariamente de forma sistemática incluía tres réplicas, y de cada réplica 6 fotografías. Es decir, la construcción de un calibrado con 6 puntos suponía realizar 108 fotografías, de las cuales había que extraer de forma manual los parámetros RGB, y posteriormente buscar posibles correlaciones con cada uno de ellos. Y es que,

en algunas ocasiones, la concentración de la especie diana se correlaciona con el parámetro R,[28] en otras con el parámetro G,[96] en otras con el parámetro B,[29] y en otras con combinaciones matemáticas de 2 de ellos o incluso de los 3.[23,25] Es más, en ocasiones el rango de concentraciones es tan amplio que se obtienen los mejores ajustes cuando se utilizan escalas logarítmicas de concentración.

En definitiva, el número de combinaciones posibles es enorme, y el Grupo invertía mucho tiempo en la búsqueda del mejor ajuste. Por esto surgió la idea de una aplicación capaz de llevar a cabo este análisis en pocos minutos, partiendo de una sola fotografía y auto calibrando en cada medida. La **Figura 4.1.** muestra un diagrama con el que la empresa burgalesa "INFORAPPS" desarrolló la aplicación bajo nuestras especificaciones.
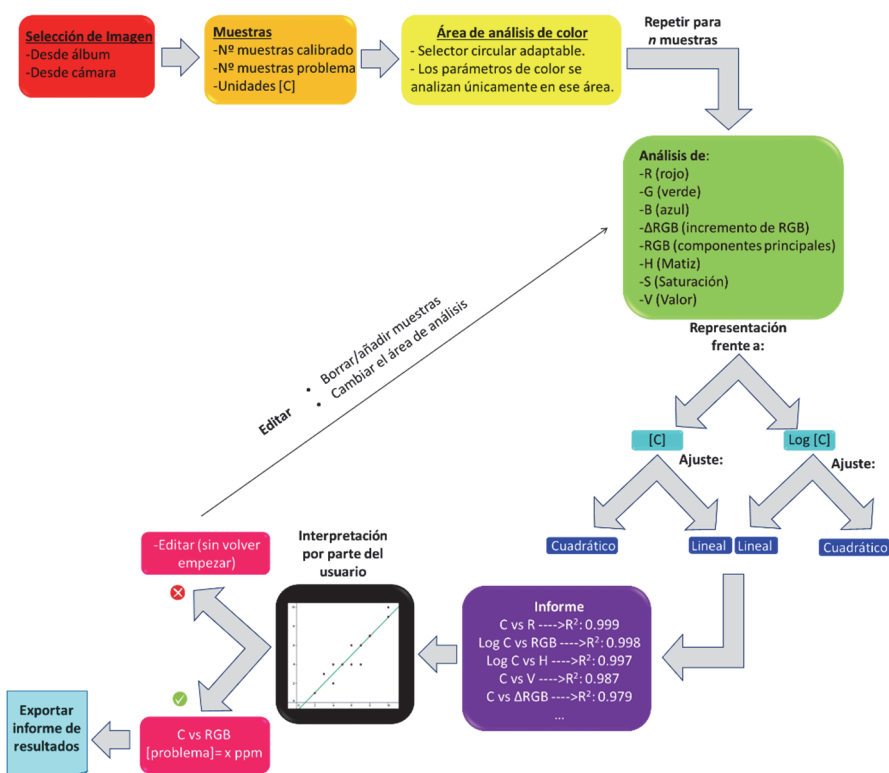
Figura 4.1. Diagrama de flujo diseñado para el desarrollo de la aplicación *Colorimetric Titration* por parte de la empresa burgalesa INFORAPPS.[100]

---

[100] Inforapps - Consultoría - Apps Web & Software. https://inforapps.es/

Aunque el desarrollo informático de la aplicación lo llevó a cabo una empresa externa, pude participar de manera activa en el proceso. Al inicio, transmitiendo a los desarrolladores la idea que habíamos madurado, y que dejamos plasmada en el esquema que se muestra en la **Figura 4.1**. En fases posteriores, trabajé en el laboratorio con las primeras versiones, optimizando el rendimiento de la aplicación y mejorando los fallos y erratas que surgían en los ensayos. Tras 10 versiones de prueba, la versión final se puede descargar de forma gratuita desde el almacén de aplicaciones de google (https://play.google.com/store/apps/details?id=es.inforapps.chameleon&gl=ES), y se ha diseñado en sistema multiplataforma, de tal forma que funciona en sistemas operativos *Android* y *iOs*.

4.3. Colorimetric Titration

La aplicación *Colorimetric Titration* nos permite, a partir de distintos parámetros del color (espacios de color RGB y HSV) de una fotografía digital, construir una recta de calibrado y calcular la concentración de una especie de interés en distintas muestras problema. La elección de los espacios de color que analiza la aplicación (RGB y HSV) vino determinada por la experiencia previa del grupo en el espacio RGB, así como por las posibilidades que creímos que podría aportar el análisis de un nuevo espacio de color. De hecho, no descartamos incluir más espacios de color en nuestra aplicación para teléfonos inteligentes a medio plazo.

La aplicación tiene una interfaz muy sencilla y fácil de utilizar (**Figura 4.2**). En la esquina superior derecha podemos encontrar tres puntos verticales que nos abren un desplegable con dos opciones (**Figura 4.2.b**). "*Help*", que nos muestra un tutorial de cómo utilizar la aplicación y "*About us*", donde encontramos toda la información acerca del Grupo de Polímeros, la Universidad de Burgos, y la financiación que ha hecho posible el desarrollo de la aplicación.

El usuario deberá pulsar el icono (+) en la esquina inferior derecha de la pantalla (**Figura 4.2.d)** para empezar el análisis, lo cual le dará la opción de

tomar la fotografía en el momento o utilizar una fotografía almacenada en la memoria (**Figura 4.2.e**).

a)

b)

c)

d)

e)

f)
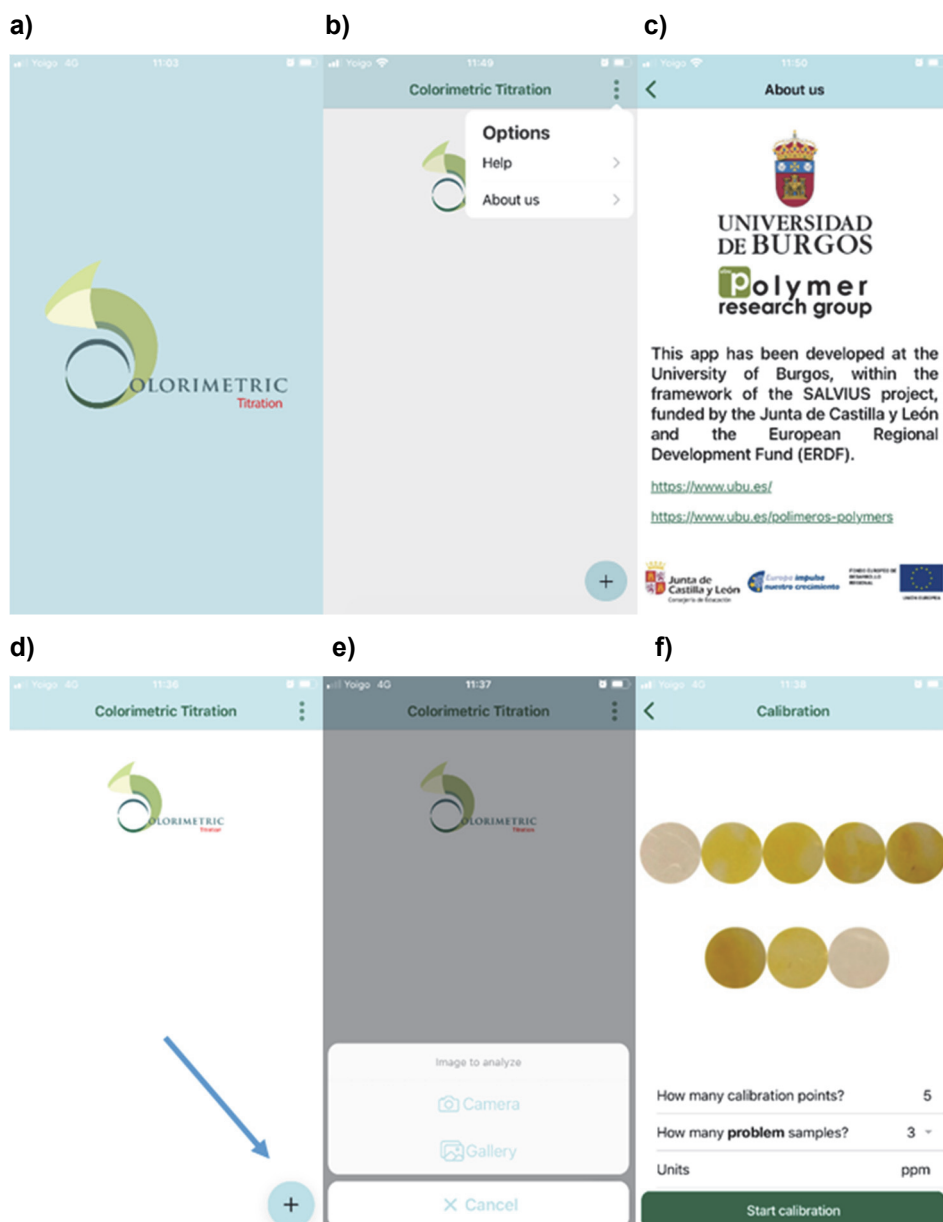
Figura 4.2. Interfaz de inicio de la aplicación: a) presentación de la aplicación "Colorimetric Titration"; b) menú opciones; y c) *About Us*. Interfaz de la aplicación para la selección de datos: a) interfaz inicial; b) carga de la imagen a través de la cámara o de la galería de imágenes; y c) selección del número del puntos del calibrado, muestras problema y unidades.

Una vez elegida la imagen, debemos indicar el número de puntos del calibrado (entre 3 y 20), el número de muestras problemas (entre 1 y 3) y las unidades de concentración (**Figura 4.2.f**).

En los pasos sucesivos, y hasta completar el número de puntos del calibrado, debemos indicar cada uno de los puntos con el selector circular y sus respectivas concentraciones (**Figura 4.3.a**). Del mismo modo, debemos indicar cuales son las muestras problema para poder concluir esta primera etapa, que dependiendo del número de puntos puede consumir entre 2 y 10 minutos.

Una vez hemos completado esta información, la aplicación nos muestra la imagen original con las zonas que hemos seleccionado como puntos del calibrado (círculos rojos) y como muestras problemas (círculos morados) (**Figura 4.3.b**).
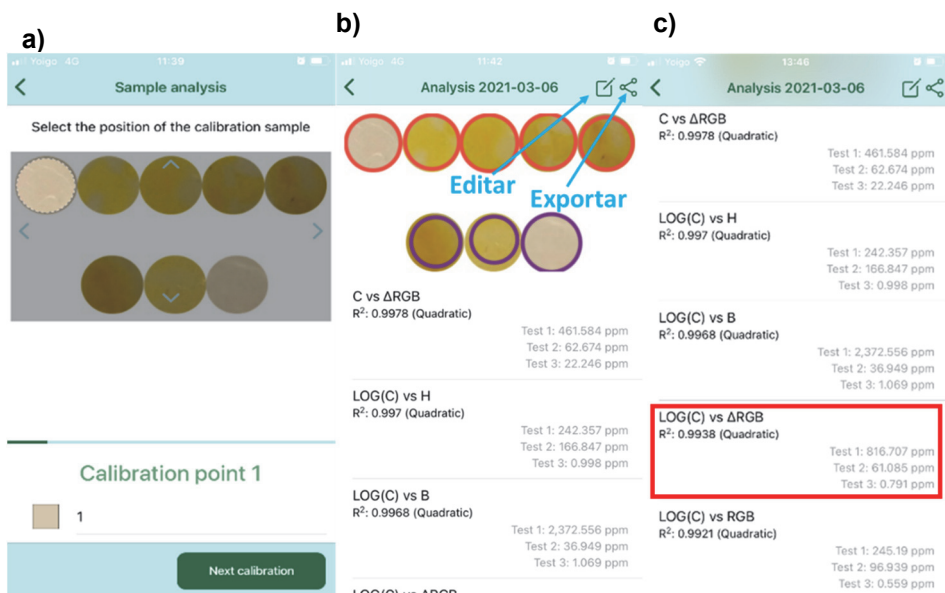
Figura 4.3. Interfaz de la aplicación para la selección de datos y muestra de resultados: a) selección de puntos del calibrado y muestras problemas sobre la imagen original; b) muestra de resultado, opciones del tratamiento de datos; y c) lista de resultados.

En ese punto, la aplicación realiza en 1 segundo y de forma simultánea 32 ajustes diferentes, correlacionado 8 parámetros distintos de color (R, G, B, H, S, V, RGB, ΔRGB) con respecto a la concentración y al logaritmo de la

concentración, y además valorando en cada uno de los casos un ajuste lineal y uno cuadrático.

Una vez realizados los 32 ajustes, la aplicación los muestra ordenados, de mejor a peor ajuste, teniendo en cuenta el parámetro R^2 (**Figura 4.3.c**). Seleccionado cualquiera de los resultados, podemos ver una gráfica tanto de su ajuste lineal (y = a + bx) (**Figura 4.4.a**), como su ajuste cuadrático (polinomio de grado 2, y = ax^2 + bx + c) (**Figura 4.4.c**).

En ambos casos, vemos la línea del ajuste en color rojo, los puntos del calibrado en azul y las muestras problema en amarillo. La aplicación permite eliminar cualquiera de ellos pulsando en la leyenda correspondiente (**Figura 4.4.b**). En esta pantalla también se incluyen los resultados de las muestras problemas y la ecuación del calibrado.
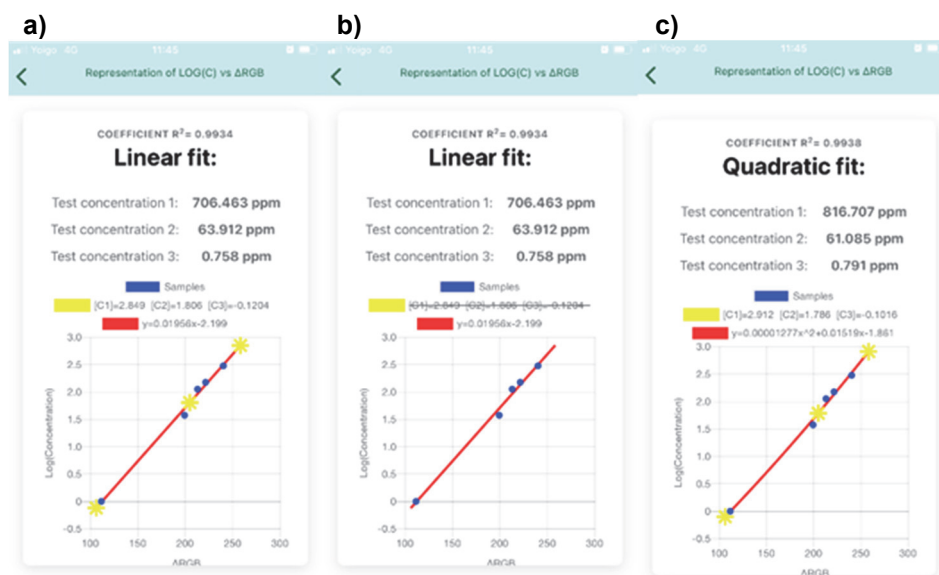

Figura 4.4. Interfaz de muestra de resultados: a) muestra de resultado, ajuste lineal; b) muestra de resultado, selección de opciones de representación; y c) muestra de resultado, ajuste cuadrático.

Por último, *Colorimetric Titration* permite exportar y editar los resultados (**Figura 4.3.b**) sin necesidad de comenzar todo el proceso desde el inicio. Es posible tanto eliminar como añadir puntos al calibrado o a las muestras problema

(**Figura 4.5.a**), y la opción de exportar nos permite realizar una descarga masiva de todos los análisis, parámetros de color, ajustes y concentraciones en formato CSV (**Figura 4.5.b**). Además, la aplicación guarda un histórico de todos los análisis realizados (**Figura 4.5.c**), de tal forma que se pueden recuperar, modificar, o borrar en cualquier momento.
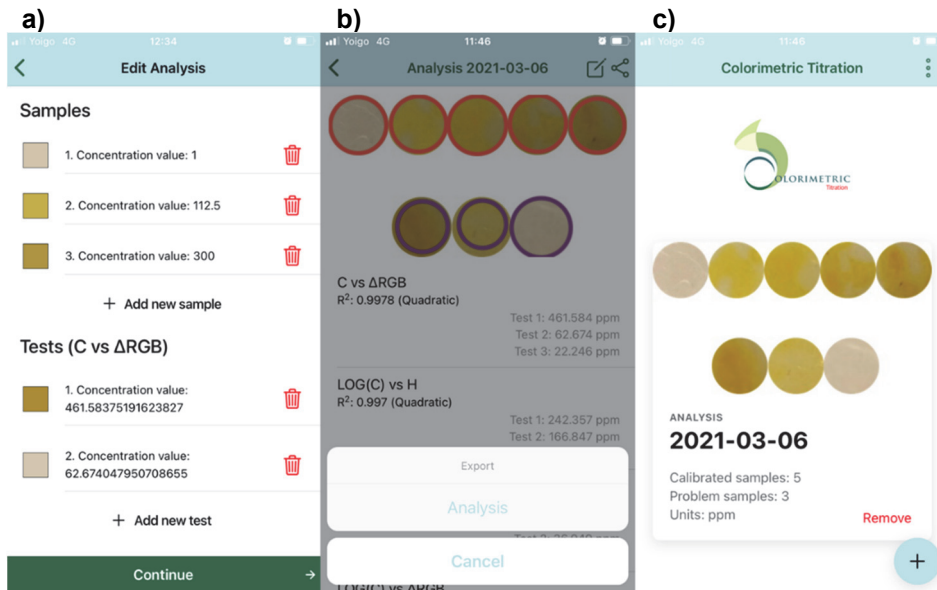

Figura 4.5. Interfaz de exportación y edición de resultados: a) edición de datos; b) de exportación de datos; y c) Interfaz de almacenaje de resultados.

Por todo lo descrito, la aplicación supone el complemento ideal de los polímeros sensores que he desarrollado en mi tesis, y nos permite realizar un análisis cuantitativo con una sola imagen, en poco tiempo y de forma muy sencilla.

4.4. Resultados

Con el fin de proteger el contenido de la invención y sus posibles usos y/o explotaciones, este software ha sido registrado en el registro de la propiedad intelectual, tal como se muestra en la **Figura 4.6.**

OFICINA PROVINCIAL DEL REGISTRO GENERAL DE LA PROPIEDAD INTELECTUAL EN BURGOS

SOLICITUD NÚMERO: BU-122-20
FECHA: 22/12/2020 HORA: 10:15

OBRA: "COLORIMETRIC TITRATION"
CLASE DE OBRA: PROGRAMA DE ORDENADOR
AUTOR: SAÚL VALLEJOS CALZADA, CÉSAR REPRESA PÉREZ, JOSÉ MIGUEL
GARCÍA PÉREZ, FÉLIX CLEMENTE GARCÍA GARCÍA Y MARTA GUEMBE
GARCÍA
TITULAR DEL DERECHO: EL AUTOR
SOLICITANTE: NOMBRE: MANUEL PÉREZ MATEOS
DOMICILIO: C/ HOSPITAL DEL REY S/N
CIUDAD: 09001 – BURGOS
TELÉFONO: 947 92 20 36

LIQUIDACION NUMERO 990036000533 1	Unid.	Precio	€uros
Tramitación de expediente de solicitud	1	13,46	13,46
Anotación preventiva		13,46	
Cancelación de asiento registral		13,46	
Modificación de asiento registral		13,46	
Traslado de asiento registral y de expediente		13,46	
Expedición de Certificado, positivo ó negativo, por cada uno		16	
Expedición de Nota Simple, positiva ó negativa, por cada una		4,47	
Diligencia de autenticación de firma	6	4,47	26,82
		Total €	40,28

De acuerdo con lo dispuesto en el artículo 22 de la Ley 62/2003, del 30 de diciembre de Medidas Fiscales, Administrativas y del Orden Social y en la Ley de Presupuestos Generales del Estado para el año 2.018 se practica la presente liquidación, correspondiente a la tasa por servicios del Registro de la Propiedad Intelectual.

CUARENTA EUROS CON VEINTIOCHO CÉNTIMOS

Burgos, a 22 de diciembre de 2020

EL RESPONSABLE DE LA OFICINA PROVINCIAL

Figura 4.7. Registro de la propiedad intelectual.

CONCLUSIONES

El desarrollo de este trabajo ha permitido establecer un procedimiento sencillo y rápido para evaluar el estado de las heridas crónicas mediante la utilización de distintos sensores poliméricos.

Las conclusiones particulares derivadas del trabajo son las siguientes:

- La matriz polimérica genera un entorno protector de las unidades receptoras, que disminuye las interacciones de los receptores con el disolvente, y por consiguiente aumenta la eficiencia de la interacción con las dianas con respecto a lo que ocurre en disolución.

- La concentración de aminoácidos de una herida está directamente relacionada con el estado y evolución de la herida.

- El sensor para aminoácidos basado en receptores de ninhidrina permite la cuantificación de forma rápida y sencilla de la concentración de aminoácidos en una herida.

- El sensor de Zn(II) basado en un derivado de la quinolina posibilita la determinación de la concentración de Zn(II) en muestras biológicas de manera sencilla y, aunque todavía no se ha demostrado la relación directa entre el estado de la herida y la cantidad de Zn(II), es un sensor que muestra mucho potencial.

A mi entender, el futuro de los sensores poliméricos para la evaluación de las heridas crónicas, así como para la determinación de otras enfermedades,

debe dirigirse hacia la detección directa de la actividad enzimática. Una de las aproximaciones más viables es mediante receptores con secuencias peptídicas fácilmente reconocibles por las enzimas estudiadas, que permitan determinar su actividad mediante señales colorimétricas o fluorescentes.